Permeability evolution in chalk linked to stress and thermochemical aspects of North Sea reservoir conditions

by

Emanuela I. Kallesten

Thesis submitted in fulfilment of
the requirements for the degree of
PHILOSOPHIAE DOCTOR
(PhD)

Faculty of Science and Technology
Department of Energy Resources
2020

University of Stavanger
NO-4036 Stavanger
NORWAY
www.uis.no

ISBN: 978-82-7644-972-3
ISSN: 1890-1387
PhD: Thesis UiS No. 564

To my dear
Børge, Maya and Kristoffer

Acknowledgements

Few people have had as much impact in my life and even fewer have so selflessly invested in me as my main supervisor, Professor Dr. Merete Vadla Madland, and co-supervisors Professor Dr. Udo Zimmermann, Dr. Reidar Korsnes, Dr. Pål Andersen Østebø and Dr. Edvard Omdal. Your combined academic competence, experience, skills, and knowledge are out of this world and I am honored and grateful to have had the opportunity to benefit from it.

I am forever grateful for your personal approach to supervision: Merete, thank you for the unconditional support, generosity, and for giving me wings to fly; Udo, you believed in me even when I did not, and always had my back; Reidar, thank you for patiently introducing me to rock mechanics and for answering my dumb questions without a flinch; Pål, thank you for always being there for me and for encouraging me to reach higher; Edvard, you challenged me to see things from new perspectives and enabled my commitment to concise writing.

I would like to thank Yosra Cherif, Dr. Silvana Bertolino, and Dhruvit Berawala for their indispensable contribution to various studies in the project. I owe a special thank you to Tonje Rafshol Hovden for her lab assistance and friendship.

I would like to thank the National IOR Centre of Norway, UiS and the industry partners for trusting me with this project, for providing an exceptional sample set, opportunities to travel to exciting conferences, and not least for taking the bill.

A heartfelt appreciation goes to my friends and colleagues who saw me through good and bad times; it has been a pleasure to get to know you, eat lunches together, and discuss ideas. To my friend and former colleague, Dr. Mona W. Minde, thank you for grabbing me with you on this journey, for your friendship and collaboration through many years.

I would like to thank my parents for implanting the value of education in me from an early age; my whole family – siblings and in-laws – and friends for their love and sustained support. But mostly, I would like to thank my husband and children for allowing me to live my dream and for making the sacrifices that it took, without hesitation.

Summary

The project was initiated by The National IOR Centre of Norway within the University of Stavanger and it aligns with the overall goal of the centre to improve oil recovery on the Norwegian Continental Shelf. It contributes to several of the centre's tasks, such as development of IOR methods, IOR mechanisms, fluid flow simulations, and evaluation of economic potential and environmental impact.

The chalk reservoirs are among the most prolific hydrocarbon fields in the North Sea, Ekofisk field alone accounting for approximately 10% of the produced net oil equivalents on the Norwegian Continental Shelf. Primary and secondary oil recovery methods induce a complex set of alteration in the reservoir properties. With more and more mature fields and reports of descending production trend, developing and implementing EOR techniques tailored to the specifics of each field is timelier than ever. Besides the mechanical changes due to fluctuations in the stress state of the reservoir during production, chalk interacts with the injected fluids, leading to chemical reactions that further affect its mineralogy, structure, and strength. It is therefore essential to understand the particularities of the reservoir rocks and the interplay of all these processes and their effect on fluid flow.

The main purpose of this project is to study the relationship between the stress state, rock-fluid interactions on one side, and the permeability of compacting chalk cores on the other side, by investigating pore- and core-scale effects of stress state, temperature, and reactive fluid flow on the permeability of fractured chalk – an essential parameter in improved oil recovery, yet still insufficiently understood. A complementary objective is to describe the mineralogy and geochemistry of North Sea reservoir and non-reservoir chalk, as well as to model and predict permeability evolution in chalk under relevant North Sea reservoir conditions based on the interpretation of the experimental data.

The approach of the project is therefore threefold:

- factual: in-depth mineralogical and chemical characterization of the North Sea chalk and an evaluation of the mineralogical and geochemical impact of hydrocarbons and EOR fluids on reservoir chalk
- experimental: geomechanical tests investigating permeability evolution in shear failing outcrop chalk exposed to thermochemical influence and the geomechanical and chemical response of North Sea reservoir chalk to reactive fluid flow
- theoretical: simulation of permeability evolution investigating the role of fracture width, flooding rate and brine concentration on the mechanical and chemical compaction in water-wet fractured chalk and relative quantification of the mechanical and chemical contribution to permeability evolution

The studies have been conducted on oil-bearing reservoir chalk from Ekofisk and Eldfisk fields in the North Sea, as well as on outcrop chalks saturated with various brines. The main finds are disseminated in four papers.

A rare and coveted sample set consisting of chalk cores from several wells in the North Sea provided a unique opportunity to obtain mineralogical and geochemical data describing reservoir and non-reservoir chalks, as well as reservoir chalk before and after flooding with EOR fluids. **Paper I** (see subsection 4.1) shows that the mineralogical composition of the North Sea chalk is typical for regional marine deposits of the Upper Cretaceous, consisting of micritic carbonate matrix, microfossils and diverse authigenic and detrital minerals. Non-carbonate mineral phases consist mostly of quartz, illite, smectite, kaolinite. Carbon isotope ratios align well with primary trends for Upper Cretaceous stages; oxygen isotopes on the other hand, are far from

primary, considerable deviation from the Upper Cretaceous trends is seen in all samples. Burial diagenesis, paleotemperature fluctuations, or meteoric water input with different thermal gradient can plausibly explain the disturbed oxygen isotopes. The presence of hydrocarbon fluids was most likely not the cause of the negative $\delta^{18}O$, as both the reservoir and the non-reservoir successions show similar oxygen isotope pattern. Dolomite is detected only in the reservoir cores, but it is interpreted to be diagenetic rather than anthropologic (i.e., due to EOR flooding) as it is present in both flooded and unflooded samples.

Paper II (subsection 4.3) presents the results of geomechanical tests on reservoir chalk from the North Sea that facilitate a valuable and needed comparison between the response of reservoir chalk and outcrop chalk to mechanical and chemical compaction. Synthetic seawater (SSW) and simplified seawater (0.219 M $MgCl_2$) injection through reservoir cores induced increased strain rates in the reservoir chalk, linked to retention of magnesium and production of calcium during flooding, which results in precipitation of secondary magnesium-bearing minerals or anhydrite. Adding calcium to the $MgCl_2$ aqueous solution effectively reduced the creep strain rate, likely because the dissolution of primary calcite is inhibited. Most interestingly, the results from this study match very well the results gained from previous studies on water-wet outcrop chalks, thus validating decades of chalk research on outcrop chalk regarding brine-chalk chemical interactions and geomechanical behaviour.

The experimental approach also includes a set of geomechanical tests on shear fractured outcrop chalk cores from the Cretaceous Niobrara Formation (Utah and Kansas, USA), often denoted “Kansas chalk”, exposed to deviatoric stress cycles and thermochemical influence, monitoring the effects of the test parameters on the permeability evolution of the cores. The results are presented in **Paper III** (see subsection 4.2)**.** Deviatoric stress state together with low confining pressure induced shear fracturing at a steep angle (over 70°),

close to flooding direction, corresponding to a simultaneous permeability increase. This was the main permeability-altering event. Subsequent deviatoric loadings had little effect on permeability in all tests, regardless of injecting brine (aqueous solutions of NaCl, Na_2SO_4, and synthetic seawater) and test temperature (50° C and 130° C). During creep, permeability generally declined slightly, or remained unchanged. The results indicate that once chalk has fractured under deviatoric stress conditions, the effective permeability is little responsive to compaction cycles and reactive flow, both at high and low temperature. Despite fracturing and exposure to different stress states, temperature and brine conditions, the end core permeability seems to remain within the same order of magnitude as the original value, ranging between the initial and double of the initial value. This indicates a notable insensitivity to changes in reservoir conditions.

Theoretical predictions of permeability evolution in fractured and intact cores were obtained from simulations of reactive fluid flow through outcrop chalk. The model was calibrated to match nine previous geomechanical tests on intact chalk cores from Aalborg and Liège and four tests on pre-fractured Kansas and Mons chalk cores. **Paper IV** addresses the main finds from this study (see subsection 4.4). The model quantifies the permeability loss related to mechanical and chemical compaction. The simulations predict that porosity and axial strain are sensitive to fracture width, reactive brine concentration and injecting rate. However, while the permeability trend in time is affected by the brine composition, it remains insensitive to injection rate and fracture width. The results also underline that fracture permeability, in another order of magnitude compared to the matrix permeability, dominates the effective permeability evolution and that the mineral alterations and any significant permeability loss in the matrix are strongest at the core inlet.

List of publications

Paper I:

Kallesten, E., Zimmermann, U., Madland, M. V., Bertolino, S. R. A., Omdal, E., Andersen, P.Ø.

Mineralogy and geochemistry of reservoir and non-reservoir chalk from the Norwegian continental shelf

Journal of Petroleum Science and Engineering (2nd review)

Paper II:

Kallesten, E., Cherif, Y., Madland, M.V., Korsnes, R.I., Omdal, E., Andersen, P.Ø., Zimmermann, U

Validation study of water weakening research from outcrop chalks performed on Eldfisk reservoir cores

Journal of Petroleum Science and Engineering, (in press)

Paper III:

Kallesten, E., Andersen, P.Ø., U., Madland, M.V., Korsnes, R.I., Omdal, E., Zimmermann, U.

Permeability evolution of shear failing chalk cores under thermochemical influence

ACS Omega 2020, 5, 9185 – 9195

Paper IV:

Kallesten, E., Andersen, P.Ø., U., Berawala, D.S., Korsnes, R.I., Madland, M.V., Omdal, E., Zimmermann, U.

Modelling of Permeability and Strain Evolution in Chemical Creep Compaction Experiments with Fractured and Unfractured Chalk Cores Conducted at Reservoir Conditions

SPE Journal, in press

Conference contributions:

Kallesten, E. I., Zimmermann, U., Minde, M. W, Madland, M. V.; Petrological, Mineralogical and Geochemical Constraints on Hydrocarbon Bearing North Sea Reservoir Chalk. IOR 2017 - 19th European Symposium on Improved Oil Recovery; 2017-04-24 - 2017-04-27; UIS

Kallesten, E. I., Zimmermann, U., Minde, M. W., Madland, M. V.; Petrological, Mineralogical and Geochemical Constraints on Hydrocarbon Bearing North Sea Reservoir Chalk. 2nd Reservoir Characterization Conference - NPF 2017-12-05; Sola, Norway

Kallesten, E.I., Madland, M.V., Korsnes, I.R., Zimmermann, U., Andersen, P.Ø.; Permeability and Stress State. IOR Norway 2018, Smart Solutions for Future IOR. 2018-04-24 - 2018-04-25, Stavanger, Norway

Kallesten, E. I., Madland, M.V., Korsnes, R.I., Omdal, E., Zimmermann, U., Andersen, P.Ø.; Permeability evolution of shear failing chalk cores under thermochemical influence. IOR Norway 2019, All for IOR, IOR for All 2019-03-19 – 2019-04-20, Stavanger, Norway

Kallesten, E. I., Madland, M.V., Korsnes, R.I., Omdal, E., Zimmermann, U., Andersen, P.Ø.; Permeability evolution of shear failing chalk cores under thermochemical influence. IOR 2019 – 20th European Symposium on Improved Oil Recovery; 2019-04-08 – 2019-04-11, Pau, France

Kallesten, E. I., Andersen, P.Ø., Berawala, D. S., Madland, M.V., Korsnes, R.I., Omdal, E., Zimmermann, U.; Modelling of Permeability and Strain Evolution in Chemical Creep Compaction Experiments with Fractured and Unfractured Chalk Cores Conducted at Reservoir Conditions; Abu Dhabi International Petroleum Exhibition and Conference (ADIPEC), 11-14 November 2019, Abu Dhabi, UAE

Table of Contents

Part I

1 Introduction

1.1. Background

In the broad Earth science context, permeability is an intrinsic property of a porous medium that denotes the medium's ability to permit fluids to flow through it, and it is closely related to the volume, shape and connectivity of the available pore space – porosity. In the petroleum geoscience context, porous sedimentary rocks such as sandstones and carbonates are recognized potential hosts of vast petroleum accumulations, still a widely used energy source in the contemporary society, whose producibility is evaluated in close connection to the ease of fluid flow towards a production well.

If permeability is a key parameter in any petroleum reservoir, it plays an even more important role for the Norwegian petroleum industry. The first discovery on the Norwegian Continental Shelf (NCS) in 1969 and to this day one of the main hydrocarbon accumulations in the Norwegian sector of the North Sea has been found in the Ekofisk field, a chalk reservoir, in which the most producing horizons are within the Hod (Turonian – Campanian), Tor (Campanian – Maastrichtian) and Ekofisk (Danian) Formations. The surprisingly high potential of this discovery at that time is well expressed in the rhetorical question in the title of a landmark article – "Oil from chalks, a modern miracle?" (Scholle, 1977). Chalk is a fine-grained marine carbonate, consisting largely of a mud-sized background – matrix – composed predominantly of coccolithophore fragments of nano- and micrometer size. In rocks of such small grain sizes, permeability is naturally very low (Scholle, 1977), and accordingly, matrix permeability in Ekofisk field is evaluated between 1 – 5 millidarcies (mD) (Sulak and Danielsen, 1989). As a comparison, Statfjord field, a sandstone reservoir, and the largest oil field in the North Sea, has a matrix permeability of up to 8 darcies, averaging at 1500 mD (Kirk, 1979).

However, one of the redeeming features of the Ekofisk field is the intricate natural fracture system dominated by steeply dipping conjugate sets of fractures, which enhances the reservoir permeability by up to two orders of magnitude (Haper and Shaw, 1974; Brown, 1987; Sulak and Danielsen, 1989; Teufel and Rhett, 1992). Another key aspect that made Ekofisk field into a hydrocarbon giant is the preserved primary matrix porosity sometimes over 40 %, which should virtually be eliminated entirely by mechanical compaction given that the reservoir is buried at 3000 m below the seafloor, or even greater depths in certain areas (Scholle, 1977).

Although among one of the key reservoir parameters and essential in hydrocarbon recovery, a clear understanding of permeability evolution in chalk reservoirs is still insufficient, simply because the porosity dependency is only one of the many and complex permeability influencing factors, acting simultaneously during hydrocarbon production and enhanced oil recovery (EOR) processes (Agarwal et al., 1997; Blasingame, 2008; Meireles et al., 2017).

1.2. Stress influence on permeability of a fractured chalk reservoir

Changes in the pressure state of a petroleum reservoir, closely associated to the different production stages, have a direct effect on the porosity and permeability of the reservoir and consequently on the oil recovery. The primary recovery of Ekofisk hydrocarbons has been by pore pressure depletion, hydrocarbons being spontaneously displaced from the porous reservoir. Under these circumstances, the reservoir effective stress σ', defined by Terzaghi's law as a function of the total stress (overburden load and confining pressure) σ and the pore pressure σ_{pore}

$$\sigma' = \sigma - \sigma_{pore} \tag{1}$$

naturally increased, leading to compaction of the reservoir rock. The compaction, or gradual loss of porosity of the reservoir facilitated the hydrocarbon expulsion but at the same time it had significant effects on the mechanical properties of the chalk, and lead to severe seafloor subsidence – a massive environmental impact and a real challenge to the production facilities (Hermansen et al., 1997; Johnson et al., 1988; Hermansen et al., 2000). Yet, despite the clear porosity loss, reservoir permeability was unaffected (Sulak and Danielsen, 1989; Sulak, 1989). Studies attributed this seeming paradox to the contribution of fracture permeability, which is a dominant factor in effective permeability and whose evolution is strongly related to the fracture orientation and the stress path. In case of Ekofisk, the steeply dipping fractures aligned with the maximum horizontal stress and the deviatoric stress conditions contribute to permeability preservation despite matrix compaction (Teufel, 1991; Teufel and Rhett, 1992). The studies revealed a clear distinction between hydrostatic and deviatoric stress effects on permeability, as permeability declines steadily with increasing hydrostatic stress, while it is often preserved under deviatoric stress conditions, typical for reservoirs (Teufel, 1991; Suri et al., 1997; Yale and Crawford, 1998; Korsnes et al, 2006; Minde et al., 2018).

1.3. Thermochemical effects on the mechanical strength of chalk

Dramatically decreasing production rates following primary recovery as well as seafloor subsidence prompted the implementation of a seawater injection program at Ekofisk field in 1987 which successfully contributed to reservoir re-pressurization and a remarkable increase in oil production rates. However, the non-equilibrium between the injecting seawater the chalk surface triggered several chemical mechanisms that altered the chalk's physical, geomechanical and mineralogical properties, all encompassed under the common notion of water weakening.

Although seawater injection had a positive EOR effect, the initial water-chalk interactions caused an abrupt decrease in mechanical strength of the chalk, which explained the continued compaction of the Ekofisk field despite reservoir re-pressurization. The deformation continued thereafter, but at a lower, stable rate (Schroeder et al., 1998). Studies show that chemical and mineralogical alterations that occur in the presence of surface active ions in the seawater, such as Ca^{2+}, Mg^{2+} and SO_4^{2-} through adsorption, calcite dissolution, substitution and new mineral precipitation are decisive in water weakening of chalk during this second deformation stage (Korsnes et al., 2006; Madland et al., 2011; Nermoen et al., 2015; Ahsan and Fabricius, 2010; Megawati et al., 2013; Bergsaker et al., 2016; Andersen et al., 2018; Sachdeva et al., 2019a; Zeng et al., 2020).

These mineralogical and textural changes do not only affect the mechanical stability of the chalk, but they also impact the chalk porosity and permeability as well, and studies linked the dissolution of calcium to precipitation of permeability-inhibiting minerals such as anhydrite and gypsum (Madland et al. 2011). Additionally, elevated temperatures such as 130° C in the case of Ekofisk reservoir, facilitate and enhance the rock-fluid interactions (Austad et al., 2005; Heggheim et al. 2005; Austad et al. 2008; Korsnes et al. 2008; Madland et al. 2011; Megawati et al. 2015; Bergsaker et al., 2016; Polat et al. 2017; Minde et al. 2018).

1.4. Research rationale

Chalk research on the NCS dates back to the early 1970s (Scholle, 1975; Jensen et al., 2000), when it was clear that the primary recovery at Ekofisk will leave behind a considerable fraction of the hydrocarbons in place with possibly large economic impact. Although the waterflooding injection program was extraordinarily successful, leaving certain zones of the reservoir with as little as 30 % irreducible oil saturation, the volume of resources left behind in the flooded zones is substantial, merely due to the size of the reservoir.

As Ekofisk, many of the producing fields on the NCS are mature and report a descending production trend, while new discoveries are likely to be fewer and smaller. Developing and implementing EOR techniques tailored to the specifics of each field is timelier than ever, focusing not only on sustained profitability and resource optimization on the NCS, but also on finding better suited solutions to streamline production, while at the same time reducing the environment footprint in an effort to support the Norwegian government's climate pledge.

Maximizing reserve growth and extending field life requires among many aspects, a long-term commitment to obtain key knowledge of the actual reservoir characteristics, to building reliable reservoir models and continuous monitoring of reservoir evolution throughout production (Agarwal et al., 1997; McKinney et al., 2002; Schulte, 2005; MacGregor et al., 2005).

Extensive chalk research over the past few decades has contributed to tremendous advances within understanding mechanical behavior of chalk and evaluating the chemical effects of waterflooding on chalk for EOR purposes. Much of this research, however, is performed on chalk from outcrops, as the actual reservoir core samples are extremely scarce, and not least, the costs related to obtaining reservoir chalk samples are exceptionally high. An important knowledge gap that this project addresses is how does North Sea reservoir chalk respond mechanically and chemically to the same test parameters used in outcrop chalk studies. The results can contribute to validation of decades of chalk research and serve as grounds for selecting suitable analogues for future studies.

The use of outcrop chalk is justified, as not only it is easier and cheaper to obtain, but its relatively simple mineralogy – often over 95 % calcite – is also a convenient aspect when considering knowledge transfer from one chalk type to another. Still, depositional environment with all its geological implications, clay mineralogy, diagenesis, burial

depth, as well as reservoir stress history, exposure to EOR fluids can strongly influence chalk engineering properties and so, data from any outcrop chalk research is not always relevant in the reservoir chalk context (Scholle, 1977; Brasher and Vagle, 1996; Hjuler & Fabricius, 2009; Minde et al., 2016). There are very few published contributions that characterize the North Sea chalk in terms of petrology, mineralogy, diagenesis, or engineering properties (e.g., Scholle, 1975; Schatzinger et al., 1985; Egeberg and Saigal, 1991; Stoddart et al., 1995; Hjuler and Fabricius, 2009; Gennaro et al., 2013), and the focus is mostly on the Southern part of the North Sea and/or are often limited to a reduced number of samples.

This project offers a novel contribution to the reservoir chalk characterization by investigating a remarkably large sample set of chalk cores from several locations on the NCS, both with and without hydrocarbon content; additionally, the hydrocarbon-bearing cores are both unflooded and flooded for EOR purposes. Therefore, besides a petrophysical characterization, the sample set allows an exciting investigation of mineralogy and geochemistry effects of hydrocarbons and EOR fluids on North Sea chalk, an essential aspect in the EOR decision-making process and future research.

Further, most of the chalk research has been conducted on whole, intact cores and studied the individual or combined effects of fluctuating effective stress, temperature and brine composition on chalk and the impact on fluid flow properties. There are a limited number of studies have considered fractured cores, deviatoric stress, or repeated stress cycles that describe the stress dynamics of a producing reservoir (e.g., Milsch et al., 2016; Kluge et al., 2017; Hu et al., 2018). Even more, the complex porosity-permeability behavior in carbonate reservoirs triggered by the interplay between specific stress paths and thermochemical influence is not yet sufficiently documented and very often permeability models for the NCS are based on limited data (Jensen et al., 2000; Talukdar et al., 2002; Minde and Hiorth, 2020).

The study of permeability evolution within this project proposes a distinct approach from other studies, by incorporating several permeability-influencing factors in the test design, intending to replicate the production-related dynamics of a chalk reservoir. By considering shear fractured chalk cores exposed to cyclic deviatoric stress states while systematically changing either the test temperature, or the injected brine, different combinations highlight the individual contribution of temperature, brine chemistry and cyclic deviatoric stress on permeability evolution.

The project also includes a permeability model that considers both intact and fractured chalk, focusing mostly on interpreting the fracture's response to inert and reactive brines. The sensitivity analyses can help investigate the interplay between chemical and mechanical compaction in fractures cores and quantify the porosity-permeability relationship in non-uniformly chemically compacting intact and fractured cores.

1.5. Objectives

This project focuses primarily on permeability evolution in fractured chalk and with this it aims to contribute to a clearer grasp of one of the most significant, yet not fully understood, reservoir characteristics. The research takes a standpoint in the context of North Sea chalk reservoir, providing factual, experimental, and theoretical data and insight relevant to the particularities of the North Sea reservoir chalk and challenges of hydrocarbon production on the NCS. The objectives of the project are therefore:

- to characterize the mineralogy and geochemistry of the North Sea chalk and investigate its diagenetic overprint, as well as the effect of hydrocarbon and seawater injection on the reservoir chalk (**Paper I**)
- to investigate the geomechanical behaviour of North Sea reservoir chalk exposed to reactive brine injection and compare the results with similar tests on outcrop chalk (**Paper II**)

- to investigate permeability evolution in shear fractured chalk cores exposed to repetitive deviatoric stress cycles, different brine composition and temperature, relevant to the production-related dynamics of chalk reservoirs on the NCS (**Paper III**)
- to model permeability and strain evolution in fractured and intact chalk cores undergoing chemical and mechanical creep compaction under relevant reservoir conditions (**Paper IV**)

The results aim to bridge an important knowledge gap by enhancing the understanding of permeability evolution in chalk under stress conditions and thermochemical exposure relevant to the North Sea reservoir conditions, and eventually contribute to increase efficiency of the EOR techniques from existing and future chalk reservoirs.

2 Materials

2.1. Chalk samples used in this study

In this project we used an exceptional array of samples that includes both offshore and onshore chalk.

2.1.1 North Sea chalk

The offshore chalk used in this study is sampled from various wells in the North Sea from the Hod, Tor and Ekofisk Formations. They represent both non-reservoir and reservoir successions, which facilitates observations of the effect of hydrocarbons presence on the chalk mineralogy and geochemistry.

The non-reservoir samples are cores from 6 exploration wells spanning from the Ekofisk Field and up to Balder/Grane area in the North Sea. The samples from two of these wells, drilled in the Ekofisk Field area, represent Tor and Ekofisk Formations, while the samples from the remaining 4 wells (7/1-1, 15/12-4, 16/2-3, 25/11-17) are from Hod and Tor Formations.

140 reservoir samples used for various geochemical analyses are horizontal core plugs from production wells in the Ekofisk Field. Due to the confidential nature of these wells, their ID and exact geographic location remains undisclosed. The cores represent the hydrocarbon rich Tor and Ekofisk Formations and have experienced different exposures to EOR fluids: either flooded over a long period of time, assumingly with seawater, or unflooded (i.e., were not exposed to seawater injection). The injecting fluid temperature is not reported beyond hot and cold, and the exact distance between the injectors and the flooded cores is not given. Comparing flooded and unflooded cores is used for insight into the effect of EOR fluid injection on reservoir chalk.

A second set of reservoir chalk cores is used for geomechanical tests and consists of two cylindrical cores from the Eldfisk field, Ekofisk Formation with measured porosity between 18-19 %. Mineralogically, Eldfisk chalk is comparable to the Ekofisk chalk, with calcite content up to 97 % and a non-carbonate phase consisting mostly of quartz, kaolinite, and scarce dolomite, feldspar, pyrite, apatite, smectite and illite (Madsen, 2010).

2.1.2 Onshore chalk

Kansas chalk

Outcrop chalk from in Kansas/Utah, USA (Niobrara Formation) is considered a relevant analogue to North Sea chalk in terms of physical properties and mineralogy, with a non-carbonate phase content of less than 5 % bound mostly in quartz, clays and pyrite (Tang and Firoozabadi, 2001). The porosity (32 % ±1%) and permeability (1 mD ± 0.3 mD) properties of Kansas chalk used in this study are within the same range of the North Sea chalk (Scholle, 1975; Andersen et al., 2018; Nourani et al., 2019). In this study, Kansas chalk is used for geomechanical tests in triaxial cells to investigate the combined effects of stress, temperature, and fluid chemistry on permeability evolution in chalk cores.

Additionally, Kansas chalk cores are used for flooding experiments that serve as input data for permeability modeling.

Mons chalk

Outcrop chalk collected from the Mons Basin in Belgium (Trivières Formation, Upper Cretaceous) is one of the two chalk types used for permeability modeling calibration. Unlike Kansas chalk, Mons chalk has an extremely high carbonate content, over 99 % (Pradhan et al., 2015; Andersen et al., 2018) and the comparison between the two chalk types gives an indication of the role of non-carbonate content in permeability evolution related to rock-fluid interactions. Additionally, Mons chalk is often used as an analogue to Ekofisk chalk in the North Sea in terms of petrography, porosity, and permeability (Papamichos and Stroggylis, 2019).

Liège and Aalborg chalk

The Liège and Aalborg outcrop chalks are not directly tested in this project, but experimental data from previous studies (Madland et al., 2011; Nermoen et al., 2015; Andersen et al., 2018; Minde et al., 2018) provided input for model parametrization in **Paper IV**, along with Kansas and Mons chalk, and consequently condition the permeability model simulations.

Outcrop chalk from Liège (Belgium) is from Gulpen Formation, of Late Campanian to Early Maastrichtian age (Molenaar et al., 1997) and it is viewed as analogue to the North Sea chalk in terms of mechanical behavior (Collin et al., 2002). It also bears mineralogical similarities to the North Sea chalk, with high carbonate content (95 %) while the remaining non-carbonate phase consist of mainly quartz, smectite and mixed smectite-illite layers, mica, apatite and feldspar, among others (Hjuler and Fabricius, 2009). The typical porosity for this chalk lies between 40 – 43 %, while the matrix permeability is 1 – 2 mD (Cui et al., 1996; Schroeder et al., 1998).

Aalborg chalk was obtained from the Rørdal quarry near Aalborg, Denmark, from the exposed Rørdal Member of the Tor Formation (Upper Maastrichtian age). The carbonate content is between 90 – 95 % with a relatively high clay and quartz (commonly opal-CT) content, beside smectite, kaolinite, mica, apatite, and feldspar (Håkonsson et al., 1975). The chalk used for parametrization had an initial porosity of 47 % and 1 – 2 mD matrix permeability.

2.2 Sample preparation and properties calculations

Each method required a careful and customized sample preparation, from hand- or machine-milled powder to drilled cores. All the samples, apart from polished thin sections made at Acme Laboratories, Canada, were prepared at the University of Stavanger.

2.2.1 Hand- and machine milling

Hand-milled samples were used for X-ray diffraction, a measurement which relies on the integrity of the crystals. Approximately 2 g of the bulk sample were carefully ground to a very fine powder in an agate mortar. The material used for geochemistry was pulverized to a fine mesh in an automated, ultra-clean agate mill (Retsch RS200) for 2 – 3 min. at 700 rpm.

2.2.2 Separation of the non-carbonate phase

The mineralogy and geochemistry of the non-carbonate content in the chalk was measured for 23 reservoir samples. To isolate the non-carbonate phases, the chalk was treated cautiously with acetic acid (2 M) for several days, until the carbonate dissolved entirely. The insoluble residue (IR) left after acid treatment including quartz, clays, pyrite, was cleaned with distilled water and dried.

2.2.3 Core preparation

Geomechanical testing of cores is described in **Papers II, III** and **IV**. The Kansas and Mons chalk cores (**Papers III** and **IV**) are drilled with an oversized bit and lathed to 38.1 mm (1.5 inch) diameter. The cores are cut to approximately 75 mm lengths using a Struers Discotom-5 cutting machine. The length-diameter of approximately 2:1 should accommodate the steeply dipping shear fracture plane expected to occur during deviatoric stress loading. The reservoir cores from Eldfisk field (**Paper II**) were drilled by an external contractor, but the uneven end facets were cut and grinded at the University of Stavanger with a Delta LF-350 machine to obtain right cylinders (sides perpendicular to the parallel bases) compatible with triaxial cell testing. Since the length of these reservoir cores is between 52 – 53 mm, during testing an additional steel spacer (19.3 mm length) is placed on top of the cores to compensate the reduced core length.

The experiments in **Papers II** and **III** required intact cores, while for **Paper IV**, the cores were pre-fractured in a Brazilian cell to obtain a controlled fracture through the entire length of the core, parallel to the axial direction. Just before the testing started, all Kansas and Mons cores were saturated with distilled water (DW), while the oil-bearing reservoir cores were brought to 100 % saturation with NaCl brine.

2.2.4 Porosity calculation

The parameters used for calculating the initial porosity of the cores were measured by gas pycnometry (**Paper II**) and by saturation method (**Papers III, IV**).

Gas pycnometry (Micromeritics Gas Pycnometer model AccuPyc II 1340) was used to obtain the reservoir cores' solid volume (V_s) by measuring the how much helium gas did the porous core displace

when placed in a sealed 100 cm^3 chamber. The pore volume (V_p) was calculated from the relation (2)

$$V_b = V_s + V_p \quad (2)$$

where V_b (bulk volume) is the volume of the cylindrical cores with known diameter and length.

The saturation method was used on the outcrop chalks to calculate the pore volume of the cores. The dry cores were immersed in distilled water with known density under vacuum conditions. The cores were weighed before and after saturation and the mass difference was assumed to represent the mass of distilled water penetrating the pore space in the core. The pore volume could be derived from the expression for density:

$$\rho = \frac{m}{V} \quad (3)$$

where ρ is the density of distilled water at ambient temperature ($\approx 1\ g/cm^3$), m is the mass of distilled water (g) and V is the volume of distilled water, and in this case the same as the pore volume (V_p, cm^3).

The core porosity (ϕ) was then calculated as the ratio between the pore volume V_p and the bulk volume V_b as shown in (4) and it is reported in percentage (Table1).

$$\phi = \frac{V_P}{V_b} \quad (4)$$

2.2.5 Permeability calculation

Permeability evolution in chalk cores was monitored during triaxial cell testing. The value registered once the cores were mounted, fully saturated with brine, the differential pressure was stable, prior to the

initiation of mechanical testing was considered the cores' initial permeability. The effective permeability (k) calculation is derived from Darcy's law (Darcy, 1856), assuming a steady, laminar fluid flow and symmetric axial and radial deformations:

$$k = \frac{4\,\mu\,(L_i + \Delta L)Q}{\pi\,(D_i + \Delta D)^2\,\Delta P} \quad (5)$$

where μ is fluid viscosity as a function of salinity and temperature (cP; after c), L_i is the initial length of the core (cm), ΔL is the change in core length (cm), Q is flow rate (cm^3/sec), D_i is the initial diameter of the core (cm), ΔD is the mean change in core diameter (cm) and ΔP is the pressure drop over the core during flooding (atm).

An overview of the cores' initial dimensions and properties before mechanical testing is listed in Table 1.

Table 1: Overview of the cores' initial length (L), diameter (D), porosity (ϕ) and permeability (k)

Paper	Chalk type	Core ID	L	D	ϕ	k
			$[mm]$	$[mm]$	[%]	$[mD]$
II	Eldfisk	E2	53.00	37.93	18.00	0.71
	Eldfisk	E3	52.40	37.98	18.93	0.19
III	Kansas	KE4	70.3	38.12	32.6	1.24
	Kansas	KE20	70.9	38.11	32.6	0.94
	Kansas	KE44	76.5	38.10	32.2	0.64
	Kansas	KE45	74.5	38.10	31.7	0.59
	Kansas	KE48	78.9	38.09	32.9	0.70
	Kansas	KE75	75.9	38.14	32.4	0.62
	Kansas	KE22	72.8	38.09	32.4	0.66
	Kansas	KE55	75.9	38.10	32.6	0.61
	Kansas	KE47	75.4	38.10	32.9	0.81
	Kansas	KE77	75.5	38.12	33.0	0.68
	Kansas	KE51	77.1	38.10	32.1	0.58
	Kansas	KE73	76.4	38.12	32.4	0.66
IV	Kansas	KR15	73.7	38.1	33.0	0.65
	Kansas	KE71	74.7	38.1	32.2	0.65
	Mons	ME5	75.5	38.1	44.0	1.40
	Mons	ME4	75.5	38.2	43.8	1.40

2.3 Overview of injecting brines used in this study

During the mechanical tests, several brines were injected through the chalk cores to identify the role of brine chemistry in rock-fluid interactions under various test conditions and its effect on permeability evolution. Table 2 shows the chemical composition of the brines, including the ionic strength and ion concentrations.

Table 2: Ionic strength and ion concentrations of the brines used in the project

	NaCl	$MgCl_2$	$MgCl_2$ + $CaCl_2$	Na_2SO_4	SSW
Ionic strength [-]	0.657	0.657	1,047	0.657	0.657
Cl^- [mole L^{-1}]	0.657	0.438	0,698	0.585	0.525
Na^+ [mole L^{-1}]	0.657			0.633	0.450
Mg^{2+}[mole L^{-1}]		0.219	0,219		0.045
SO_4^{2-} [mole L^{-1}]				0.024	0.024
Ca^{2+} [mole L^{-1}]			0,130		0.013
HCO_3^- [mole L^{-1}]					0.002
K^+ [mole L^{-1}]					0.010

The brines were prepared at room temperature with calcite-equilibrated distilled water.

3 Methods

The studies involved a large array of analytical, geomechanical and theoretical methods. The methods' name, application and measuring parameters are briefly described below.

3.1 Optical petrography

Optical petrography was used as a preliminary method for characterization of reservoir chalk. The method uses a transmitted light microscope (light passes through the sample), whose essential application is that it polarizes bulk source light (filter electric wave vectors to a single plane) in order to enhance the contrasts in a sample.

The method was performed at the University of Stavanger using a Zeiss AXIO polarized microscope and it provided first data on the

texture and petrography of 40 reservoir and 19 non-reservoir thin sections of offshore chalk from the North Sea (**Paper I**).

3.2 Scanning electron microscopy

Scanning electron microscopy (SEM) is a widely used method for high-resolution images of surface topography with application for mineral identification, textural and morphological analyses. The method was applied on both fresh surface fragments and thin sections of reservoir cores and it was used for characterization of North Sea reservoir chalk (**Paper I**) and identification of mineral alterations as a result of flooding reactive brines through reservoir chalk (**Paper II**).

The method requires high-quality samples with an electronically conductive surface that ensures a steady flux of electrons across the sample surface and counteracts build-up of electrical charge during the radiation. Since chalk is non-conductive, the samples were sputter-coated with a conductive layer of carbon or palladium.

Because the reservoir cores were assumed to be wet sedimentary rocks, the unwashed reservoir chalk inner fragments were examined with cryo-SEM, a non-routine procedure that prevents vaporization of the hydrocarbons in the pores during electron scanning and consequently the contamination of the SEM column, with the use of liquid nitrogen.

The measurements took place at the University of Stavanger using a Zeiss Supra 35VP Field emission gun scanning electron microscope (FEG-SEM) equipped with cryogenic unit (Polar Prep 2000T), backscattered electron detector (BSED) and energy dispersive spectroscopy (EDS). Additionally, a SEM and BSED study of polished thin sections took place at the Technical University of Freiberg.

3.3 X-ray powder diffraction

X-ray diffraction (XRD) is – after sample preparation – a non-destructive method that bases its premise on the unique pattern that each mineral diffracts X-rays. XRD method was used for mineral identification and relative quantification of reservoir chalk (**Paper I**) and it was performed on randomly oriented powder.

The measurements took place at Instituto Jaime Almera - C.S.I.C.Barcelona (Bruker D5005 diffractometer, Cu Kα x-ray radiation at 40 mA and 40 kV intensity, 0.1 mm receiving slit size, between 3 – 65° 2Θ in increments of 0.02° 2Θ, 6 seconds per increment) and at University of Stavanger (Bruker D8 ADVANCE ECO diffractometer with a Lynxeye detector, Cu Kα x-ray radiation at 40 kV and 25 mA intensity, 0.6 mm receiving slit, 4 – 70° 2Θ in increments of 0.01°, 0.2 seconds per increment).

Mineral identification was performed on DIFFRAC.EVA software for semi-quantitative relative mineral proportions of whole rock patterns while for the siliciclastic fraction quantitative mineral proportions were obtained by Rietveld refinement with TOPAS5®.

3.4 Carbon and oxygen stable isotopes

Analysing the oxygen and carbon stable isotopes in carbonates was used to gain insight into the depositional environment of the chalk, paleo-climate and diagenetic overprint (**Paper I**). The method is based on the partitioning of isotopes in an element caused by ambient influences (temperature, biological and chemical processes, etc), leading to the enrichment of an isotope relative to another. The stable isotope ratios are calculated in terms of their deviation from the corresponding ratios of Vienna Pee Dee Belemnite (V-PBD) standard and are reported in units per mil notation (‰).

The measurement took place at the Wolfson Laboratory, School of Geosciences Grant Institute, Edinburgh University. The samples were collected from fresh surfaces of offshore (reservoir and non-reservoir) chalk. The carbonate powder was reacted with 100 % orthophosphoric acid at 90° C in an ISOCARB automatic carbonate preparation system and the resulting carbon dioxide was analyzed in a VG Isoglas PRISM III stable isotope mass spectrometer.

3.5 Geochemistry

Inductive Coupled Plasma Mass Spectrometry (ICP-MS) was used to quantify the concentrations of oxides and elements in fused samples and gain further insight in the offshore chalk depositional environment and diagenetic overprint (**Paper I**). Loss on ignition (LOI) was measured after igniting the samples at 1000° C for one hour and the total carbon and sulphur were obtained by the LECO® method.

The measurements were performed at Bureau Veritas Minerals laboratories (Canada) on offshore chalk, representing bulk samples both reservoir and non-reservoir successions as well as insoluble residue from 5 reservoir cores.

3.6 Triaxial cell tests

3.6.1 Equipment

The geomechanical tests of chalk cores involved in triaxial cells equipped with an outer heating jacket and a regulating system (Omron E5CN) with precise Proportional Integral Derivative (PID) temperature control. The system includes two Quizix QX-2000HC pumps that control the axial and confining pressures independently, and a fluid injection pump (Gilson 307HPLC) as well as a backpressure regulator that controls the pore pressure.

The cores were saturated with distilled water or brine prior to cell mounting; they were isolated from the oil bath in the confining chamber by a fluorinated ethylene propylene heat shrinkage sleeve (0.5 mm wall thickness). An extensometer surrounded the core at mid length and measured the changes in diameter throughout the test (radial strain). Changes in the cores' length (axial strain) were monitored by an external axial linear variable displacement transducer (LVDT) placed on top of the cell piston (Figure 1).

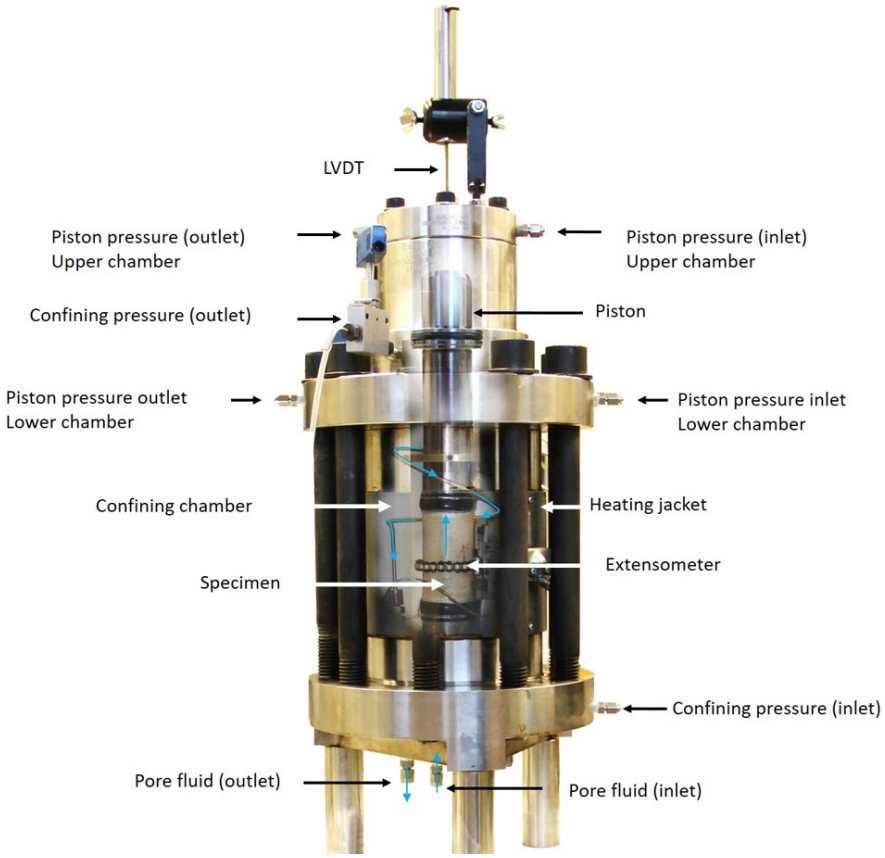

Figure 1: Fully mounted triaxial cell; overlay images of the specimen, extensometer in the confining chamber and the piston in the piston chamber are internal parts. Blue arrows indicate fluid flow direction.

3.6.2 Test procedures

After the cell mounting was complete, the cores were flooded with at least 3 pore volumes (PVs) of brine before the test start. During this time, the pore pressure and confining pressure were increased simultaneously to 0.7 MPa and 1.2 MPa, respectively, at ambient temperature. Further, before the tests begun, the temperature was increased to the desired value and the cell piston was lowered to contact with the core. The test measurements started only when the system was in equilibrium (the cell temperature has stabilized at the right value, the differential pressure was stable, and axial and radial strain rates were close to zero).

Thereafter, the test conditions were adjusted according to the study purpose, varying the type of stress (hydrostatic, deviatoric), the number of stress cycles (loading, creep, unloading), the injecting brine and test temperature. The procedures are briefly described below, and a summary is presented in Table 3 on page 23.

Paper II – Validation study of water weakening research from outcrop chalks performed on Eldfisk reservoir cores

The test setup described in **Paper II** was used to investigate how oil-bearing reservoir chalk cores from active fields in the North Sea respond to similar test conditions as those used in previous tests on water-saturated outcrop chalk such as Madland et al., 2011 and Megawati et al., 2011, in an effort to verify the relevance of outcrop chalk research to the North Sea chalk context.

The cores were loaded hydrostatically to 50 MPa, while flooded with NaCl. Then they were allowed to deform (creep) under constant stress (50 MPa) over several weeks, during which time the injecting brine was changed from NaCl to SSW in the first series, and from NaCl to $MgCl_2$ and subsequently to $MgCl_2$+$CaCl_2$ in the second series. This was done to highlight the effect of reactive brines on the compaction rate of

chalk and to verify whether excess calcium in $MgCl_2$ brine would reduce the compaction rate.

After the measurements, the cores were flooded with distilled water to avoid salt precipitation. Additionally, one of the reservoir cores was washed with methanol and toluene to eliminate salts and hydrocarbon residue in preparation for further analyses.

Paper III: Permeability evolution of shear failing chalk cores under thermochemical influence

The test setup used in **Paper III** focuses on the permeability evolution of fractured outcrop cores under repetitive cycles of deviatoric stress conditions and various thermochemical conditions, relevant to the chalk fields on the Norwegian Continental Shelf.

The cores were loaded deviatorically (the principal stresses are not equal). The confining stress was kept constant at 1.2 MPa, while the axial stress increased steadily from 0.5 MPa above yield, and until shear failure (fracture occurrence). Immediately after, the axial stress was set to constant at a value slightly below the failure point, allowing the cores to creep for 3 days. The axial stress was then lowered to the starting point at the same rate as the loading.

This stress sequence (deviatoric loading, creep, unloading) was repeated twice, after the system had reached equilibrium. In the second and third cycles, the creep phases were shorter (1 day).

Each test series involved one injecting brine throughout the test and the experiments were repeated at different temperatures (Table 3) to highlight the thermo-chemical aspect of rock-fluid interactions. After the third cycle, the cores were washed with distilled water (4 PVs).

Paper IV: Modelling of Permeability and Strain Evolution in Chemical Creep Compaction Experiments with Fractured and Unfractured Chalk Cores Conducted at Reservoir Conditions

A third test setup provided calibration input for modelling of permeability evolution during chemical compaction of fractured outcrop chalk and it is described in **Paper IV**. The pre-fractured cores were flooded under constant, low hydrostatic stress conditions (1.2 MPa) to minimize the role of mechanical compaction and rather emphasize the brine chemistry effect on the permeability of a fracture-matrix system. The tests were performed on chalks with different degrees of purity in terms of the ratio of carbonate/non-carbonate phases and flooded with inert and reactive brines (Table 3).

Table 3: Overview of test parameters used in triaxial cell tests

Paper	Chalk	Stress	Stress cycles	Flooding fluids	Temperature
II	Eldfisk	Hydrostatic	1	NaCl, SSW	130° C
	Eldfisk	Hydrostatic	1	NaCl, $MgCl_2$, $MgCl_2$+$CaCl_2$	130° C
III	Kansas	Deviatoric	3	NaCl	50° C
					130° C
	Kansas	Deviatoric	3	Na_2SO_4	50° C
					130° C
	Kansas	Deviatoric	3	SSW	50° C
					130° C
IV	Kansas	Hydrostatic	1	NaCl	130° C
	Kansas	Hydrostatic	1	$MgCl_2$	130° C
	Mons	Hydrostatic	1	NaCl	130° C
	Mons	Hydrostatic	1	$MgCl_2$	130° C

3.7 Ion Chromatography

The effluent brines from the mechanical experiments on reservoir chalk (**Paper II**) were sampled at regular intervals, 4 samples per day during

the first 9-12 PVs of each brine, thereafter once per day. The Na^+, Cl^-, Mg^{2+}, Ca^{2+} and SO_4^{2-} concentrations in the injected and produced brines were measured with a Dionex Ion Chromatography System (ICS)-5000$^+$. IonPac AS16 and IonPac CS12A were used as anion and cation exchange columns, respectively. Prior to the analyses, the were diluted 500 times with DW in a Gilson GX-271 dilution machine.

Comparing the effluent composition to the original injecting brine composition provided an insight in the chemical interactions between the chalk and the different brines during the test.

3.8 Permeability simulations

Numerical modelling performed in a commercial software (Matlab) was used to build on a previous model developed by Andersen and Berawala (2019), which focused on the mechanical and chemical creep compaction of Belgian (Liège) and Danish (Aalborg) outcrop chalks. In this study, the model was extended to match the permeability evolution during chemical compaction in the Liège and Aalborg chalks, and to also include a fracture-matrix geometry (data input from Kansas and Mons chalk), representative for flow in a naturally fractured reservoir, such as Ekofisk or Valhall.

The model was based on several simplifying assumptions:

- the matrix and the fracture were considered as two non-communicating domains, each with its specific fluid flow properties
- fracture width remains constant throughout the simulations, compaction occurs only in the matrix
- surface reactions and dispersion are overlooked in favor of advection-reaction mechanisms
- chemical reaction rates are equal in both matrix and fracture domains

Permeability calibration, according to the model assumptions, distinguished between matrix and fracture permeability (K^m and K^f respectively), by considering the porosity component only in the matrix domain, while the chemical alteration was a permeability-influencing factor in both domains. The matrix permeability was described by (6)

$$K^m = K^{m0} F_\phi(\phi^m) F_\rho^m(\rho_m^m) \quad (6)$$

where K^{m0} is the initial matrix permeability, F_ϕ is permeability reduction factor due to porosity change, ϕ^m is matrix porosity, F_ρ^m is the permeability reduction factor due to mineralogical change and ρ_m^m is the concentration of magnesite in the matrix.

The fracture permeability was expressed as

$$K^f = K^{f0} F_\rho^f\left(\rho_m^f\right) \quad (7)$$

where K^{f0} is the initial fracture permeability, F_ρ^f is permeability reduction factor in the fracture due to mineralogical changes, and ρ_m^f is magnesite concentration in the fracture.

Table 4 summarizes the large array of analytical, geomechanical and theoretical methods used in this project and the key insight they provide.

Table 4: Overview of methods used in this project

Method	Test chalk	Sample type	Purpose	Paper
Optical petrography	Offshore	Thin sections	First data of sample petrography	I
Scanning Electron Microscopy	Offshore	Thin sections, chalk fragments	Imaging, mineral identification and characterization	I, II
X-ray Diffraction	Offshore	Powder from bulk rock and insoluble residue	Mineral identification and relative quantification	I
C-O isotope geochemistry	Offshore	Powder from bulk rock	Examine indications of depositional environment and diagenesis	I
Geochemistry	Offshore	Powder from bulk rock and insoluble residue	Major, minor and trace element quantification	I
Ion Chromatography	Offshore	Brine effluent	Trace changes in ionic composition of injecting brines during testing	II
Triaxial cell tests	Offshore	Intact cores, non-fractured	Monitor the response of reservoir chalk to stress and thermochemical influence	II
	Onshore	Intact cores, fractured during test	Monitor permeability evolution during repeated stress cycles under various thermochemical conditions	III
	Onshore	Pre-fractured cores	Monitor brine chemistry effect on permeability of fractured chalk	IV
Numerical modeling (Matlab)	Onshore	Assumed fractured cores	Predict permeability of fractured cores under reservoir conditions	IV

4 Main results and discussion

4.1 Petrological, mineralogical, geochemical characteristics of North Sea chalk

A comprehensive look into the petrology, mineralogy and geochemistry of the North Sea chalk (**Paper I**) highlighted the particularities of this type of chalk and the complex sample set allowed identifying reservoir chalk's potential geochemical response to hydrocarbons and EOR fluids.

4.1.1 Depositional environment

The sediment composition of the North Sea chalk is consistent with a deep marine depositional environment typical for Upper Cretaceous chalks, comprising micritic carbonate matrix, nano- to macrofossils (mostly calcareous, but also siliceous and phosphatic) and diverse authigenic and detrital non-carbonate minerals. SEM micrographs (Figure 2) reveal a matrix composed of 1-2 μm size calcite crystals from broken, disaggregated coccoliths, but also intact coccolith platelets and coccospheres. There is an abundance of single- and multichambered foraminifera Figure 2d) and although many may have retained their globular shape, some are deformed, broken, or filled with new calcite crystals (Figure 2b), or coccolith debris (Figure 2c).

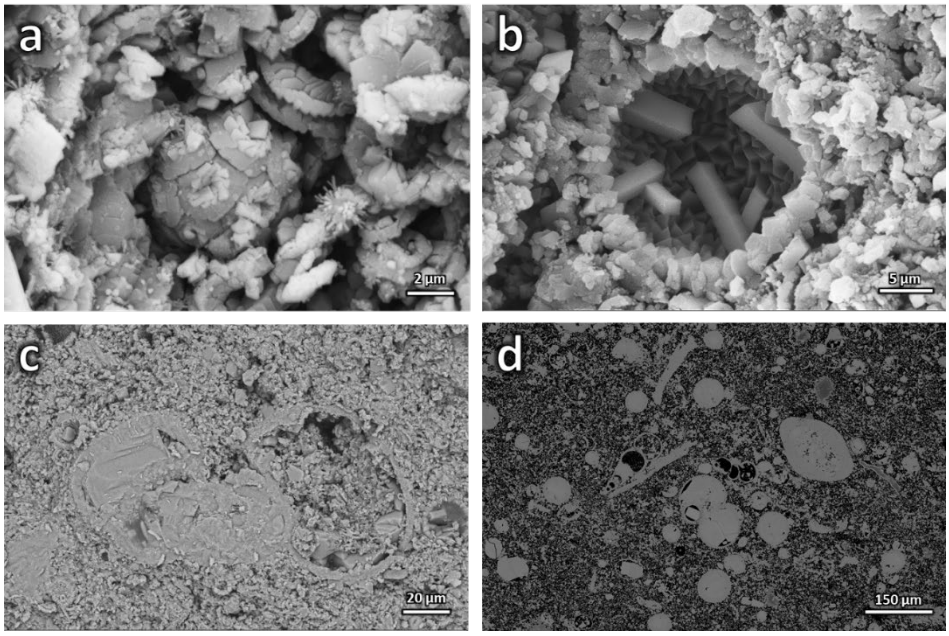

Figure 2: Cryo-SEM micrographs of waterflooded and unflooded reservoir core plug from well 3 (a-c); a – preserved cocosphere,, cocolith platelets and broken coccolith fragments as the main constituents of the chalk matrix (unflooded sample); b - new calcite crystals precipitated inside cavity of well-preserved foraminifer test (unflooded sample); c – foraminifer chambers entirely filled with calcite or cocolith debris (waterflooded sample); d – BSE micrograph of thin section representing large variety of faunal content in matrix (well 1, waterflooded sample)

The typical marine petrographic features expressed by the faunal content are alike in all North Sea samples, describing reservoir and non-reservoir chalk, as well as flooded or unflooded reservoir chalk. However, the geochemical analyses indicate that the carbonate precipitation in both reservoir and non-reservoir chalk was influenced by a secondary fluid flow. This is seen in the Rare Earth Element (REE) and Yttrium concentrations, where the depletion pattern relative to shale standard (PAAS) follows the typical open marine seawater signature (enrichment in lanthanum (La), depletion of cerium (Ce) and a positive Y anomaly), but less than what is expected for (pure) chalk deposits.

The positive covariation between carbon and oxygen isotope ratios (Figure 3) confirm this observation and together with the narrow $\delta^{13}C$ variability compared to the $\delta^{18}O$, points towards a marine-meteoric mixing zone (Allan and Matthews, 1982).

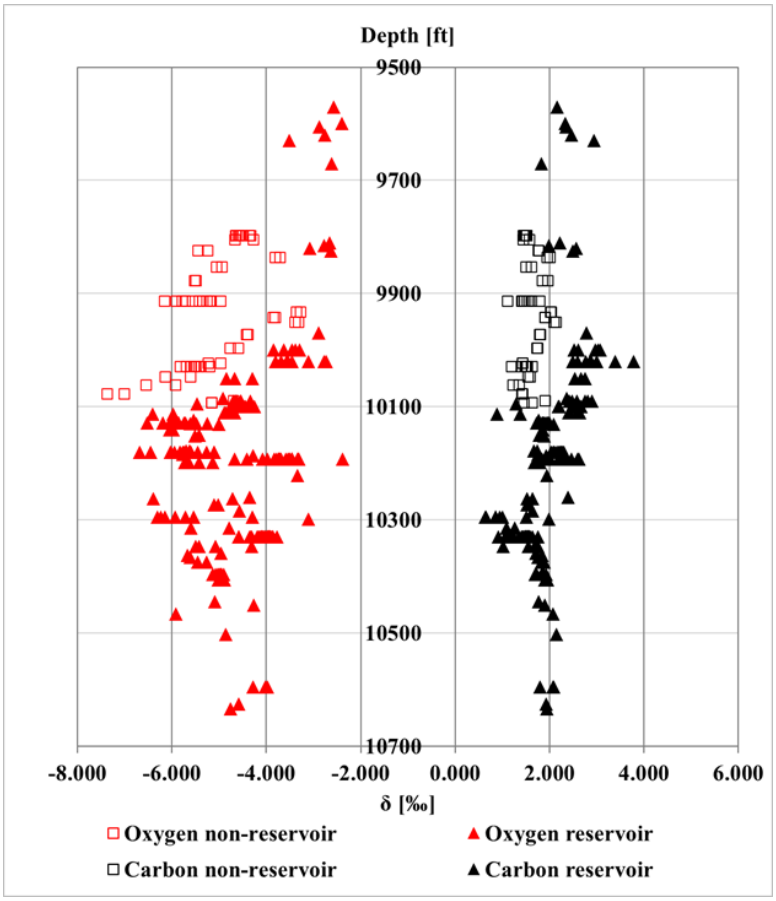

Figure 3: Oxygen (red markers) and carbon (black markers) stable isotope curves of reservoir (full triangles) and non-reservoir (empty squares) rock samples from shallower (top) to deeper layers (bottom)

The hydrothermal influence is supported by the SEM investigation of the reservoir chalk. Although the origin of this fluid-flow and the timing of its circulation was outside of the scope of this study, its presence is underlined by occurrence of minerals typically related to such an

environment (Laudise et al., 1965; Simmons and Browne, 2000; Scott et al., 2009), e.g., framboidal pyrite, albite, sphalerite, etc. (Figure 4).

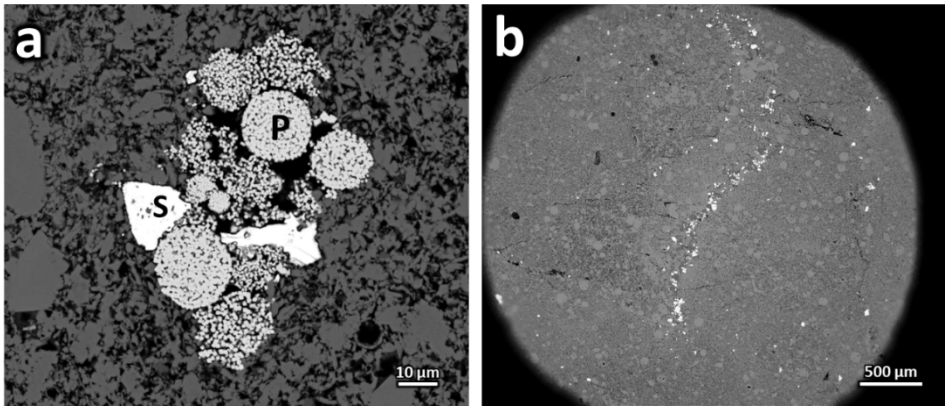

Figure 4: BSE micrographs of a – framboidal pyrite (P) and (S) sphalerite (unflooded sample, well 4); b – bright pyrite along stylolites (cold waterflooded sample, well 1)

4.1.2 Clastic input and its role in permeability evolution

The non-carbonate content is particularly relevant in the context of hydrocarbon production, as studies show that impure chalk (non-carbonate – mainly quartz and clay – content above 5 %) are mechanically stronger, but more readily affected by reactive brines than pure chalk (Risnes and Flaageng, 1999; Madland et al., 2011).

The type of clastic input has an obvious effect on permeability evolution in chalk. The model described in **Paper IV** matched permeability data from experiments on Aalborg and Liège chalk flooded with $MgCl_2$ at 130° C during creep; it is estimated that the permeability reduction factor due to compaction (F_ϕ) and mineral alteration (F_ρ) can be several orders of magnitude higher in Aalborg chalk than Liège chalk (Figure 5). This can be attributed to the presence of presence of opal-CT – an amorphous form of silica – in Aalborg chalk, making it more susceptible to mineral alterations (Minde et al., 2018).

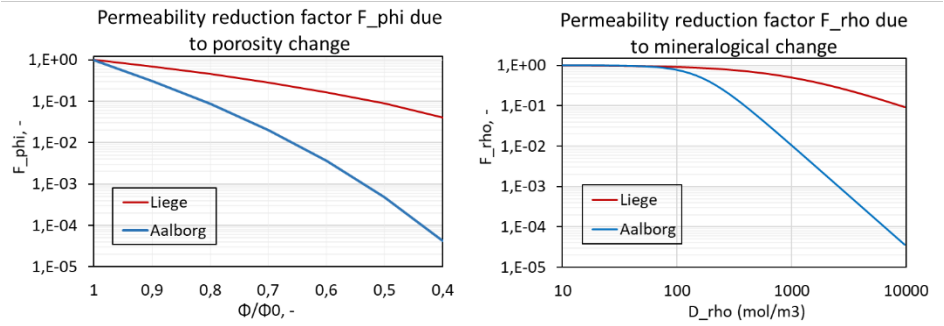

Figure 5: Permeability correlation functions due to porosity change ($\boldsymbol{F_\phi}$, left) and due to mineralogical change ($\boldsymbol{F_\rho}$, right) for outcrop chalk from Liège and Aalborg as obtained from matching experimental data. Permeability reduction factor is strongly dependent on chalk mineral composition when flooded with reactive brines.

All North Sea chalk samples contain non-carbonate phases, confirmed by XRD, SEM and whole-rock geochemical analyses. Quartz represents the fraction of non-carbonate phases, but not as opal CT. Phyllosilicates are present in minor abundance relative to quartz, and include mostly smectitic minerals, illite, (Figure 6), kaolinite, chlorite.

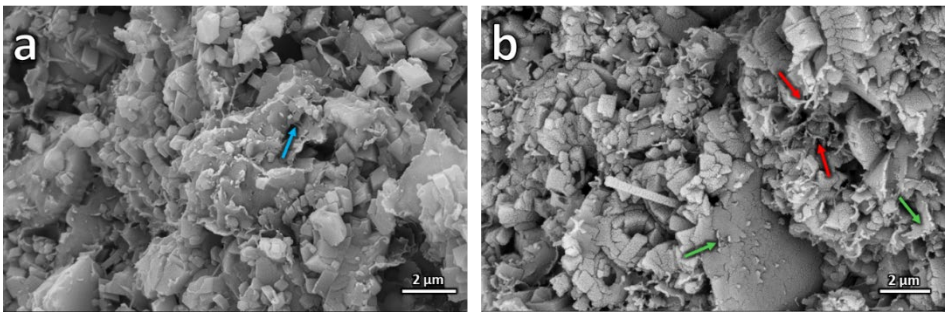

Figure 6: Cryo-SEM micrographs of unflooded reservoir core plug from well 3: a – inhomogeneous unflooded sample with bridge of acicular illite joining flakes (blue arrow); b – authigenic acicular illite (red arrows) and smectitic clays (green arrows)

An important aspect for hydrocarbon production, besides the qualitative evaluation of clastic input is the quantitative aspect. Due to the unavailable non-reservoir testing material, the XRD analyses focused only on the reservoir chalk. The results, together with geochemistry results indicate that chalks in the reservoir wells differ strongly regarding the proportion of clastic contamination, with some wells only represented by mineralogically impure chalk within the Ekofisk Formation. Major element geochemistry shows a large variation in the silica (SiO_2) content with values ranging from 0.3 % up to 20 %, which lead to characterize several layers as marls. The introduction of clastic material seems to start mostly at the bottom of the Ekofisk Formation, but rarely already during deposition of the older Tor Formation (Tables 3, 4 in **Paper I**). This variation is of utmost importance when modelling or estimating rock-fluid interactions in possible reservoirs (see also section 4.1.4) and should be considered in comparison to onshore chalk composition and flooding results (Andersen et al., 2018).

4.1.3 Diagenetic overprint

If carbon isotope ratios are often indicators of depositional environment, oxygen isotopes may be used additionally as indicators of diagenetic overprint, as carbon isotopes are too robust to be affected (Clayton and Degens, 1959; Shields and Veizer, 2002). The oxygen isotope ratios in the North Sea chalk, in both reservoir and non-reservoir samples, show clear deviation from the secular Upper Cretaceous composition (i.e, 0 to -1.5 ‰, Gradstein et al., 2012) averaging at -4.6 ‰ in the non-reservoir chalk and -5.0 ‰ in the reservoir chalk. Previous studies showed that oxygen isotopes in carbonates are influenced by burial diagenesis, becoming increasingly negative with depth (Hudson, 1977; Scholle, 1977; Allan and Matthews, 1982), a trend seen here as well (Figure 3). However, generally, the oxygen isotope ratios are not sufficiently

negative (i.e., all ratios are above -10 ‰) to define an unequivocal diagenetic overprint.

The occurrence of dolomite is linked to either a substantial fluid flow, or a slowly developing diagenesis. Secondary dolomite crystals were detected in all thin sections from the Ekofisk area, mostly in pores and along fractures, but not in the northern, non-reservoir wells (Figure 7). The presence of dolomite is of importance in the context of smart water injection for EOR processes, as studies show that dolomite is less reactive to EOR fluids such as seawater than calcite (Shariatpanahi et al., 2016).

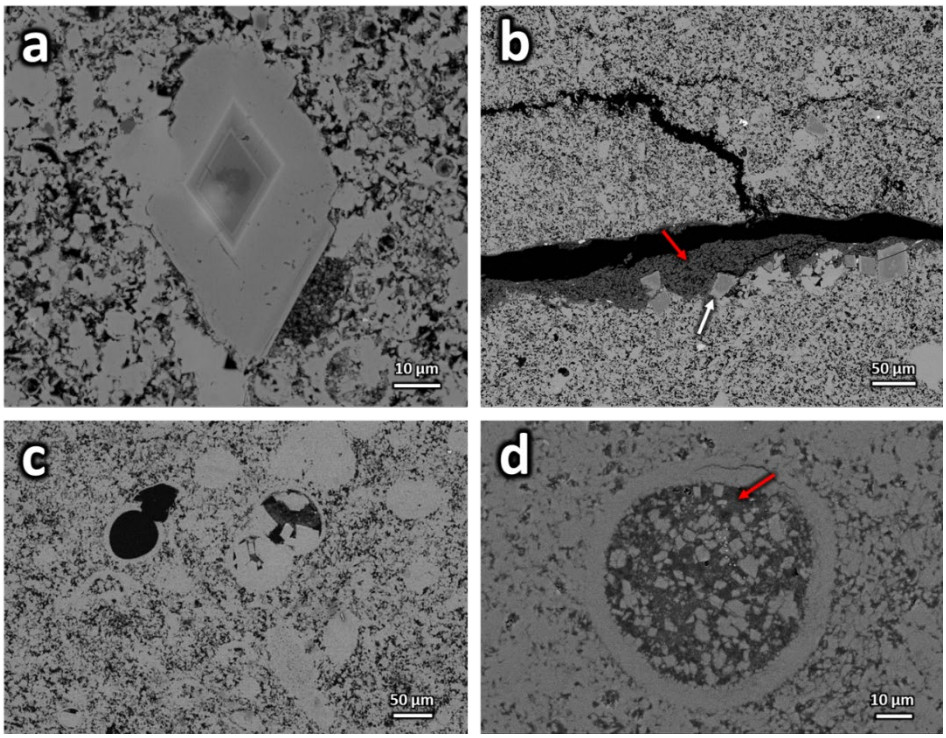

Figure 7: BSE micrographs of a – secondary dolomite crystal with light ankerite rim (unflooded sample, well 3); b – kaolinite (red arrow) and in-situ dolomite crystals (white arrow) along fracture walls(unflooded sample, well4); c – foraminifers from empty to fully cemented with calcite in coccolith matrix (non-reservoir sample, well 8); d – foraminifer filled with aluminosilicate phase (red arrow, non-reservoir sample from well 9). See Paper I for well reference.

Reservoir and non-reservoir chalk share similar post-depositional features, in terms of geochemical composition, texture, mineral assemblage, and relative mineral proportions. Common for both lithotypes is a reworked material consisting of brecciated calcite fragments, quartz, kaolinite in pore spaces, or along fracture walls, sometimes entirely filling fracture apertures (Figure 7b and d, red arrow). However, while this material often contains dolomite in the reservoir samples (Figure 7b, white arrow) it is not associated with dolomite in any of the investigated non-reservoir samples, although it is Mg-rich.

4.1.4 Effect of hydrocarbons and EOR fluids on North Sea reservoir chalk

The isotope ratios from both reservoir and non-reservoir samples deviate from the typical paleo-seawater isotopic composition still preserved in a number of Late Cretaceous samples of onshore chalk from Aalborg, Stevns Klint, Liège and Mons Basin (Andersen et al., 2018, Figure 8, black diamonds). Therefore, it is unlikely that the presence of hydrocarbons is responsible for the negative $\delta^{18}O$.

However, the cross-plot in Figure 8 shows often higher oxygen and carbons isotope ratios in reservoir (green markers) compared to non-reservoir samples (blue markers), which might be related to the presence of hydrocarbons. It may be that the processes that stabilized the chalk (early hydrocarbon entry, overpressuring, Nygaard et al., 1983; Brasher and Vagle, 1996) and were responsible for the early change of the REE concentrations, also retarded further change in the O isotope ratios during early, very low-grade diagenesis.

Further, the similarity between REE values of unflooded and flooded high porosity reservoir chalk excludes that artificial flooding events are decisive for the observed negative oxygen ratio shift, which is therefore interpreted as natural, rather than anthropogenic.

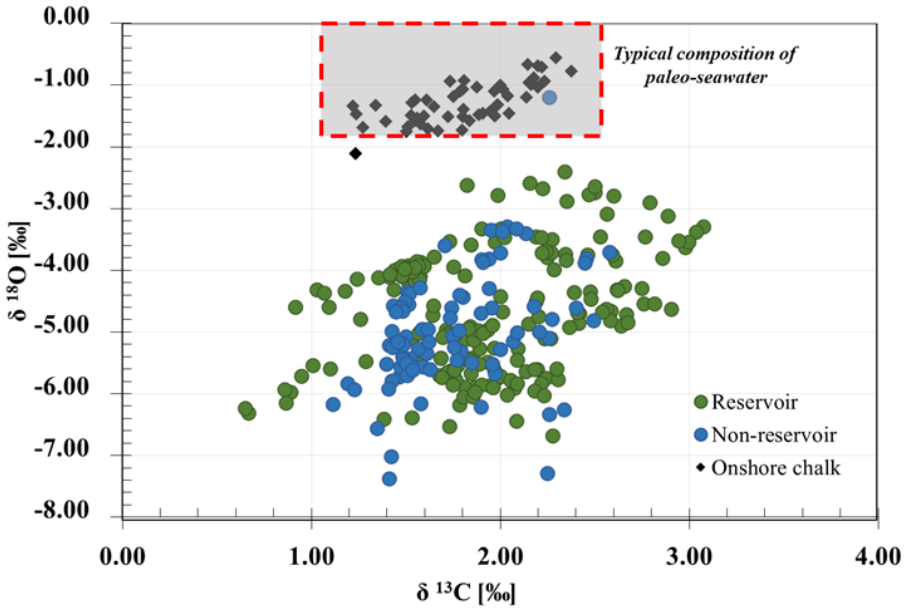

Figure 8: Cross-plot of carbon and oxygen isotopic composition of offshore and onshore chalk from Danish outcrop locations (Andersen et al., 2018); the dashed red frame marks the expected plot area for undisturbed Cretaceous carbon and oxygen stable isotopes (after Gradstein et al., 2012).

Yet, field observations and laboratory studies confirm that NCS chalk is prone to mineralogical and textural changes when in contact with reactive EOR brines, and the effects of rock-fluid interactions are enhanced with higher injecting brine temperature (Sylte et al, 1999; Austad et al., 2008; Madland et al. 2011; Megawati et al. 2015). The main mineralogical alterations are explained in terms of calcite dissolution and precipitation of new minerals such as magnesite, or anhydrite (Madland et al. 2011; Minde et al., 2018) and mineral alteration is most obvious close to the injection inlet (Minde et al., 2018). Mineral precipitation is seen in flooding experiments of Eldfisk reservoir chalk (**Paper II,** see also section 3). Simulations of reactive fluid flow through fractured cores described in **Paper IV** also predict that the main rock-fluid interactions take place at the inlet where the core also experiences more compaction and permeability reduction.

The effects of waterflooding are possibly seen in the reservoir samples, as XRD results show waterflooded cores which contained less calcite than the unflooded cores. However, this correlation is not evident in all wells, and SEM analyses show that the mineral assemblage is similar in all reservoir wells and that the mineral and textural differences (e.g., presence of dolomite, pore morphology) are rather depositional, independent of flooding status. Geochemistry results confirm this observation. Still, this does not necessarily rule out the effect of EOR fluids on chalk mineralogy, and the newly precipitated minerals might be more clearly seen closer to the brine injectors.

4.2 Permeability evolution in fractured onshore chalk

The main premise of the geomechanical study reported in **Paper III** was to replicate the production-related dynamics of a chalk reservoir, by considering shear fractured outcrop chalk cores exposed to cyclic deviatoric stress states while systematically changing either the test temperature, or the injected brine.

Deviatoric loading beyond yield (when the strain rate accelerates relative to the loading rate) together with low confining pressure caused shear fracturing at a steep angle (over 70°), close to flooding direction (Figure 9, left). This corresponded with a simultaneous permeability rise (Figure 9, right) and it was the only event that changed permeability decisively, as the shear fracture provided an instantaneous "highway" for brine flow.

The permeability model (**Paper IV**) confirmed this phenomenon, showing that the fluid flow is to great extent diverted from the matrix into the fracture. Further, sensitivity analyses on the impact of fracture showed that although generally the permeability decreased with time, the decreasing rate did not change with fracture width, as long as the

residence time of the reactive fluid in the fracture is short enough (see section 4.4).

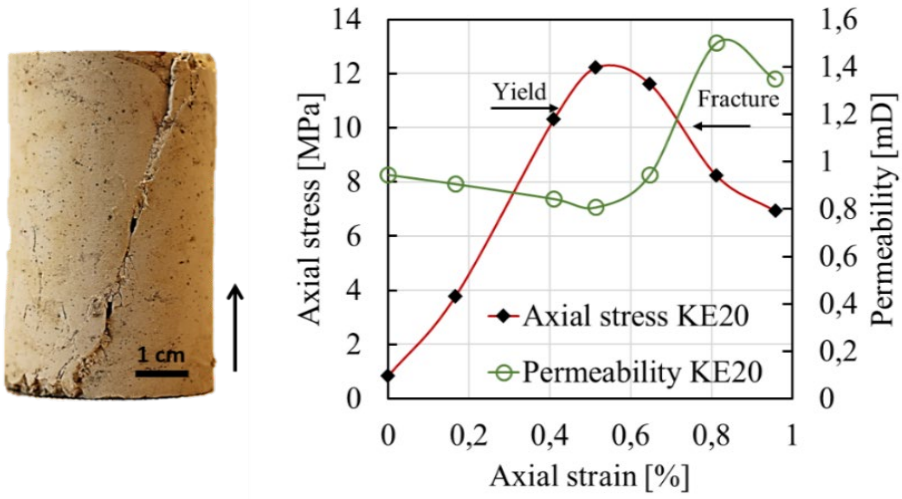

Figure 9: Left: High-angle shear fracture, typical for deviatoric loading at low confining pressure. The arrow indicates the flooding direction. Right: Typical example of axial stress-strain relationship (red curve) and permeability evolution (green curve) during first deviatoric loading above yield, here data from KE20 experiment (NaCl series, 50° C). Permeability generally decreases during deviatoric loading; the shear fracture event causes a concomitant drop in axial stress and increase in permeability.

4.2.1 Impact of deviatoric stress cycles on chalk permeability

Successive deviatoric loadings had little effect on permeability in all tests, regardless of injecting brine and test temperature. The cycles naturally weaken the cores, each loading-unloading adding more fatigue and deformation to the rock and alter its elastic properties. Figure 10 shows that the cores yielded at lower axial stress during the second and third loadings. At the same time, the core stiffness increased, as pointed out by the red arrow in Figure 10, and the cores deform axially approximately 50-60 % less during the second and third loading compared to the first cycle, although the loading rate is the same.

The diminutive consequence of cyclic deviatoric loading on permeability is in agreement with Ekofisk field observations, where even though matrix permeability declined with matrix compaction, the effect was of no apparent consequence to the effective permeability (Sulak, 1991).

During creep, permeability declined slightly or remained unchanged, but generally the deviatoric creep conditions did not override the permeability gain related to fracturing (Figure 11). Teufel (1991) pointed out that the deviatoric nature of the reservoir stress state seems to control the permeability of fractures, such that steeply dipping fractures aligned with the maximum horizontal stress, as seen at Ekofisk, will suffer least permeability loss. The results in this study confirm this behaviour. In contrast, under hydrostatic conditions, permeability declines steadily with increasing hydrostatic stress (Suri et al., 1997; Yale and Crawford, 1998; Korsnes et al., 2006; Fernø et al., 2010; Minde et al., 2018).

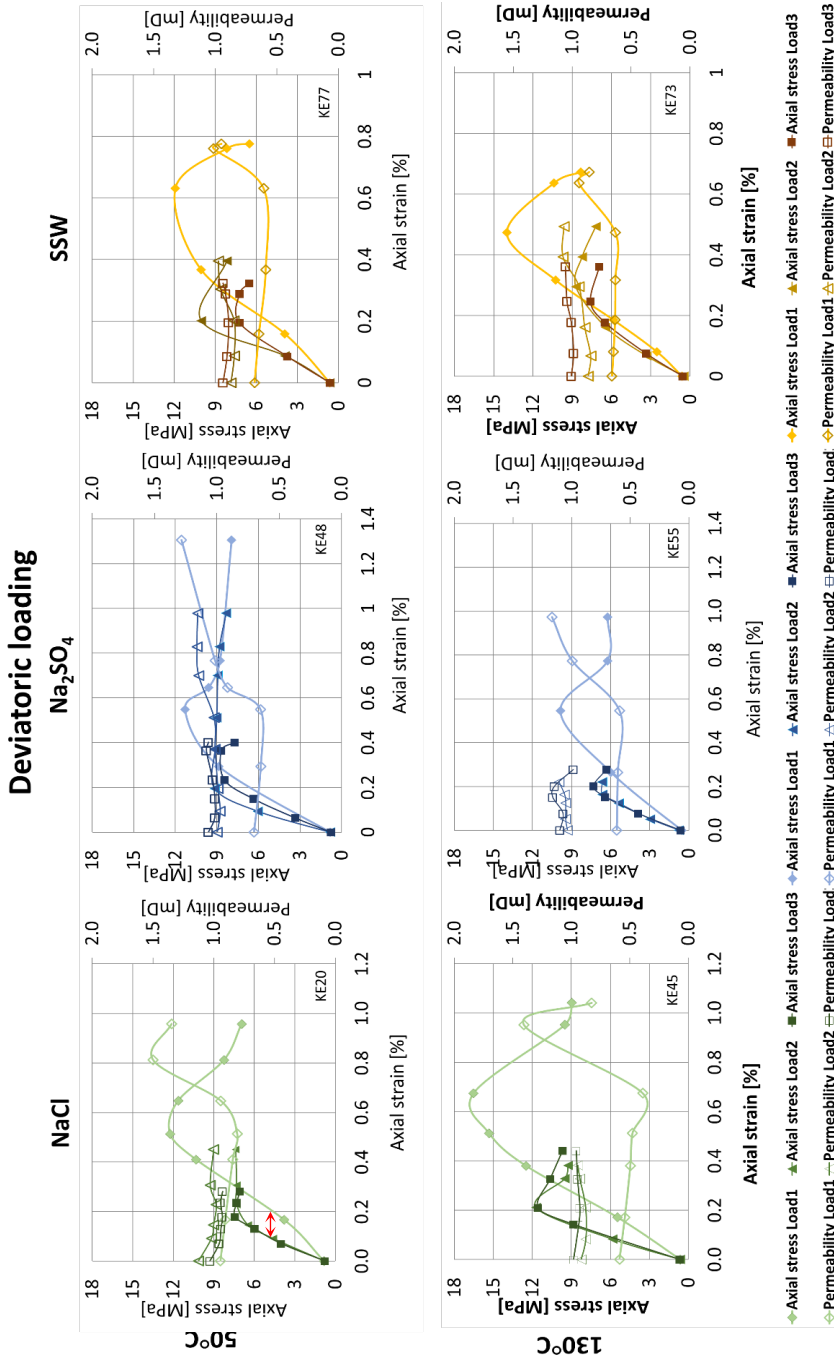

Figure 10: Permeability response to three cycles of deviatoric loading at 50° C (top row) and 130° C (bottom row) and NaCl (green), Na_2SO_4 (blue) and SSW (yellow) brines; the graphs represent one selected test from each series. Second and third cycles are shorter and are represented with darker colors. Permeability changes decisively only as a response to first fracturing. Subsequent stress cycles affect the mechanical strength of the cores, (red arrow) but not the core permeability in all test series.

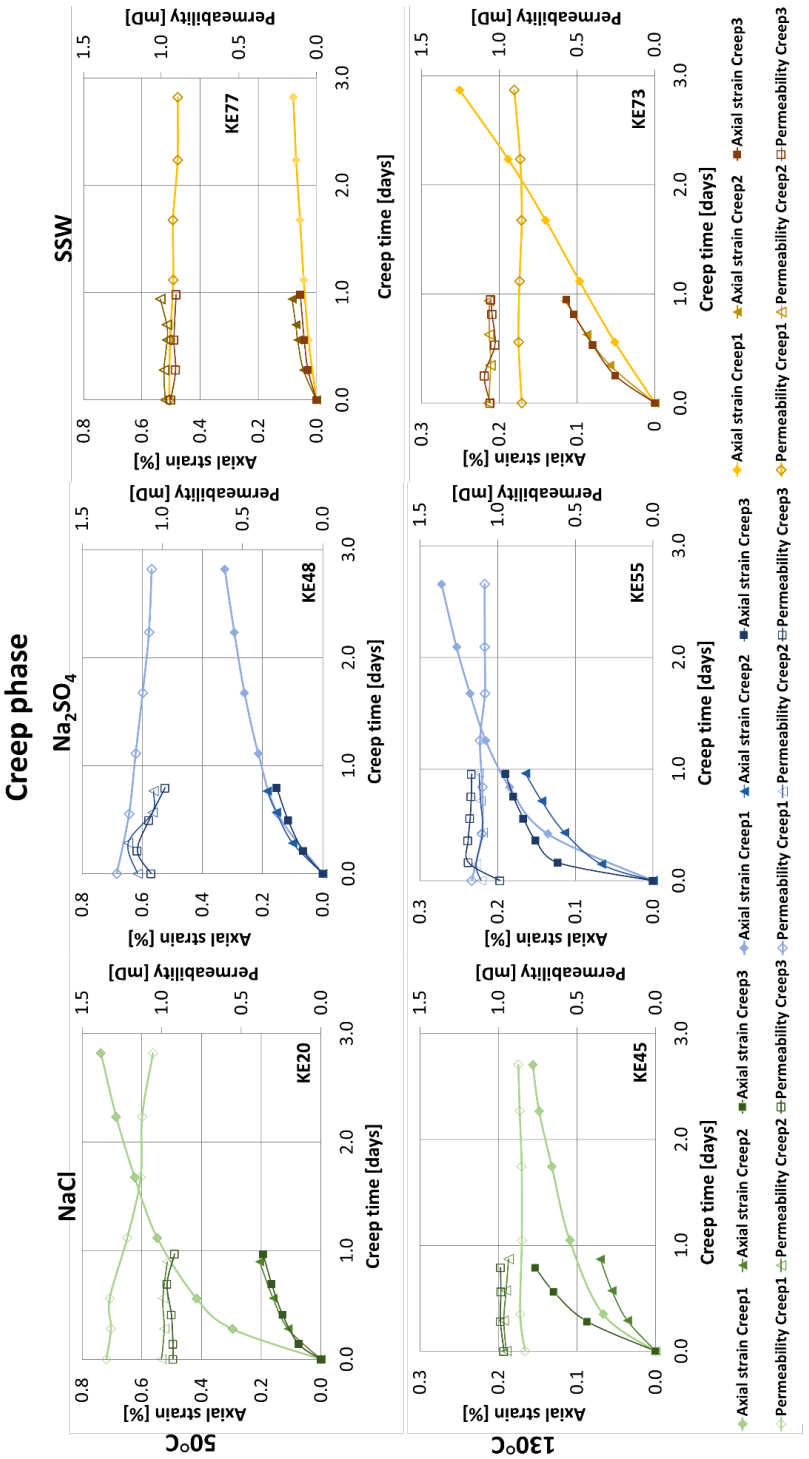

Figure 11: Permeability response to three cycles of creep at 50° C (top row) and 130° C (bottom row) and three brines with the same test selection as in Figure 10. Graphs follow the same color code as Figure 10. Permeability suffers either a slight decline or remains unchanged during deformation under constant stress over time.

4.2.2 Role of brine chemistry and temperature in permeability evolution

Figure 12 shows the permeability evolution throughout the tests at 50° C (top) and 130° C (bottom) while flooding NaCl (green lines), Na_2SO_4 (blue lines) and SSW (yellow lines). The first data point is the beginning of the first deviatoric cycle, and each line segment represents the permeability behaviour during consecutive stress states, including unloading.

The Na_2SO_4 test series stand out with the highest final permeability at both temperatures. This is likely a result of sulfate adsorption on the calcite grain surface as suggested by Megawati et al., 2013, creating enough disjoining force at granular contact to preserve permeability. In addition, calcite equilibration during brine preparation may have prevented calcium displacement and consequently anhydrite ($CaSO_4$) precipitation.

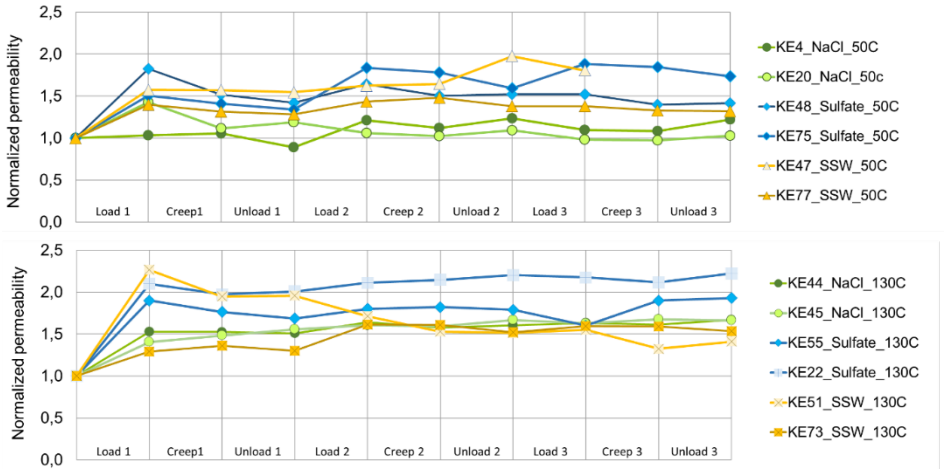

Figure 12: Overview of permeability evolution in all tested cores at 50° C (top chart) and 130° C (bottom chart). Permeability is normalized to the initial core permeability at the start of the first

If flooding Na_2SO_4 through fractured chalk seems to sustain the permeability gain related to shear fracturing, flooding reactive brine such as SSW at high temperature has an opposite effect on permeability

evolution. SSW test series registered most permeability loss at 130° C, most likely due to chemical alteration, possibly precipitation of anhydrite.

Another notable aspect from Figure 12 is that the degree of permeability rise related to fracturing (load 1) correlates with test temperature: overall, permeability increased 70 % in average the beginning of the tests at high temperature and only 40 % average at low temperature. There was also higher variation in permeability rise among high temperature tests, compared to low temperature tests, where four out of six tests had almost identical permeability increase. Additionally, end permeability at 130° C increased in average by a factor of 1.7, while at 50° C the average increasing factor was 1.3 (see detailed values in **Paper III**).

4.2.3 Combined effect of stress, brine, and temperature on permeability evolution

The results of geomechanical testing of chalk exposed to repetitive deviatoric cycles and various thermo-chemical conditions indicate that the main drive for permeability evolution is the shear fracturing of the core. The deviatoric and low confining stress conditions preserve permeability. Although injecting SSW reduces the chalk mechanical stability and alters its mineralogy, and more so at higher temperature, the effects do not seem to successfully compete with the impact of deviatoric stress in fractured chalk.

When flooding equilibrium brines that do not alter chalk mineralogy (NaCl and Na_2SO_4), brine temperature can play a significant role in mechanical compaction (strain), a key permeability-controlling factor. At 50° C the cores suffered approximately 70 % more net axial strain than the 130° C tests for both brine series, and consequently registered less end permeability increase. In average end permeability

was approximately 80 % less in NaCl series and 45 % less when injecting Na_2SO_4 at 50° C compared to the high temperature tests.

Evaluating the combined contribution of all test parameters indicated that, despite fracturing and exposure to repetitive different stress states, temperature and brine conditions, core permeability at the end of the test seems to remain within the same order of magnitude as the original value (ca 1 mD), ranging between the initial and double of the initial value. This indicates that permeability has an apparent insensitivity to changes in reservoir conditions.

4.3 Applicability of onshore chalk research in the North Sea reservoir chalk context

The results from geomechanical testing of Eldfisk reservoir chalk cores described in **Paper II** offer a unique opportunity to evaluate the application significance of the outcrop chalk research in the North Sea reservoir chalk context.

Of particular interest are the compaction behavior of reservoir chalk exposed to thermo-chemical influence and the rock-fluid interactions that influence this behavior. The results show that, under hydrostatic stress conditions, at 130° C and exposed to chemical perturbation, generally Eldfisk reservoir chalk showed similar behavior as outcrop chalk described by several previous studies (e.g., Madland et al., 2011; Megawati et al., 2011; Korsnes et al., 2013; Megawati et al., 2015; Zimmermann et al., 2015; Andersen et al., 2018; Minde et al., 2018; Nermoen et al., 2018; Wang et al., 2018; Sachdeva et al., 2019a) in terms of mechanical and chemical response. This is a novel and important result.

Figure 13 shows that as soon as the cores are flooded with a reactive brine (SSW) the axial strain rate (dotted line) increases compared to when injected with NaCl. This is attributed to the major

reactive divalent ions i.e. magnesium, calcium, and sulphate present in seawater. The ionic concentrations in the effluent water throughout the test show that magnesium ions are retained in the core (Figure 13, purple line) and calcium ions are produced (red line), a clear deviation from the original brine concentrations (corresponding dashed lines). The excess calcium and the loss of magnesium can indicate dissolution of calcite and precipitation of magnesium-bearing minerals, seemingly the ongoing processes during seawater injection.

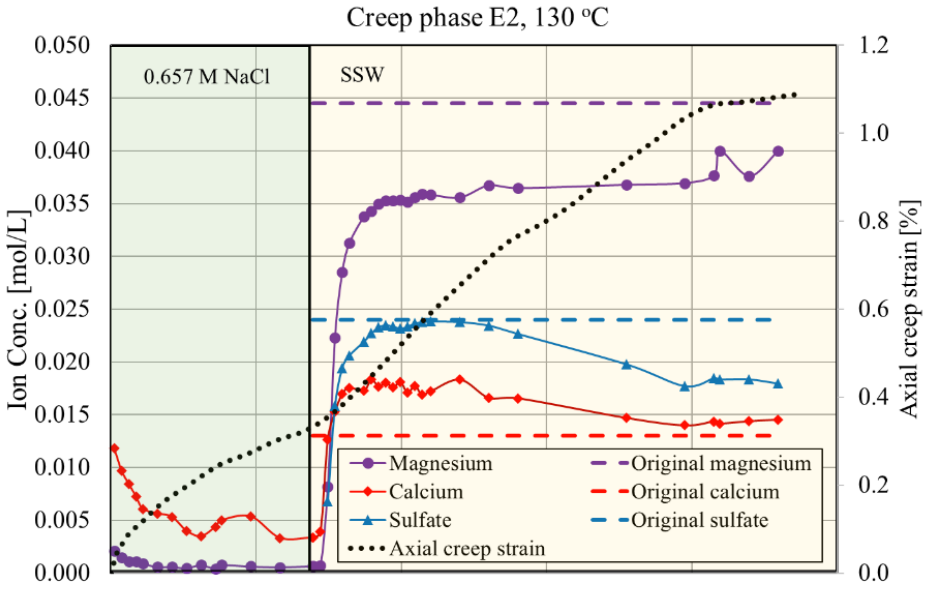

Figure 13: Axial deformation (dotted black line) and magnesium (purple line), calcium (red line) and sulfate (blue line) concentrations of effluents [mol/L] during creep time [days] and flooding inert (green shade) and reactive (yellow shade) brine of core E2. Dashed lines indicate original ion concentrations.

Additionally, the sulfate concentration in the effluent (blue line) declined compared to the original seawater, following closely the decline in calcium production. This led to precipitation of anhydrite ($CaSO_4$), which caused clogging of the outlet tubing, consequently increasing the pore pressure of the core, and reducing the effective stress. The impact

of lower effective stress is reflected in the flattening of the deformation curve (dotted black line) around day 20 of the experiment.

Similar to core E2, a clear mechanical response is observed in core E3 after switching from NaCl to the reactive brine. The chemically induced creep deformation rate is shown in the plot of axial strain along (dotted black line) and the effluent concentration profiles as a function of creep time in Figure 14.

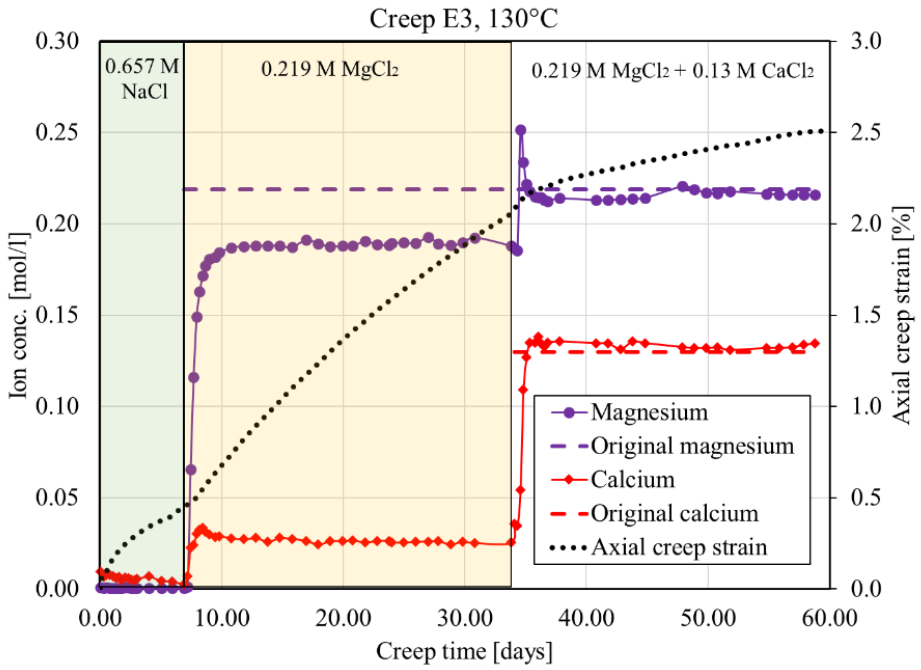

Figure 14: Axial deformation (dotted black line) and magnesium (purple line) and calcium (red line) concentrations of effluents [mol/L] during creep time [days] and flooding inert brine (green shade) magnesium chloride (yellow shade) and calcite-enhanced magnesium chloride (unshaded) of core E3. Dashed lines indicate original ion concentrations.

The axial strain rate increased (Figure 14, dotted line) as a response to the non-equilibrium nature of the rock-fluid interface. This effect has been observed in multiple earlier studies on outcrop chalk which investigated the isolated role of magnesium in mineral alteration of chalk such as calcite dissolution followed by precipitation of magnesium

bearing minerals (Madland et al., 2008; Madland et al., 2011; Megawati et al., 2015; Andersen et al., 2018; Minde et al., 2018; Wang et al., 2018). This is indicated here as well, secondary precipitated minerals, identified by SEM-EDS analysis as magnesium-bearing also having been detected in the inlet of E3 (Figure 15, red circle). Although not clearly identified, due to their minute size, the newly precipitated crystals are most likely magnesite, according to their position and form, agreeing to previous studies on outcrop chalk at similar conditions (Korsnes et al., 2013; Zimmermann et al., 2015, Minde et al., 2018).

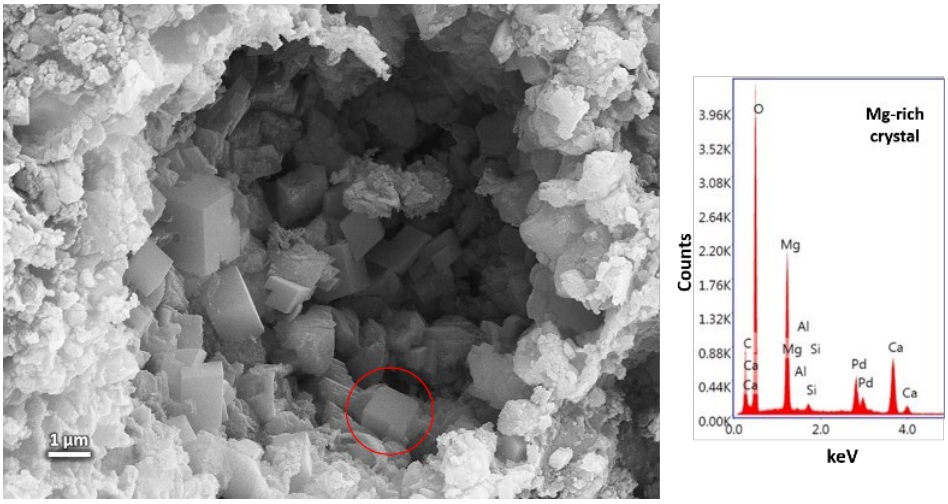

Figure 15: Left: SEM micrograph of flooded chalk fragment from the inlet of core E3; red circle shows Mg-rich crystal. Right: EDS spectrum of the encircled crystal, possibly magnesite.

The ionic concentration profiles shown in Figure 14, with mirrored magnesium loss and calcium production around 0.03 mol/L align very well with the ion chromatography studies on outcrop chalk (Andersen et al., 2018). The axial deformation rate observed in outcrop chalk studies (Madland et al., 2011), is higher than what was observed in the Eldfisk chalk tests (although it remains in the same order of magnitude), most likely due to core properties (over 40 % in tested outcrop chalk) and/or test parameters (flooding rate, stress conditions).

Adding $CaCl_2$ to $MgCl_2$ produced a similar effect in the Eldfisk reservoir core as described in Megawati et al. (2011) which tested this effect on Liège chalk. Figure 14 shows that as soon as $CaCl_2$ is added to the $MgCl_2$ brine, the magnesium (purple line) and calcium concentrations (red line) lay steady around the original ion concentrations of the injected brine, together with a clear reduction in creep compaction rate (dotted black line).

Not only does this confirm that the mechanical and chemical response of outcrop chalk from Liège is relevant for North Sea reservoir chalk, but it also reinforces the observations made by Sachdeva et al., 2019b, that the initial wettability of the chalk cores was inconsequential regarding the effect of the imposed fluids on the mechanical behavior of chalk. The presumed presence of hydrocarbons in the cores used in this study did not seem to hinder the water weakening effect, indicating that application of rock-fluid interactions observed in water-wet experiments can be valid also in a reservoir context.

4.4 Permeability predictions for mechanically- and chemically-compacting, fractured chalk

One of the main motivations behind the series of experiments in this project was to provide experimental data as input for developing a permeability model relevant to the reservoir conditions in the North Sea. The model, presented in **Paper IV**, built on the stress- and chemistry-related compaction model in Aalborg and Liège chalk, was extended to capture the permeability behavior in intact chalk cores, and further developed to consider the role of fractures in permeability evolution.

A direct application of matching experimental data was the quantification of permeability loss relative to mechanical and chemical compaction (section 4.1.2, Figure 5) where it is estimated that mineralogical impact on permeability becomes significant when more than approximately 100 mol/m^3 magnesite has precipitated.

Simulations of the fracture width on permeability evolution show that wide-fractured cores maintain a higher porosity than cores with narrow fractures (Figure 16 a and c). At the same time, permeability decreases with time for all fracture apertures (Figure 16 b and d) at a rate that is width-independent. This seeming paradox indicated that fracture permeability, in another order of magnitude compared to the matrix permeability, dominates the effective permeability evolution.

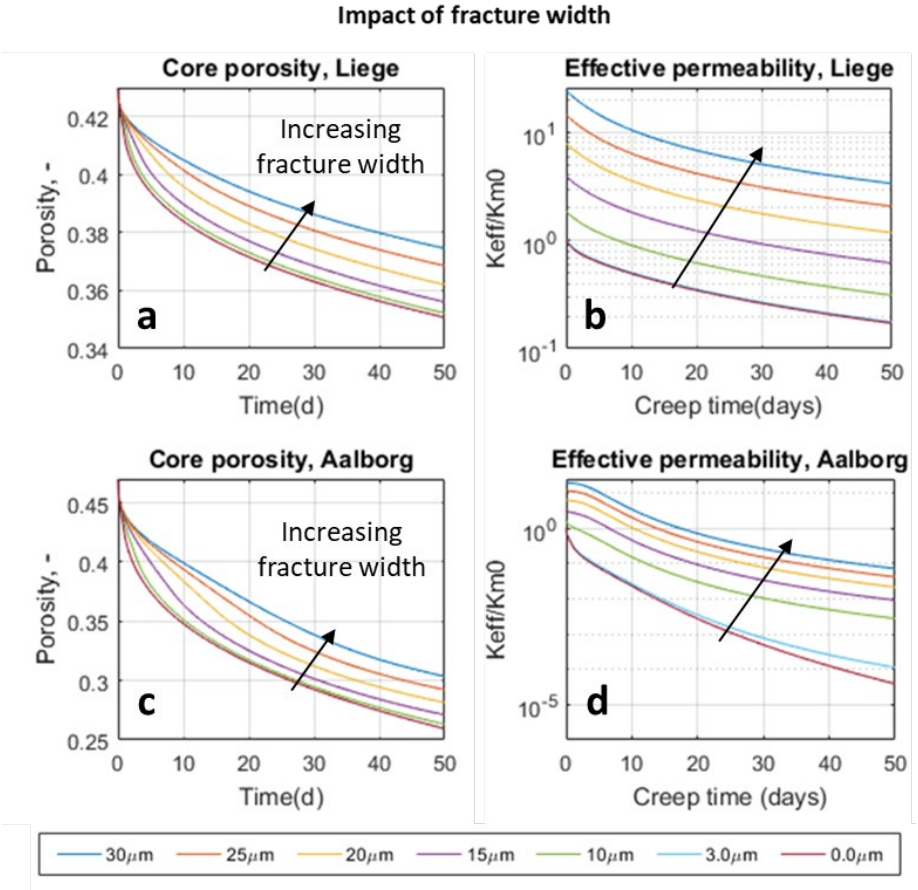

Figure 16: Simulated time evolution of porosity and effective permeability for fractured Liège (a, b) and Aalborg (c, d) chalk cores injected with 0.219 M $MgCl_2$ at 1 PV/d assuming different fracture widths $\boldsymbol{w_0}$ (in μm). Wider fractures induce less porosity reduction, but fracture width does not influence the permeability reduction rate.

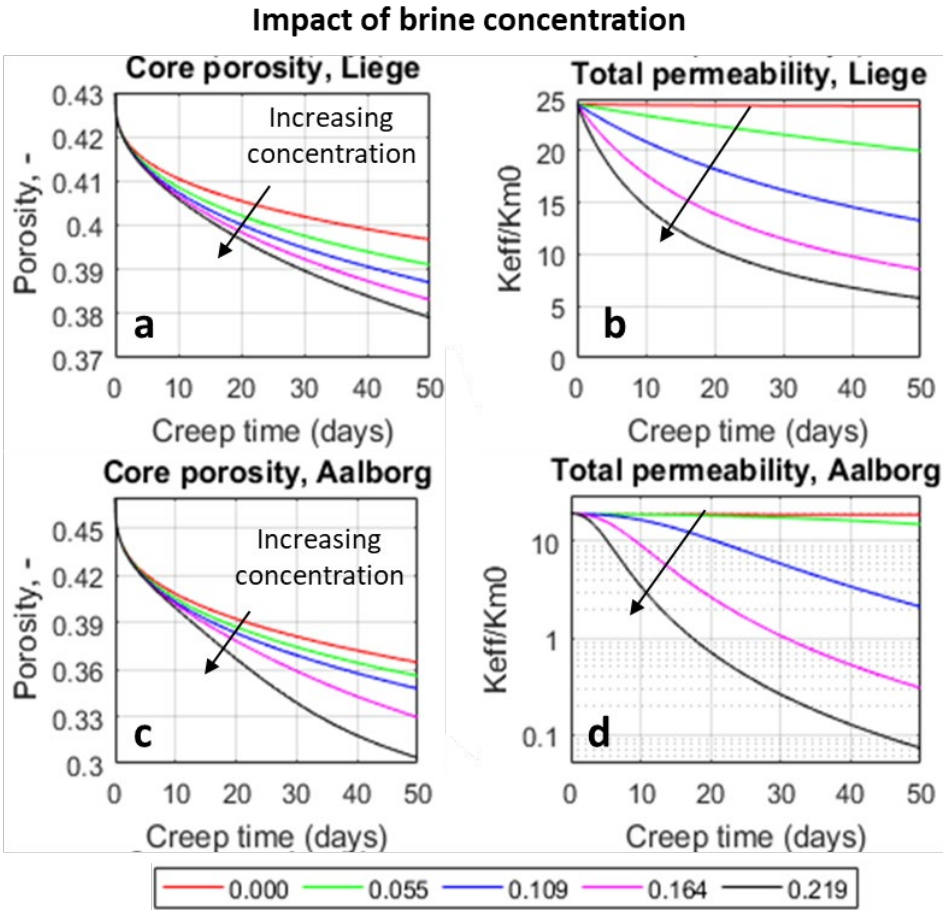

Figure 17: Simulated evolutions of core porosity and total permeability during injection of $MgCl_2$ at different concentrations (indicated in mol/L) with rate 1 PV/d. Fractured Liège (a, b) and Aalborg (c, d) cores were assumed. For both chalk types, porosity and permeability decrease with increasing brine concentration.

The model predicts that increasing magnesium concentration in the flooding medium also increases porosity and permeability loss in the fractured chalk (Figure 17). For this simulation, the fracture was set to 30 µm. The porosity and permeability distribution along the core indicates that increasing the concentration affects the fracture permeability more than the matrix (in the fracture, magnesite precipitation lowered the permeability by as much as three orders of

magnitude) and that any significant permeability reduction in the matrix is isolated to the inlet.

Finally, varying the injection rate for 0.219 M $MgCl_2$ in fractured Liège and Aalborg cores, the model forecasts a strongly rate dependent evolution of porosity (Figure 18 a and c). Higher injection rate leads to more fluid in the core so that a greater fraction of the matrix is exposed to the reactive brine, consequently compacting more. However, the permeability evolution seems insensitive to injection rates (Figure 18 b and d), as the fluid flows sufficiently fast through the fracture even at the lowest injection rates, to maintain a constant dissolution rate.

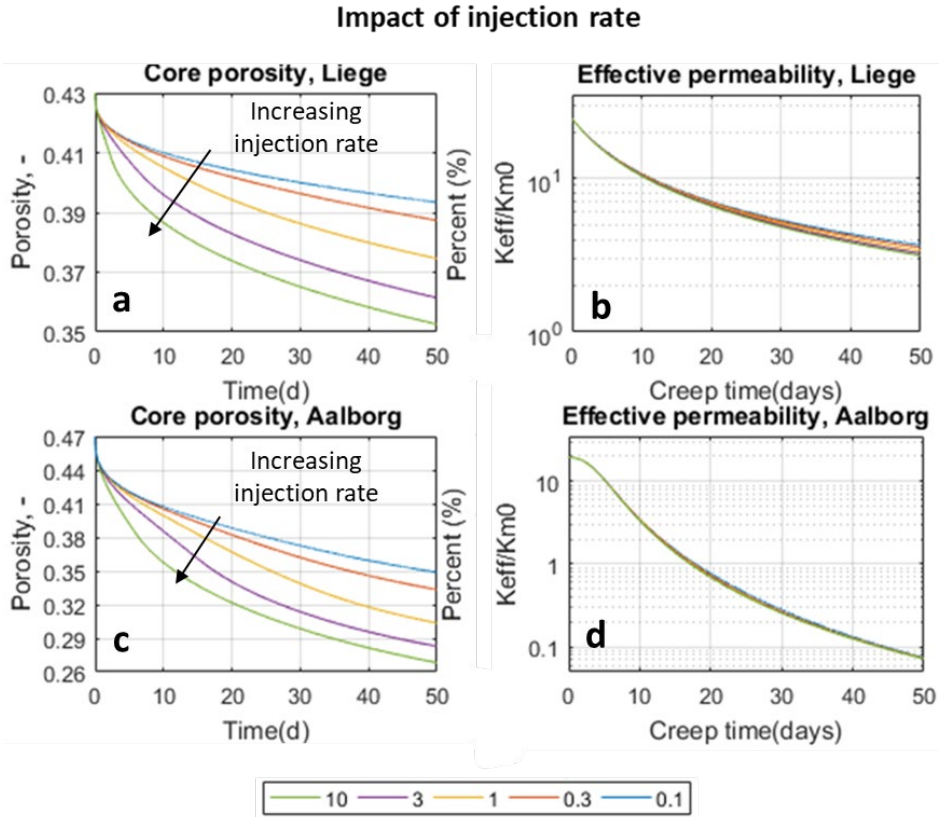

Figure 18: Simulated porosity change and effective permeability at varying injection rates (PV/day) in Liège (a, b) and Aalborg (c, d) chalk. For both chalk types, core porosity decreases with increasing injection rate, while effective permeability decreases irrespective of injection rates.

Even though the matrix compacts more, the permeability reduction associated with it is not significant enough to cause a clear impact the effective permeability. This underlines that the permeability of the fracture and its rate-independent behavior, several orders of magnitude greater than that of the matrix, dominates the permeability of the core.

5 Impact and relevance of permeability research for the petroleum industry

The broad spectrum of experiments and analyses in this project addresses a series of data and knowledge gaps with direct and indirect applicability for the petroleum industry.

A thorough description of North Sea reservoir chalk in terms of mineralogy, petrography, geochemistry and the potential influence of hydrocarbons and decades of seawater flooding on this chalk (**Paper I**) are central parts for selecting and developing appropriate EOR methods for hydrocarbon production on the Norwegian Continental Shelf.

The EOR efforts involving reactive waterflooding must not underestimate the importance of the clastic content in chalk, as rock-fluid interactions and their effects on chalk properties (porosity, permeability, mechanical strength) may be amplified or accelerated in the presence of certain non-carbonate mineral phases. The varying spatial distribution and abundance of clastic material observed in the reservoir chalk should count as essential criteria for customizing future EOR methods.

Having confirmed similar mechanical and chemical effects of reactive flow in both water-wet outcrop and oil-bearing reservoir chalk (**Paper II**) has significant economic implications for sustained chalk research. With extremely scarce and expensive reservoir cores, research

on the more easily available outcrop chalk can provide relevant data instead.

The results described in **Paper III** document several aspects of the relationship between permeability and permeability-influencing parameters in chalk reservoirs, a subject that still poses many unanswered questions. The study brings a closer look at permeability evolution in a reservoir context by showing that, at core scale, chalk permeability seems little responsive to production-related changes in the reservoir parameters (effective stress cycles, temperature fluctuations, brine composition), once the chalk is fractured and under deviatoric stress conditions. Further, the quantification of permeability reduction factor (see section 4.1.2 and **Paper IV**) as a function of mechanical compaction and chemical alteration and the role of non-carbonate mineral phases is a valuable and concrete contribution to describe permeability behavior in reservoir chalk.

Knowledge of mineralogy characteristics of the North Sea reservoir chalk, as well as diagenetic features (**Paper I**) is useful input for refining of existing reservoir models. Reservoir models relevant for the NCS are instrumental for the hydrocarbon industry, as they are economical and time-saving tools that support EOR decision-making processes, thus making their reliability essential. The permeability model developed in this project (**Paper IV**) although simplified, seems to successfully identify and describe permeability-influencing factors in chalk at reservoir conditions.

6 Conclusions and future work

6.1 Concluding remarks

The results generated in the present project were intended to further the understanding of permeability evolution in fractured chalk reservoirs during field lifetime. The research approach included obtaining factual

data regarding the mineralogy, geochemistry of reservoir chalk representative for the NCS and the impact of hydrocarbons and EOR fluids on the chalk, as well as experimental data comprising a systematic analysis of permeability evolution in shear failing chalk and geomechanical and chemical effects on reservoir chalk. Additionally, the project included theoretical simulations of fluid flow in fractured cores.

The main outcome of the project is that permeability evolution of fractured outcrop chalk is strongly dependent on fracture permeability. Systematic combinations of repetitive deviatoric stress cycles, brine chemistry (either NaCl, Na_2SO_4, SSW) and temperature (50° C or 130° C) acting simultaneously on chalk cores indicated that the main permeability influencing event was the occurrence of the shear fracture under deviatoric stress conditions (**Paper I**). The core permeability gain following fracturing and exposure to different stress states, temperature, and brine conditions, at the end of the test seems to remain within the same order of magnitude as the original value, ranging between the initial and double of the initial value.

Although all cores registered a positive net change in permeability at the end of the tests, regardless of brine and temperature, flooding Na_2SO_4 through fractured chalk seems to sustain the permeability gain related to shear fracturing better than flooding SSW. Injecting Na_2SO_4 lead to the highest final permeability at both temperatures compared to the other brines. Injecting SSW at elevated temperature caused most permeability loss compared to the other brines.

The clearer permeability decline during SSW injection may be related to precipitation of anhydrite, a recognized permeability inhibiting mineral. Anhydrite precipitation was also suspected to have occurred after several days of SSW flooding during the geomechanical testing reservoir chalk cores from Eldfisk Field (**Paper II**).

Yet, the geochemical analyses of the North Sea reservoir chalk (**Paper I**) do not point to evident mineral or geochemical alterations

expected to occur after seawater injection for EOR purposes, as seen in numerous onshore chalk experiments (e.g., calcite dissolution and magnesite or anhydrite precipitation). However, this does not rule out the effects of EOR fluids on chalk, as studies show that rock-fluid interactions are more likely to occur close to the injectors; in this case, it is possible that the distance between the studied samples and the seawater injectors was large enough for the effects to lessen.

Still, the use of onshore chalk for laboratory testing substituting authentic North Sea reservoir chalk can be justified from a mechanical and thermochemical point of view (**Paper II**), as the stress and brine composition seem to generate a similar strain effect and rock-fluid interactions on both lithotypes. Under hydrostatic stress, the injecting brine composition conditions the creep deformation rate: brines containing surface-reactive ions lead to higher deformation rates than inert brines. Increasing calcium concentration tenfold reduced the deformation rate severely. However, the large variations in mineralogy, particularly the silica content, observed in the North Sea reservoir chalk (**Paper I**) should be taken into consideration before transferring data from one chalk type to the other.

The presence of hydrocarbons in the Eldfisk cores did not seem to impact the effect of the imposed fluids on the mechanical behavior of chalk, an observation also reported in studies on onshore chalk. Also, there was no evidence of hydrocarbon influence in sediment composition, textures, and mineralogy of the North Sea reservoir chalk (**Paper I**), given the similarities between samples both with and without hydrocarbon accumulations, indicating that application of rock-fluid interactions observed in water-wet experiments on onshore chalk can be valid also in a reservoir context.

A thorough knowledge of the reservoir chalk mineralogy is also important for parametrization of permeability models for the NCS. Based on the available experimental data, the permeability model

developed in this project (**Paper IV**) was able to quantify the loss of permeability relative to the mineralogical alteration (magnesite precipitation) and mechanical compaction. The presence of fragile, amorphous quartz (opal CT) in the outcrop chalk had a strong influence on the permeability evolution, reducing it at a much higher rate than chalk without opal CT. However, more data is needed to quantify these relations for an accurate description of how chalk would behave under fracture conditions.

When simulating injection of reactive $MgCl_2$ brine into fractured chalk cores, there was a clear impact of injected concentration on permeability evolution, as well as porosity. Higher concentration led to greater permeability and porosity reduction, and higher axial strain due to the chemical weakening of the matrix and the precipitation of new minerals in the fracture. However, simulations of varying fracture widths and increasing injection rate for a given fracture width resulted in greater porosity reduction and increased strain but had no practical effect on permeability evolution.

This reinforces the dominant role of fracture permeability, greater than that of matrix permeability, in permeability evolution. It also supports a key observation from geomechanical testing under deviatoric stress conditions that, once the chalk core has fractured, effective permeability is little responsive to certain aspects relevant to the dynamics of petroleum reservoir development, such as fluctuations of the stress state and exposure to reactive fluid flow, both at high and low temperature.

6.2 Future work

For future research, data acquisition regarding reservoir characterization, dynamically changing reservoir parameters that influence fluid flow through chalk during reservoir production is still needed for considering potential EOR methods and optimizing the EOR strategy.

Permeability studies should include the effects of longer-term stress cycles or several stress cycles at actual reservoir stress conditions on permeability evolution in fractured chalk cores.

A challenge in the modeling study was the lack of representative parameterization of fracture behavior. With more experimental data, the model can be improved by allowing fracture deformation and thus a more accurate balance between flow in matrix and fracture can be obtained. Deviatoric stresses, typical for reservoirs, are also a more favorable state for preserving fractures open than hydrostatic conditions used in this work. The model can be thus further extended to include the effect of deviatoric stress, which is more representative to reservoir conditions.

Upscaling the permeability evolution of chalk from core to reservoir scale is a major challenge when considering EOR methods. This project provides a significant amount of data at pore and core scale but applying this knowledge to field scale should happen gradually both theoretically (better models) and experimentally (intermediate scale experiments). For example, at a core scale the model predicted uniform fracture permeability based on the limiting assumptions. However, for low permeable fractures at reservoir scale, giving relatively high residence time of fluid in the fractures, this behavior might change.

7 References

Agarwal, B., Allen, L. R., & Farrell, H. E. (1997). Ekofisk Field reservoir characterization: mapping permeability through facies and fracture intensity. *SPE Formation Evaluation*, *12*(04), 227-234.

Agarwal, B., Hermansen, H., Sylte, J. E., & Thomas, L. K. (1999, January). Reservoir characterization of Ekofisk field: a giant, fractured chalk reservoir in the Norwegian North Sea—history match. In *SPE Reservoir Simulation Symposium*. Society of Petroleum Engineers.

Ahsan, R., & Fabricius, I. L. (2010, June). Sorption of magnesium and sulfate ions on calcite. In *72nd EAGE Conference and Exhibition-Workshops and Fieldtrips* (pp. cp-161). European Association of Geoscientists & Engineers.

Allan, J. R., & Matthews, R. K. (1982). Isotope signatures associated with early meteoric diagenesis. *Sedimentology*, *29*(6), 797-817.

Andersen, P. Ø., Wang, W., Madland, M. V., Zimmermann, U., Korsnes, R. I., Bertolino, S. R. A., ... & Gilbricht, S. (2018). Comparative study of five outcrop chalks flooded at reservoir conditions: chemo-mechanical behaviour and profiles of compositional alteration. *Transport in Porous Media*, *121*(1), 135-181.

Andersen, P. Ø., & Berawala, D. S. (2019). Modeling of Creep-Compacting Outcrop Chalks Injected with Ca-Mg-Na-Cl Brines at Reservoir Conditions. *SPE Journal*, 24(3), 1378-1394.

Austad, T., Strand, S., Høgnesen, E. J., & Zhang, P. (2005). Seawater as IOR fluid in fractured chalk. In *SPE international symposium on oilfield chemistry*.

Austad, T., Strand, S., Madland, M. V., Puntervold, T., and Korsnes, R. I. (2008) Seawater in Chalk: An EOR and Compaction Fluid. *SPE Reservoir Evaluation & Engineering: 11*(4), 648-654.

Bergsaker, A. S., Røyne, A., Ougier-Simonin, A., Aubry, J., & Renard, F. (2016). The effect of fluid composition, salinity, and acidity on subcritical crack growth in calcite crystals. *Journal of Geophysical Research: Solid Earth*, *121*(3), 1631-1651.

Blasingame, T. A. (2008, January). The characteristic flow behavior of low-permeability reservoir systems. In *SPE Unconventional Reservoirs Conference*. Society of Petroleum Engineers.

Brasher, J. E., & Vagle, K. R. (1996). Influence of lithofacies and diagenesis on Norwegian North Sea chalk reservoirs. *AAPG bulletin*, *80*(5), 746-768.

Brown, D. A. (1987). The flow of water and displacement of hydrocarbons in fractured chalk reservoirs. *Geological Society, London, Special Publications*, *34*(1), 201-218.

Clayton, R. N., & Degens, E. T. (1959). Use of carbon isotope analyses of carbonates for differentiating fresh-water and marine sediments. *AAPG Bulletin*, *43*(4), 890-897.

Collin, F., Cui, Y. J., Schroeder, C., & Charlier, R. (2002). Mechanical behaviour of Lixhe chalk partly saturated by oil and water: experiment and modelling. *International journal for numerical and analytical methods in geomechanics*, *26*(9), 897-924.

Cui, P. D. C. S. Y., Delage, P., & Schroeder, C. (1996). Subsidence and capillary effects in chalk. In *Proceedings of Eurock* (Vol. 96, pp. 1291-1298).

Darcy, H. P. G. (1856). Les Fontaines publiques de la ville de Dijon. Exposition et application des principes à suivre et des formules à employer dans les questions de distribution d'eau, etc. V. Dalamont.

Egeberg, P. K., & Saigal, G. C. (1991). North Sea chalk diagenesis: cementation of chalks and healing of fractures. *Chemical Geology*, *92*(4), 339-354.

Ferno, M. A., Haugen, A., & Graue, A. (2010, January). Visualizing Oil Displacement In Fractured Carbonate Rocks-Impacts On Oil Recovery At Different Hydrostatic Stress And Wettability Conditions. In *44th US Rock Mechanics Symposium and 5th US-Canada Rock Mechanics Symposium*. American Rock Mechanics Association.

Gennaro, M., Wonham, J. P., Sælen, G., Walgenwitz, F., Caline, B., & Faÿ-Gomord, O. (2013). Characterization of dense zones within the Danian chalks of the Ekofisk Field, Norwegian North Sea. *Petroleum Geoscience*, *19*(1), 39-64.

Gradstein, F. M., Ogg, J. G., Schmitz, M. B., & Ogg, G. M. (Eds.). (2012). *The geologic time scale 2012*. Elsevier, 181-232

Harper, M. L., & Shaw, B. B. (1974). Cretaceous-Tertiary carbonate reservoirs in the North Sea: Offshore North Sea Technology Conference. *Stavanger, Norway, Paper G IV/4*, *20*.

Heggheim, T., Madland, M. V., Risnes, R., & Austad, T. (2005). A chemical induced enhanced weakening of chalk by seawater. *Journal of Petroleum Science and Engineering*, *46*(3), 171-184.

Hermansen, H., Thomas, L. K., Sylte, J. E., & Aasboe, B. T. (1997, January). Twenty five years of Ekofisk reservoir management. In *SPE annual technical conference and exhibition*. Society of Petroleum Engineers.

Hermansen, H., Landa, G. H., Sylte, J. E., & Thomas, L. K. (2000). Experiences after 10 years of waterflooding the Ekofisk Field, Norway. *Journal of Petroleum Science and Engineering*, *26*(1-4), 11-18.

Hjuler, M. L., & Fabricius, I. L. (2009). Engineering properties of chalk related to diagenetic variations of Upper Cretaceous onshore and offshore chalk in the North Sea area. *Journal of Petroleum Science and Engineering*, *68*(3-4), 151-170.

Hu, C., Agostini, F., Skoczylas, F., & Egermann, P. (2018). Effects of gas pressure on failure and deviatoric stress on permeability of reservoir rocks: initial studies on a Vosges sandstone. *European Journal of Environmental and Civil Engineering*, 22(8), 1004-1022.

Hudson, J. D. (1977). Stable isotopes and limestone lithification. *Journal of the Geological Society*, *133*(6), 637-660.

Håkansson, E., Bromley, R., & Perch-Nielsen, K. (1975). Maastrichtian chalk of north-west Europe—a pelagic shelf sediment. *Pelagic Sediments: on Land and under the Sea*, 211-233.

Jensen, T., Harpole, K., & Østhus, A. (2000). EOR screening for Ekofisk. In *Integrated reservoir management: how integration is breaking barriers and adding value: Paris, 24-25 October 2000* (pp. 151-161).

Johnson, J. P., Rhett, D. W., & Siemers, W. T. (1988, January). Rock mechanics of the Ekofisk reservoir in the evaluation of

subsidence. In *Offshore Technology Conference*. Offshore Technology Conference.

Kirk, R. H. (1979). Statfjord Field, North Sea Giant. *AAPG Bulletin*, *63*(3), 479-480.

Kluge, C., Blöcher, G., Milsch, H., Hofmann, H., Nicolas, A., Li, Z., & Fortin, J. (2017). Sustainability of fractured rock permeability under varying pressure. *Poromechanics VI,* (pp. 1192-1199).

Korsnes, R. I., Risnes, R., Faldaas, I., & Norland, T. (2006). End effects on stress dependent permeability measurements. *Tectonophysics*, *426*(1-2), 239-251.

Korsnes, R. I., Madland, M. V., Austad, T., Haver, S., and Røsland, G. (2008) The effects of temperature on the water weakening of chalk by seawater. *Journal of Petroleum Science and Engineering, 60*(3), 183-193.

Korsnes, R. I., Zimmermann, U., Madland, M. V., Bertolino, S. A. R., Hildebrand-Habel, T., & Hiorth, A. (2013, June). Tracing Fluid Flow in Flooded Chalk under Long Term Test Conditions. In *75th EAGE Conference & Exhibition incorporating SPE EUROPEC 2013* (pp. cp-348-00392). European Association of Geoscientists & Engineers.

Laudise, R. A., Kolb, E. D., & DeNeufville, J. P. (1965). Hydrothermal solubility and growth of sphalerite. *American Mineralogist: Journal of Earth and Planetary Materials*, *50*(3-4), 382-391.

MacGregor, A. G., Trussell, P., Lauver, S., Bedrock, M., Bryce, J., & Moulds, T. (2005, January). The Magnus Field: extending field life through good reservoir management and enhanced oil recovery. In *Geological Society, London, Petroleum Geology Conference series* (Vol. 6, No. 1, pp. 469-475). Geological Society of London.

Madland, M. V., Midtgarden, K., Manafov, R., Korsnes, R. I., Kristiansen, T., & Hiorth, A. (2008, October). The effect of temperature and brine composition on the mechanical strength of Kansas chalk. In *International Symposium of the Society of Core Analysts, Abu Dhabi*.

Madland, M., Hiorth, A., Omdal, E., Megawati, M., Hildebrand-Habel, T., Korsnes, R., Evje, S., Cathles, L. (2011) Chemical Alterations Induced by Rock–Fluid Interactions When Injecting Brines in High Porosity Chalks. *Transport in Porous Media, 87*(3), 679-702.

Madsen, H. B. (2010). Silica diagenesis and its effect on porosity of upper Maastrichtian chalk–an example from the Eldfisk Field, the North Sea. *Bulletin of the Geological Society of Denmark*, *20*, 47-50.

McKinney, P. D., Rushing, J. A., & Sanders, L. A. (2002, January). Applied reservoir characterization for maximizing reserve growth and profitability in tight gas sands: A paradigm shift in development strategies for low-permeability gas reservoirs. In *SPE Gas Technology Symposium*. Society of Petroleum Engineers.

Megawati, M., Andersen, P. Ø., Korsnes, R. I., Evje, S., Hiorth, A., & Madland, M. V. (2011). The Effect of Aqueous Chemistry pH on the Time-Dependent Deformation Behaviour of Chalk - Experimental and Modelling Study. In *Pore2Fluid IFP Energies nouvelles Paris, Nov*, 16-18.

Megawati, M., Hiorth, A., & Madland, M. V. (2013). The impact of surface charge on the mechanical behavior of high-porosity chalk. *Rock mechanics and rock engineering*, *46*(5), 1073-1090.

Megawati, M., Madland, M. V., and Hiort, A. (2015) Mechanical and physical behavior of high-porosity chalks exposed to chemical perturbation. *Journal of Petroleum Science and Engineering, 133,* 313-327

Meireles, L. T., Alam, M. M., & Fabricius, I. L. (2017). Permeability Estimation in Chalk Using NMR and a Modified Kozeny Equation. *Poromechanics VI (pp. 1208-1215).*

Milsch, H., Hofmann, H., & Blöcher, G. (2016). An experimental and numerical evaluation of continuous fracture permeability measurements during effective pressure cycles. *International Journal of Rock Mechanics and Mining Sciences*, *100*(89), 109-115.

Minde, M. W., Zimmermann, U., Madland, M. V., Korsnes, R. I., Schulz, B., & Audinot, J. N. (2016). Fluid–flow during EOR experiments in chalk: insights using SEM–MLA, EMPA and Nanosims Applications. *In International Symposium of the Society of Core Analysts, Colorado, USA* (pp. 21-26).

Minde, M. W., Wang, W., Madland, M. V., Zimmermann, U., Korsnes, R. I., Bertolino, S. R. A., and Andersen, P. Ø. (2018) Temperature effects on rock engineering properties and rock-fluid chemistry in opal-CT-bearing chalk. *Journal of Petroleum Science and Engineering, 169*, 454-470.

Minde, M. W., & Hiorth, A. (2020). Compaction and Fluid—Rock Interaction in Chalk Insight from Modelling and Data at Pore-, Core-, and Field-Scale. *Geosciences*, *10*(1), 6.

Molenaar, N., & Zijlstra, J. J. P. (1997). Differential early diagenetic low-Mg calcite cementation and rhythmic hardground development in Campanian-Maastrichtian chalk. *Sedimentary Geology*, *109*(3-4), 261-281.

Nermoen, A., Korsnes, R. I., Hiorth, A., & Madland, M. V. (2015). Porosity and permeability development in compacting chalks during flooding of nonequilibrium brines: Insights from long-term experiment. *Journal of Geophysical Research: Solid Earth*, *120*(5), 2935-2960.

Nermoen, A., Korsnes, R. I., Storm, E. V., Stødle, T., Madland, M. V., & Fabricius, I. L. (2018). Incorporating electrostatic effects into the effective stress relation—Insights from chalk experiments. *Geophysics*, *83*(3), MR123-MR135.

Nourani, M., Meyer, A. G., Lorentzen, H. J., Sigalas, L., Taheriotaghsara, M., Olsen, D., & Stemmerik, L. (2019). Determination of the Overburden Permeability of North Sea Chalk. *Rock Mechanics and Rock Engineering*, *52*(6), 2003-2010.

Nygaard, E., Lieberkind, K., & Frykman, P. (1983). Sedimentology and reservoir parameters of the Chalk Group in the Danish Central Graben. In *Petroleum Geology of the Southeastern North Sea and the Adjacent Onshore Areas* (pp. 177-190).

Papamichos, E., & Stroggylis, P. (2019, August). Experiments and Modeling of Acid Dissolution Fingering. In *53rd US Rock Mechanics/Geomechanics Symposium*. American Rock Mechanics Association.

Polat, C., and Parlaktuna, M. (2017) A study on the effect of the chemical composition of brine to improve oil recovery from carbonates. *Energy Sources, Part A: Recovery, Utilization, and Environmental Effects, 39*(23), 2151-2156.

Pradhan, S., Stroisz, A. M., Fjær, E., Stenebråten, J. F., Lund, H. K., & Sønstebø, E. F. (2015). Stress-induced fracturing of reservoir

rocks: acoustic monitoring and μCT image analysis. *Rock Mechanics and Rock Engineering*, *48*(6), 2529-2540.

Risnes, R., & Flaageng, O. (1999). Mechanical properties of chalk with emphasis on chalk-fluid interactions and micromechanical aspects. *Oil & Gas Science and Technology*, *54*(6), 751-758.

Sachdeva, J. S., Muriel, H., Nermoen, A., Korsnes, R. I., & Madland, M. V. (2019 a). Chalk Surface Area Evolution during Flow of Reactive Brines: Does Oil Play a Role?. *Energy & Fuels*, *33*(6), 4890-4908.

Sachdeva, J. S., Nermoen, A., Korsnes, R. I., & Madland, M. V. (2019 b). Impact of Initial Wettability and Injection Brine Chemistry on Mechanical Behaviour of Kansas Chalk. *Transport in Porous Media*, *128*(2), 755-795.

Schatzinger, R. A., Feazel, C. T., & Henry, W. E. (1985). Evidence of resedimentation in chalk from the Central Graben, North Sea.

Scholle, P. A. (1975). Diagenesis of Upper Cretaceous Chalks from England, Northern Ireland, and the North Sea. *Pelagic Sediments: On Land and under the Sea*, 177-210.

Scholle, P. A. (1977). Chalk diagenesis and its relation to petroleum exploration: oil from chalks, a modern miracle?. *AAPG Bulletin*, *61*(7), 982-1009.

Schroeder, C., Bois, A. P., Maury, V., & Halle, G. (1998, January). Water/chalk (or collapsible soil) interaction: Part II. Results of tests performed in laboratory on Lixhe chalk to calibrate water/chalk models. In *SPE/ISRM Rock Mechanics in Petroleum Engineering*. Society of Petroleum Engineers.

Schulte, W. M. (2005, January). Challenges and strategy for increased oil recovery. In *International Petroleum Technology Conference*. International Petroleum Technology Conference.

Scott, R. J., Meffre, S., Woodhead, J., Gilbert, S. E., Berry, R. F., & Emsbo, P. (2009). Development of framboidal pyrite during diagenesis, low-grade regional metamorphism, and hydrothermal alteration. *Economic Geology*, *104*(8), 1143-1168.

Shariatpanahi, S. F., Hopkins, P., Aksulu, H., Strand, S., Puntervold, T., & Austad, T. (2016). Water based EOR by wettability alteration in dolomite. *Energy & Fuels*, *30*(1), 180-187.

Shields, G., & Veizer, J. (2002). Precambrian marine carbonate isotope database: Version 1.1. *Geochemistry, Geophysics, Geosystems*, *3*(6), 1-12.

Simmons, S. F., & Browne, P. R. (2000). Hydrothermal minerals and precious metals in the Broadlands-Ohaaki geothermal system: Implications for understanding low-sulfidation epithermal environments. *Economic Geology*, *95*(5), 971-999.

Stoddart, D. P., Hall, P. B., Larter, S. R., Brasher, J., Li, M., & Bjorøy, M. (1995). The reservoir geochemistry of the Eldfisk field, Norwegian North Sea. *Geological Society, London, Special Publications*, *86*(1), 257-279.

Sulak, R., & Danielsen, J. (1989). Reservoir aspects of Ekofisk subsidence. *Journal of petroleum technology*, **41**(7), 709-716.

Sulak, R. M. (1991). Ekofisk field: the first 20 years. *Journal of Petroleum Technology, 43(10), 1-265.*

Suri, P., Azeemuddin, M., Zaman, M., Kukreti, A. R., & Roegiers, J. C. (1997). Stress-dependent permeability measurement using the oscillating pulse technique. *Journal of Petroleum Science and Engineering*, *17*(3-4), 247-264.

Sylte, J. E., Thomas, L. K., Rhett, D. W., Bruning, D. D., & Nagel, N. B. (1999, January). Water induced compaction in the Ekofisk field. *In SPE Annual Technical Conference and Exhibition. Society of Petroleum Engineers.*

Talukdar, M. S., & Torsaeter, O. (2002). Reconstruction of chalk pore networks from 2D backscatter electron micrographs using a simulated annealing technique. *Journal of petroleum science and engineering*, *33*(4), 265-282.

Tang, G. Q., & Firoozabadi, A. (2001). Effect of pressure gradient and initial water saturation on water injection in water-wet and mixed-wet fractured porous media. *SPE reservoir evaluation & engineering*, *4*(06), 516-524.

Teufel, L. W. (1991) Permeability of naturally fractured reservoirs. *AAPG 1991 annual convention with DPA/EMD divisions and SEPM, an associated society, 1991, Vol.75(3),* 680.

Teufel, L. W., & Rhett, D. W. (1992). Effect of reservoir stress path on permeability of fractures in chalk. In *Proc. 4th North Sea Chalk Symposium*.

Wang, W., Madland, M. V., Zimmermann, U., Nermoen, A., Korsnes, R. I., Bertolino, S. R., & Hildebrand-Habel, T. (2018). Evaluation of porosity change during chemo-mechanical compaction in flooding experiments on Liege outcrop chalk. *Geological Society, London, Special Publications*, *435*(1), 217-234.

Yale, D. P., & Crawford, B. (1998). Plasticity and permeability in carbonates: dependence on stress path and porosity. In SPE/ISRM Rock Mechanics in Petroleum Engineering. Society of Petroleum Engineers.

Zeng, L., Chen, Y., Lu, Y., Hossain, M. M., Saeedi, A., & Xie, Q. (2020). Role of brine composition on rock surface energy and its implications for subcritical crack growth in calcite. *Journal of Molecular Liquids*, *303*, 112638.

Zimmermann, U., Madland, M. V., Nermoen, A., Hildebrand-Habel, T., Bertolino, S. A., Hiorth, A., ... & Grysan, P. (2015). Evaluation of the compositional changes during flooding of reactive fluids using scanning electron microscopy, nano-secondary ion mass spectrometry, x-ray diffraction, and whole-rock geochemistry. Compositional Changes during Flooding. *AAPG Bulletin*, *99*(5), 791-805.

Part II

Paper I: Mineralogy and geochemistry of reservoir and non-reservoir chalk from the Norwegian continental shelf

Kallesten, E., Zimmermann, U., Madland, M. V., Bertolino, S. R. A., Omdal, E., Andersen, P.Ø.

Journal of Petroleum Science and Engineering (in 2nd review)

Mineralogy and geochemistry of reservoir and non-reservoir chalk from the Norwegian continental shelf

E. Kallesten[1, 2], U. Zimmermann[1, 2], M. V. Madland[1, 2], S. Bertolino[3], E. Omdal[4], P. Ø. Andersen[1, 2]

1.University of Stavanger, Kristine Bonnevies vei 22, 4021 Stavanger, Norway

2.The National IOR Centre of Norway (same address as 1.)

3. Universidad Nacional de Cordoba, Av. Medina Allende, 2144, Cordoba, Argentina

4.ConocoPhillips, Ekofiskveien 35, 4056 Tananger, Norway

Abstract: A study of the geochemistry and mineraogy characterizing the North Sea reservoir and non-reservoir chalk is provided in this work. Such a characterization is central for refining or developing new enhanced oil recovery (EOR) methods as it provides an instrumental insight in the chemical composition, mineral structures, and textures of the North Sea chalk. Moreover, studies on reservoir core samples are extremely rare, yet paramount for research related to hydrocarbon and especially for EOR research. The study is based on 185 cores from exploration and development wells in the North Sea, representing Tor, Ekofisk and Hod formations. The cores related to reservoir development have different flooding status, from unflooded to waterflooded at lower or higher temperatures, directly sampled from the Ekofisk field.

Optical petrography shows a micritic carbonate matrix, with grains represented by various microfossils such as foraminifers and sponge spicules. Scanning electron microscopy (SEM) reveals post-depositional calcite precipitation and cementation. Dolomite is present

only in the reservoir samples, but it is discussed as a diagenetic feature, unrelated to the hydrocarbon content or EOR exposure. The non-carbonate minerals observed with SEM and X-ray diffraction (XRD) include mostly quartz but also smectite, illite, kaolinite, mica, and pyrite. The abundance of clastic input varies, and there is a clear decrease in porosity stratigraphically downwards, with stronger cementation and higher compaction (e.g., the silica content varies highly from < 2 wt % in clean chalk cores and up to 15 wt % in tight cores). $\delta^{13}C$ reflect primary trends for Upper Cretaceous stages while $\delta^{18}O$ in all samples are lower than the secular global isotopic values for this period and therefore different from onshore chalk, where $\delta^{18}O$ are often still primary. However, the $\delta^{18}O$ values are not sufficiently low to imply a strong diagenetic overprint, but rather suggest a resetting or the influence of a secondary fluid. This fluid cannot be a hydrocarbon-rich (HC) one, nor EOR fluids, as both flooded and unflooded reservoir as well as the non-reservoir samples show very similar stable isotope values and may indicate post-depositional overprint. It may have also flown syn-depositional to cause the lower Y/Ho ratios and could have had sufficient Mg concentration to trigger dolomite formation and manipulate primary $\delta^{18}O$ values.

Keywords: geochemistry; mineralogy; reservoir chalk; North Sea chalk; EOR

1 Introduction

Carbonate reservoirs hold significant amounts of the hydrocarbon reserves worldwide. Since the discovery of the Ekofisk field on the Norwegian Continental Shelf (NCS) in 1969, the chalk play remains among the most prolific hydrocarbon resources in the North Sea, Ekofisk field alone accounting for approximately 10% of the produced net oil equivalents on the NCS. After the primary oil recovery, the initiation water injection program on Ekofisk in 1987 the seawater has been remarkably efficient for oil recovery, leaving water flooded zones with irreducible oil saturation of around 30 %. However, even with this good recovery already achieved, the amount of the resources left behind in the flooded zones is significant, simply due to the size of the reservoirs. This rose the motivation for studying the factors that govern this oil replacement.

For economic and availability reasons, much of the extensive research for enhanced oil recovery (EOR) on the NCS involves outcrop samples. Yet, studies showed that, despite the predictable mineralogical and petrological aspects of this rock type, factors such as depositional environment, specific diagenetic history, can strongly influence engineering properties of chalk (Scholle, 1977; Brasher and Vagle, 1996; Hjuler & Fabricius, 2009; Minde et al., 2016), and hence a direct transfer of data from one chalk type to another is not always applicable. Although the Ekofisk discovery initiated several studies on North Sea chalk (Van Den Bark and Thomas, 1981; D'Heur, 1991; Herrington et al., 1991) field observations and further laboratory studies also show that production-related processes, such as changes in reservoir stress state, or waterflooding for EOR purposes, can further influence chalk properties (Bjørlykke and Høeg, 1997; Sylte et al., 1999; Madland et al., 2011) and that the extent of the rock-fluid interactions are closely related to the rock mineralogy (Andersen et al., 2018; Madland et al., 2011; Minde et al., 2018; Strand et al., 2007; Kallesten et al., 2020).

There are very few previously published contributions that characterize the North Sea chalk and support forecasts of the impact the EOR methods have on North Sea chalk (e.g., Scholle, 1974; Egeberg and Saigal, 1991; Stoddart et al., 1995; Hjuler and Fabricius, 2009; Gennaro et al., 2013) and very often porosity, permeability models of North Sea chalk are based on limited data (Jensen et al., 2000; Talukdar et al., 2002).

Therefore, the main objective of this study is a thorough characterization of North Sea reservoir and non-reservoir chalk in terms of geochemistry and petrology and thus provide insight on key-aspects of North Sea chalk properties relevant for hydrocarbons production. An extraordinary sample set of 185 chalk cores from various locations in the North Sea were studied to investigate the chemical composition, mineral structures and textures and diagenetic print of the North Sea chalk. A novel aspect of the study is that the sample set includes chalk cores from exploration and development wells, both with and without hydrocarbon content, and reservoir cores that have various flooding statuses. With this, we aim to evaluate the impact of hydrocarbons on the petrological, mineralogical and geochemical properties of the chalk as well as the impact of enhanced hydrocarbon recovery on chalk by comparing analytic results from waterflooded cores at various temperatures to unflooded reservoir cores. This will not only serve as a standard for selecting a suitable outcrop chalk analogue for further research but may also contribute to increased model accuracy and refined experimental designs for EOR purposes.

2 Sample set

We present extensive analytical studies on chalk successions from 11 different wells in the North Sea, including hydrocarbon-bearing (reservoir) chalk from the Ekofisk area and chalk cores free of hydrocarbons (non-reservoir). The wells are numbered 1 to 11, from south to north (Figure 1, left). The samples from wells 1 – 5 are horizontal core plugs (drilled parallel to bedding) of reservoir chalk from the Tor Formation and Ekofisk Formation (Upper Cretaceous, Lower Paleogene, Figure 1, right) and have different flooding statuses linked to hydrocarbon production – unflooded and water-flooded. The flooding fluid is seawater and the fluid temperature is not defined beyond hot and cold; also, the exact distance between the flooded cores and the injectors is not given, but it can be assumed that they have been flooded over several years at high flooding rates. Due to the confidential nature of wells 1-5, their actual ID number and exact geographic position remain undisclosed.

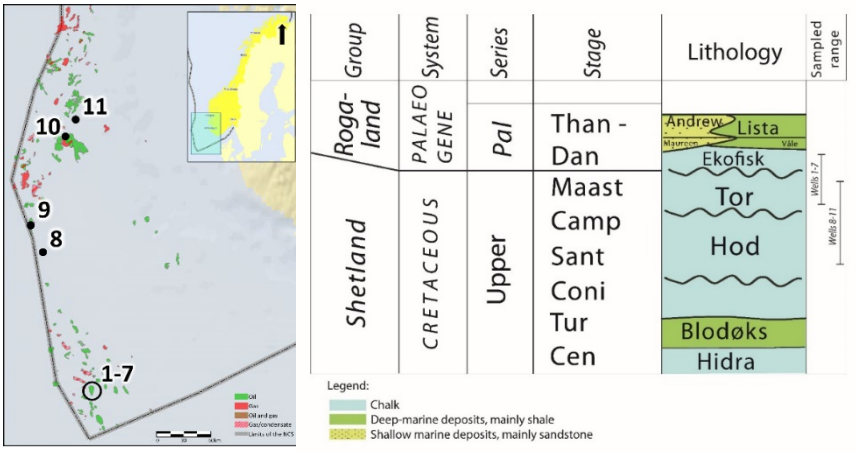

Figure 1: Left: Close-up of the shaded area in the inset map representing the section of Norwegian Continental Shelf and the approximate location of the wells in this study; Right: excerpt from lithostratigraphic chart of the North Sea. (source: npd.no)

Table 1: Overview of the sample set; well ID undisclosed for wells 1-7. Wells 6, 7 and 10 contain both reservoir and non-reservoir samples. * - including cores with unknown flooding status

Well number	Well ID	Type	Formation	Reservoir cores	Non-reservoir cores	Flooded cores	Unflooded cores
1	-	Development	Tor	51	-	33	18
2	-	Development	Tor, Ekofisk	13*	-	9	-
3	-	Development	Ekofisk	12	-	6	6
4	-	Development	Ekofisk	23	-	7	16
5	-	Development	Tor, Ekofisk	3	-	-	3
6	-	Exploration	Tor, Ekofisk	6	2	-	-
7	-	Exploration	Tor, Ekofisk	30	19	-	-
8	7/1-1	Exploration	Hod, Tor	-	8	-	-
9	15/12- 4	Exploration	Tor	-	5	-	-
10	16/2-3	Exploration	Hod, Tor	2	9	-	-
11	25/11-17	Exploration	Tor	-	4	-	-

The chalk successions from wells 6 – 11 were provided by Norwegian Petroleum Directorate (NPD) in Norway and cover mainly the Tor Formation with few from the underlying Hod Formation (Campanian, Upper Cretaceous) and the overlying Ekofisk Formation. Wells 6 – 11 are exploration wells and most of the cores from these wells are hydrocarbon-free (non-reservoir). Their location and ID are shown in Figure 1 and Table 1. However, wells 6 and 7 contains partly confidential cores and therefore their well ID remains undisclosed. Table 1 shows an overview of the number of reservoir and non-reservoir core plugs related to each well, the formations they represent, and details related to the flooding status of the reservoir cores.

3 Methods

The study is based on several analytical methods, and an overview of the measurements is listed in Table 2.

Table 2: Overview of applied methods and number of measurements; Thin sections – TS, Scanning electron microscopy – SEM, X-ray diffraction – XRD, Insoluble residue x-ray diffraction – IR-XRD, Geochemistry – GC, Insoluble residue geochemistry – IR-GC, Carbon and oxygen stable isotope – C-O; *-measurements involving cryo-SEM

Well	Methods and number of measurements						
	TS	SEM	XRD	IR-XRD	GC	IR-GC	C-O
1	15	8	16	6	19		48
2	3	3	9	4	13		13
3	12	7*	12	5	12	5	39
4	7	4	11	8	13		22
5	3		10		12		3
6	3	1			8		10
7	11	1			47		128
8	2	1			10		8
9	2	1			4		5
10	1				5		7
11					3		3

3.1 Separation of the non-carbonate fraction

23 samples from wells 1-4 were selected to separate the carbonate fraction from the non-carbonate material. For this, the samples have been treated with weak acetic acid (2 M concentration) for several days. They were then filtered, dried and again treated with acetic acid until the carbonate content was relatively low. The insoluble residue (IR) was used for geochemical analyses and XRD measurements.

3.2 Optical petrography

The characterization methods include optical petrography of polished thin sections of 40 reservoir and 19 non-reservoir cores for first data about the texture and the composition of the chalk (Zeiss AXIO polarized microscope, University of Stavanger).

3.3 Field emission gun scanning electron microscope (FEG-SEM) with cryogenic unit (cryo-SEM) backscattered electron detector (BSED) and energy dispersive system (EDS)

Fresh surface fragments from five uncleaned reservoir cores (2 unflooded and 3 water-flooded from well 3) were analysed under cryogenic conditions to avoid contaminating the SEM column. The procedure included lowering the samples into nitrogen slush (i.e., liquid nitrogen cooled under vacuum conditions) for rapid freezing, measure taken in order to avoid the vaporization of the hydrocarbons during electron scanning, and consequently contamination of the SEM column. The analysis took place at the University of Stavanger, using a Zeiss Supra 35VP SEM, equipped with a Polar Prep 2000T cryo- SEM system.

An additional SEM and BSED study of polished thin sections took place at Technical University in Freiberg (18 reservoir thin sections from wells 1-4) and University of Stavanger (2 non-reservoir thin sections from wells 8 and 9).

3.4 Stable isotope

The analytical work also includes stable carbon and oxygen isotope geochemistry (VG Isoglas PRISM III stable isotope ratio mass spectrometer, Wolfson Laboratory, Edinburgh University). The subsamples are fine powder, mainly from fresh surfaces. The carbonate powder was reacted with 100 % orthophosphoric acid at 90 °C in an

ISOCARB automatic carbonate preparation system. To test possible artefacts related to drilling, probes obtained from core sides were included, in addition to fresh surface. The data set includes 125 C and O isotope ratios from the reservoir chalk and 162 from the non-reservoir cores. Both oxygen- and carbon-isotopic data are reported in units per mil notation (‰) relative to the Vienna Pee Dee Belemnite (V-PDB) standard. The standard deviation of the powdered coral laboratory standard (COR1D, $\delta^{13}C_{PDB}$ = -0.648, $\delta^{18}O_{PDB}$ = -4.920) run as a sample on the same days as the study samples was ± 0.04 ‰ for $\delta^{13}C$ and ± 0.06 ‰ for $\delta^{18}O$.

3.5 X-ray diffraction

X-ray diffraction (XRD) was used for mineral identification and relative quantification of reservoir samples. The bulk samples were carefully hand-milled in an agate mortar to very fine powder. 12 bulk samples and 5 insoluble residue from well 3 were measured at Instituto Jaime Almera - C.S.I.C.Barcelona (Spain), where the XRD patterns were obtained from a Bruker D5005 diffractometer, Cu Kα x-ray radiation at 40 mA and 40 kV intensity, 0.1 mm receiving slit size. The measurement was between 3 – 65° 2Θ in increments of 0.02° 2Θ, 6 seconds per increment. The remainder of the samples (55 bulk rock and 17 insoluble residue) were measured at University of Stavanger, in a Bruker D8 ADVANCE ECO diffractometer with a Lynxeye detector, Cu Kα x-ray radiation at 40 kV and 25 mA intensity, 0.6 mm receiving slit, 4 – 70° 2Θ in increments of 0.01°, 0.2 seconds per increment. Mineral identification was performed on DIFFRAC.EVA software for semi-quantitative relative mineral proportions of whole rock patterns while for the siliciclastic fraction quantitative mineral proportions were obtained by Rietveld refinement with TOPAS5®.

Material from non-reservoir samples was not available for XRD measurement.

3.6 Geochemistry

Major, trace and rare earth elements geochemistry analysis took place at Acme Laboratories (Canada). The method analysed machine-milled fine powder from 69 reservoir and 77 non-reservoir cores. The material was milled and analysed at Bureau Veritas Minerals laboratories in Canada. The samples were ground in an agate mill and then mixed with $LiBO_2/Li_2B_4O_7$ flux in crucibles and fused in a furnace. The resulted bead was cooled and dissolved in ACS grade nitric acid and analysed by Inductive Coupled Plasma-Mass Spectrometry (ICP-MS). Loss on ignition (LOI) was determined by igniting the sample with a known mass in a tarred crucible at 1000 °C for one hour and calculating the difference in mass after the sample was cooled. Total Carbon and Sulphur were determined by the LECO® method. An additional 14 elements were measured after dilution in Aqua Regia solution of equal parts concentrated HCl, HNO_3, and DI-H_2O for one hour in a heating block or hot water bath. The sample volume was increased with dilute HCl-solutions. All measured concentrations were in the standard range of the possible detection limit, accuracy was between 1-2 %. Further measurement and processing details can be found at http://acmelab.com.

4 Results

4.1 Optical petrography

As chalk is very fine-grained, optical microscopic analyses are restricted to only some specific features. All thin sections reveal a mud supported fabric. All three formations (Hod, Tor and Ekofisk) contain a similar faunal group assemblage, including mainly a large variety of calcareous nano-, micro- and macrofossils (foraminifera, bivalves, crinoid stem fragments) and siliceous sponges. There is no visible distinction between reservoir (Figure 2, left column) and non-reservoir samples (Figure 2, right column) nor between flooded and unflooded samples in terms of texture and fabric. The samples can be classified as mud- to wackestone according to Dunham carbonate classification (Dunham, 1962) but local accumulations of fossils are common (Figure 2b).

Foraminifer tests appear intact, either calcite filled or hollow. Samples from Ekofisk Formation show a notable variation, as the fauna changes from mostly calcareous fossils to predominantly sponge spicules in wells 3 and 7 (Figures 2c, 2d respectively). The sponge spicules are mostly elongated rays (monaxone, Figure 2d), but triaxone spicules are also present (Figure 2c), with moldic voids filled with calcite after the original silica leached. They are often oriented, oblique to the drilling direction.

Stylolites occur in samples from both Tor and Ekofisk Formations, with the distinct serrated surface made visible by a change in color, related to the clay minerals fill (Figure 2e). Fractures and fissures appear in samples from all wells, they are mostly calcite-cemented, but are also sometimes filled with an opaque, dark material that optical petrography cannot identify (Figure 2f).

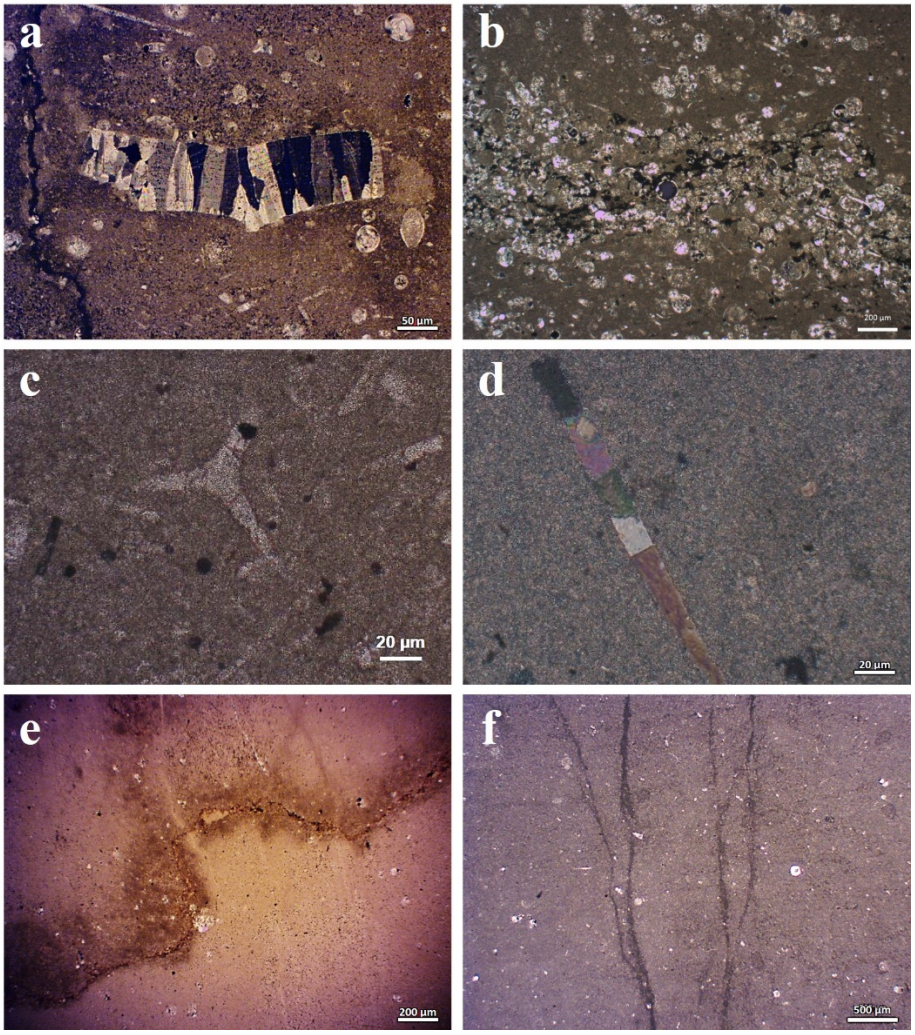

Figure 2: Micrographs showing various features in thin sections from Ekofisk Formation (a-d) and Tor Formation (e, f) representing both reservoir (left column) and non-reservoir (right column) samples;(a) plane polar micrograph of crinoid stem fragment (center), calcite-filled foraminifers of various sizes and sponge spicules; stylolite section to the left (well 1); (b) accumulation of foraminifers along stylolite (Ekofisk Formation, well 7); (c) calcite-filled triaxone spicule (center) and monoaxones (well 3); (d) cross polar view of calcite- filled sponge spicule (Ekofisk Formation, well 7); (e) stylolite (well 1, Tor Formation); (f) braided veins filled with opaque material (plane polar view, well 6).

4.2 Electron microscopy and energy dispersive spectroscopy

Cryo-SEM micrographs of fresh core surfaces from well 3 (Figure 3) show textural and compositional similarities between the water-flooded and unflooded cores. The main constituent of the deposit is the matrix composed of 1-2 μm size calcite crystals from broken, disaggregated coccoliths, but also intact coccolith platelets and coccolithosphores. Although the many foraminifera may have retained their globular shape, some are deformed, broken, or filled with new calcite crystals (Figures 3a, 3b), or coccolith debris (Figure 3c). The void left after the sponge silica dissolved is entirely or sometimes partially filled with calcite crystals (Figure 3d).

Both waterflooded and unflooded samples contain non-carbonate minerals such as quartz, biotite, muscovite, pyrite, kaolinite, or apatite. The minute amount and variety are similar in all samples but one (unflooded), which stands out with more abundant clay minerals than the others, and consequently a less homogeneous texture (Figures 3e, 3f). SEM micrographs of this sample show a conspicuous occurrence of clay flakes bent with irregular and curly edges, all features of detrital smectitic clays such as mixed layers illite-smectite and chlorite-smectite (Figure 3f, green arrows) also suggested by the x-ray diffraction (XRD) band around 5° to 9° 2Θ and the wide band at the position of illite and chlorite (8.7° and 12.3° 2Θ respectively). The flakes are also coating surfaces of voids. There is also authigenic, acicular shaped illite eventually in bundles (Figure 3f, red arrows) that seem to be growing from smectitic clays. The blue arrow in Figure 4e marks a bridge of acicular illite joining flakes.

In comparison, Figure 3b, also of an unflooded sample, exhibits completely different clay features compared to Figures 3e and 3f. Clays are minuscule and less frequent, thus hard to distinguish in the SEM images.

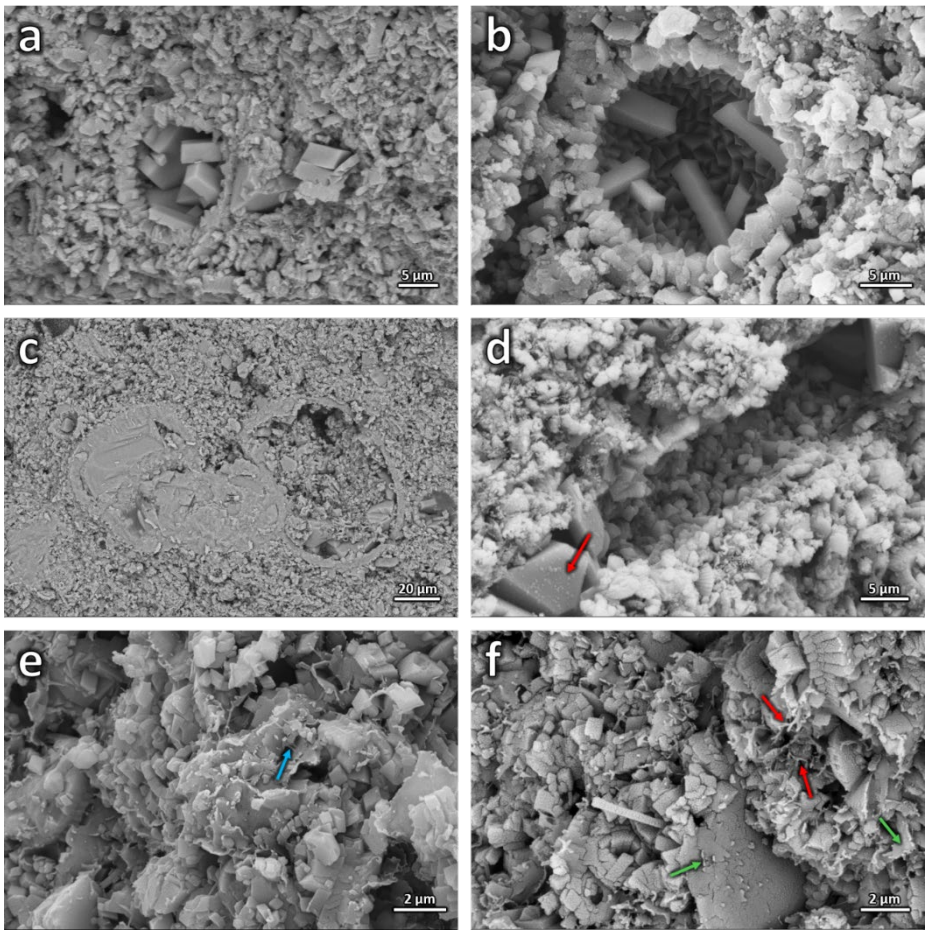

Figure 3: Cryo-SEM micrographs of waterflooded and unflooded reservoir core plug from well 3: a - new calcite crystals precipitated inside foraminifer cavity and inside an homogenous matrix (waterflooded sample); b - new calcite crystals precipitated inside cavity of well-preserved foraminifer test (unflooded sample); c – foraminifer chambers entirely filled with calcite or cocolith debris (waterflooded sample); d - cavity left after leaching of sponge spicule, with new calcite crystal growth (red arrow, waterflooded sample)); e – inhomogeneous unflooded sample with bridge of acicular illite joining flakes (blue arrow); f - inhomogeneous unflooded sample (same as featured in 4e) with authigenic acicular illite (red arrows) and smectitic clays (green arrows).

4.3 Backscatter electron analysis of thin sections

4.3.1 Reservoir samples

Further SEM and BSED analyses of thin sections reveal a similar mineral content in reservoir wells 1, 2 and 4 as seen in cryo-SEM analyses of well 3 cores. Besides calcite as the main constituent, dolomite ($CaMg(CO_2)_3$) is present in all reservoir wells, and in both formations, regardless of the flooding status (flooded at either hot or cold temperature, or unflooded). It appears both as new crystals, precipitated *in-situ*, with an ankerite ($CaFe(CO_2)_3$) rim (Figure 4a) along fractures, stylolite seams, or in pores, and as cement filling of fossils.

Veins and fractures are often calcite-cemented, but a reworked material consisting of brecciated calcite fragments, quartz, kaolinite and dolomite crystals sometimes line the fracture walls, or even fill the fracture apertures (Figure 4b). This represents the dark, opaque material that could not be identified by optical microscopy. Further, kaolinite and quartz often occur in both inter- and intraparticle pore spaces.

Framboidal pyrite (Figure 4c) is also common in all reservoir cores, often in residual stylolite seams, veins and fractures (Figure 4d) or as scattered crystals.

Apatite is here mostly linked to vertebrate remains (fish bones, scales, teeth) but occurs also as primary, detrital phase. Muscovite, biotite and albite are present as minute authigenic crystals in interparticle pore spaces. Sphalerite incapsulated in pyrite (Figure 4c), fluorite precipitates in cavities, and cassiterite, minerals associated with hydrothermal activity (Howie et al, 1992) appear in several of the thin sections.

4.3.2 Non-reservoir samples

The non-reservoir samples reveal similarities to their reservoir counterparts in terms of the faunal content, texture, mineral assemblage, and relative mineral proportions. Pelagic foraminifers are present, their chambers can be empty, but often are filled (partially or entirely) with precipitated calcite crystals (Figure 4e).

Analysed thin sections of non-reservoir cores did not contain dolomite. Re-worked material consisting of quartz and kaolinite, similar to what was observed in reservoir samples is present in veins and pore spaces in samples from wells 7, 8 and 9. This material contains magnesium, but it is not associated with dolomite, but rather associated to an aluminosilicate phase (Figure 4f).

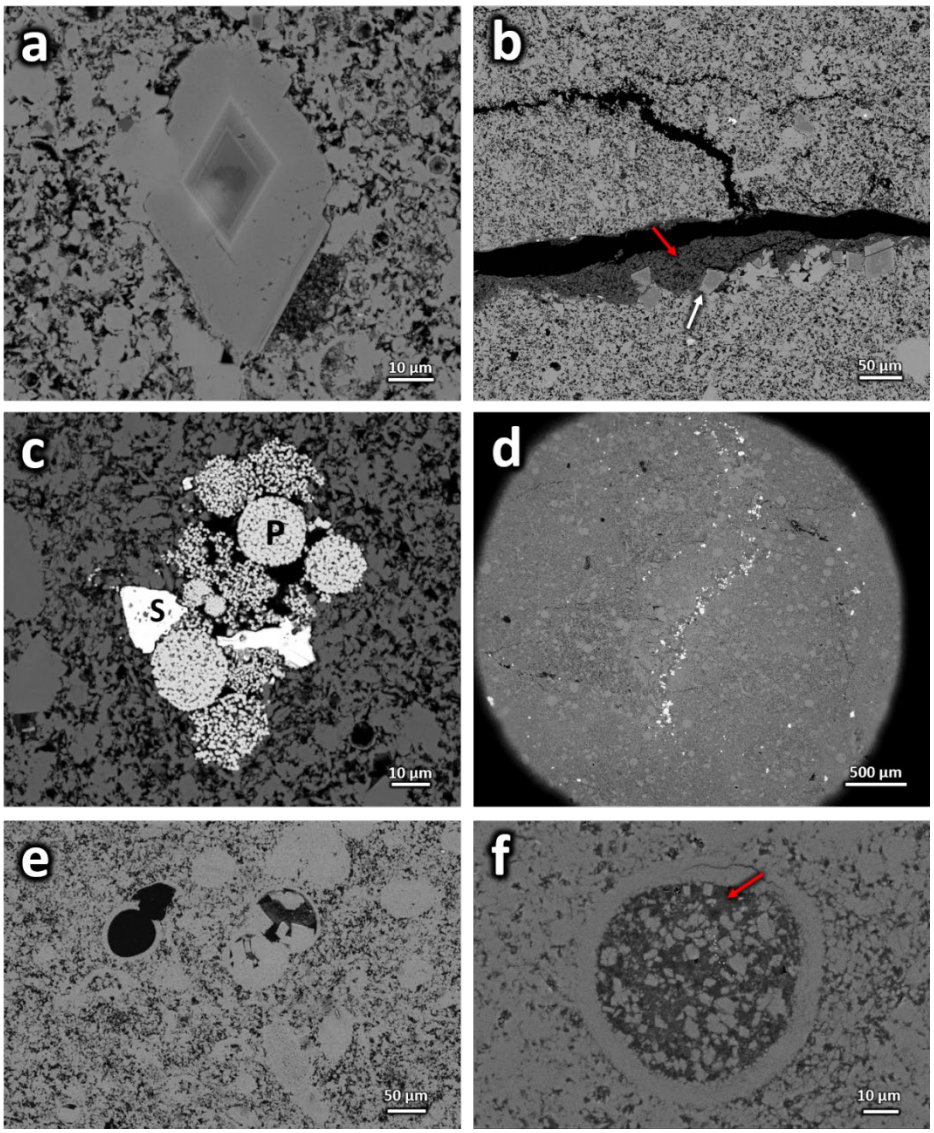

Figure 4: BSE micrographs of a – secondary dolomite crystal with light ankerite rim (unflooded sample, well 3); b – kaolinite (red arrow) and in-situ dolomite crystals (white arrow) along fracture walls(unflooded sample, well4); c – framboidal pyrite (P) and (S) sphalerite (unflooded sample, well 4); d – bright pyrite along stylolites (cold waterflooded sample, well 1); e – foraminifers from empty to fully cemented with calcite in coccolith matrix (well 8); f – foraminifer filled with aluminosilicate phase (red arrow, well 9).

4.4 X-ray diffraction of bulk and insoluble residue samples

The measurement covers only bulk and insoluble residue samples from wells 1 – 5.

Besides the high calcite content, whole-rock x-ray diffraction (XRD) scans confirm quartz as an accessory mineral in all reservoir samples. None of the silica content is related to opal. The restricted mineral assemblage is similar in all reservoir samples, both unflooded and waterflooded, but their relative abundance varies as follows:

Well 1

Samples at the top of the succession (cold-waterflooded) contain 90 – 95 % calcite, with quartz varying between 5 – 8 %. The samples contain traces of dolomite (or ankerite), phylosilicates and halite. Samples that were flooded at high temperature contain the same calcite proportion as the cold-waterflooded samples; the non-carbonate fraction consists of quartz (7 – 8 % of the bulk rock) and traces of 7 Å (d) mineral such as kaolinite or chlorite. The unflooded samples contain a higher amount of calcite (close to 100 %) than the flooded samples. Quartz is the only non-carbonate mineral detected and the highest amount (3 %) is found in one of 6 unflooded samples, other samples only showing scarce or traces of quartz.

Well 2

Besides 2 samples, all measured samples from well 2 contain approximately 100 % calcite and traces of dolomite. These two exceptions contain 88 % and 90 % calcite, and respectively 12 % and 10 % non-carbonate minerals. The 10% siliciclastic fraction consists of 92 % quartz and 8 % of clay minerals such as chlorite and smectitic clays (mixed layer clays mostly) and traces of hematite. The siliciclastic fraction of the lowest stratigraphic sample in this well has less amount

of quartz (65 %) and 18.6 % of clay minerals (chlorite and smectitic, mixed layer) and minor barite as well as analcime.

Well 3

All samples contain dominant calcite (85 – 90 %) along with quartz (10 – 15 %) and traces of dolomite or ankerite, halite and phyllosilicates. In the siliciclastic fraction quartz is the dominant phase (67.4 % to 85.2 %) along with clays and micas (11.2 % to 32.1 %) and other minerals such as plagioclase (in both waterflooded and unflooded samples) and amphibol. Clays are mostly smectite and smectitic mixed layer clays (illite-smectite I/S and chlorite-smectite C/S), illite, chlorite and kaolinite (the two latter identified in 4 out of 5 measured samples).

Well 4

The eight unflooded samples from well 4 contain 94 – 98 % calcite with minor quartz. Three of these also contain scarce to traces of dolomite (and/or ankerite), and scarce halite and minor barite. The siliciclastic fraction of the highest laying unflooded sample is composed of mainly phyllosilicate minerals, mostly clay minerals dominated by smectitic minerals (most likely mixed layer -ML- clays I/S and chlorite/smectite), kaolinite, traces of chlorite associated with abundant quartz and scarce amounts of other minerals such as plagioclase, gibbsite, gypsum and halite.

The waterflooded samples contain dominant calcite (approximately 95 – 98 %) and scarce quartz and dolomite (and/or ankerite); halite is also noticeable. The siliciclastic fraction of the highest laying waterflooded sample is dominated by quartz with minor clay minerals (mostly smectitic, mixed layers, and minute kaolinite), rare plagioclase and other minerals like fluorapatite and hollandite or proto-enstatite could be identified. One of the waterflooded samples on the other hand has a different assemblage: dominant clay minerals

(clinochlore and smectitic and mixed layer clays along with minor kaolinite), associated with quartz minor plagioclase.

Well 5

The four measured samples from the top of the succession in this well contain approximately 77 – 79 % of calcite, 17 – 18 % of quartz and scarce dolomite (and/or ankerite), kaolinite and halite. The rest of the samples are all quite similar: almost entirely consisting of calcite with ≤2 % of quartz and traces of dolomite.

4.5 Whole-rock Geochemistry

Major, minor and trace element concentrations listed in Tables 3-5 are valuable indicators for key aspects such as depositional environments and diagenetic overprint.

Major element geochemistry of the whole rock analysis from all wells shows a large variation in the silica (SiO_2) content with values ranging from 0.3 % up to 20 %. Samples with higher silica content than 10 % are arbitrarily classified as marl and marked in bold in Tables 3 and 4, while those with silica content between 5 and 10 % are classified as marly chalk and marked in italics. Table 3 shows selected element concentrations from wells 1-5 containing exclusively reservoir samples and includes information of their flooding status. The elemental concentrations for reservoir and non-reservoir samples from wells 6-11 are shown in Table 4. Element concentrations of insoluble residue from samples in well 3 are listed in Table 5.

Table 3: Major, minor and trace element concentrations in samples from reservoir wells 1-5; Fm – formation; dl - detection limit; bdl - below detection limit; WF - waterflooded (c-cold, h-hot); UF – unflooded; italics – marly chalk; bold – marl

	Flooding status	Fm	SiO_2 %	Al_2O_3 %	Fe_2O_3 %	MgO %	CaO %	Rb PPM	Sr PPM	Zr PPM	Y PPM	Ho PPM	ΣREE PPM
		dl	**0.01**	**0.01**	**0.01**	**0.01**	**0.01**	**0.1**	**0.5**	**0.1**	**0.1**	**0.02**	
Well 1	WF-C	EKO	1.83	0.11	0.17	0.83	51.41	1.6	1242.7	1.7	6.5	0.15	17.04
		EKO	4.78	0.29	0.29	1.23	48.91	2.1	1124.1	3.3	9.4	0.23	28.19
		EKO	2.75	0.12	0.21	0.75	51.30	1.5	1213.1	1.9	7.1	0.16	18.74
		EKO	2.39	0.08	0.11	0.52	52.01	1.2	1328.9	1.6	5.6	0.14	15.58
		EKO	2.19	0.13	0.38	0.48	52.60	1.2	1388.7	1.8	10.2	0.27	29.28
	WF-H	*TOR*	*8.67*	*0.69*	*0.22*	*0.25*	*47.22*	*3.1*	*1097.0*	*4.9*	*13.3*	*0.35*	*45.12*
		TOR	*6.97*	*0.45*	*0.31*	*0.26*	*48.52*	*1.5*	*1188.2*	*4.6*	*14.8*	*0.38*	*46.74*
		TOR	*5.06*	*0.46*	*0.15*	*0.22*	*49.77*	*1.8*	*1249.3*	*3.2*	*13.5*	*0.35*	*40.87*
	WF	TOR	3.14	0.25	0.17	0.23	51.34	0.6	1246.8	2.9	10.6	0.30	30.39
		TOR	3.66	0.30	0.16	0.22	50.70	1.5	1335.7	2.3	12.0	0.30	33.46
	UF	TOR	0.41	0.02	0.06	0.20	51.37	0.7	1677.2	0.8	6.9	0.13	13.66
		TOR	0.39	0.03	0.06	0.20	50.93	0.6	1562.9	0.9	5.6	0.10	9.93
		TOR	0.45	0.03	0.07	0.21	49.89	0.6	1604.3	1.2	5.6	0.11	11.70
		TOR	2.53	0.20	0.12	0.24	48.22	1.4	1357.4	3.2	9.2	0.22	26.24
		TOR	2.16	0.30	0.15	0.25	48.54	1.0	1275.7	3.5	10.1	0.24	29.79
		TOR	1.01	0.11	0.07	0.22	50.39	0.1	1496.2	1.8	7.0	0.16	15.01
		TOR	0.69	0.08	0.07	0.22	50.29	0.1	1443.6	1.4	6.6	0.14	18.95
		TOR	0.68	0.06	0.09	0.21	50.08	0.7	1483.6	1.4	6.0	0.12	13.54
		TOR	0.43	0.03	0.07	0.19	50.89	0.6	1490.1	0.9	5.4	0.13	10.09
Well 2	WF-C	**EKO**	**15.34**	**1.21**	**0.33**	**0.23**	**42.49**	**5.0**	**1138.0**	**9.1**	9.9	**0.30**	**46.32**
		EKO	*9.59*	*1.44*	*0.48*	*0.38*	*45.17*	*4.9*	*1062.5*	*9.0*	14.4	*0.42*	*62.81*
		EKO	4.28	0.31	0.14	0.38	49.20	2.4	921.3	8.2	7.9	0.19	20.78
		EKO	**11.36**	**0.39**	**0.23**	**0.40**	**46.56**	**1.5**	**1120.0**	**4.9**	12.1	**0.35**	**41.90**
		EKO	**19.22**	**0.53**	**0.27**	**0.28**	**43.00**	**1.5**	**998.3**	**5.3**	12.5	**0.35**	**53.75**
		EKO	1.83	0.22	0.07	0.27	51.10	0.6	1094.8	4.4	10.7	0.27	27.68
		EKO	**19.22**	**0.53**	**0.27**	**0.28**	**43.00**	**1.5**	**998.3**	**5.3**	12.5	**0.35**	**53.75**
		EKO	1.00	0.11	0.05	0.27	53.61	0.2	1444.3	3.6	11.8	0.28	26.02
		EKO	1.34	0.17	0.09	0.26	51.11	1.1	1329.9	2.2	11.5	0.28	29.74
		TOR	2.03	0.17	0.06	0.40	50.86	0.7	1268.3	4.0	10.2	0.21	23.62
		TOR	1.61	0.17	0.07	0.34	50.87	0.2	1219.1	1.7	8.9	0.21	25.29
		TOR	1.65	0.14	0.08	0.44	50.77	0.2	1484.9	2.6	9.6	0.22	23.98
		TOR	1.14	0.13	0.07	0.45	52.95	0.2	1505.0	1.7	9.5	0.21	21.82
Well 3	UF	**EKO**	**10.81**	**1.69**	**0.34**	**0.41**	**46.17**	**6.5**	**1197.0**	**6.5**	**13.6**	**0.42**	**55.28**
		EKO	*6.81*	*0.44*	*0.22*	*0.27*	*49.66*	*2.4*	*1268.1*	*2.8*	*11.3*	*0.28*	*40.27*
		EKO	*8.10*	*0.55*	*0.22*	*0.26*	*47.96*	*3.2*	*1097.4*	*4.7*	*10.2*	*0.27*	*39.29*
		EKO	*8.02*	*0.58*	*0.27*	*0.26*	*48.06*	*3.2*	*1161.9*	*4.2*	*11.3*	*0.31*	*39.82*
		EKO	*8.90*	*0.58*	*0.24*	*0.26*	*47.69*	*3.2*	*1152.9*	*4.4*	*12.1*	*0.33*	*43.18*
		EKO	*8.93*	*0.69*	*0.28*	*0.28*	*47.62*	*3.4*	*1145.3*	*4.9*	*11.9*	*0.33*	*46.15*
	WF	*EKO*	*9.04*	*0.58*	*0.22*	*0.26*	*47.85*	*3.2*	*1144.0*	*4.6*	*12.1*	*0.35*	*43.95*
		EKO	*8.81*	*0.57*	*0.24*	*0.26*	*47.89*	*3.1*	*1113.2*	*4.3*	*10.8*	*0.32*	*42.30*
		EKO	*9.26*	*0.63*	*0.23*	*0.27*	*47.80*	*3.3*	*1147.1*	*5.0*	*11.9*	*0.33*	*45.63*
		EKO	*9.55*	*0.68*	*0.35*	*0.28*	*47.63*	*3.3*	*1203.1*	*4.9*	13.2	*0.37*	*47.47*
		EKO	*8.99*	*0.65*	*0.23*	*0.27*	*48.24*	*3.6*	*1159.7*	*5.1*	*12.6*	*0.33*	*45.11*
		EKO	*8.75*	*0.64*	*0.24*	*0.27*	*48.37*	*3.4*	*1166.7*	*4.6*	*11.7*	*0.34*	*46.11*
Well 4	WF	EKO	3.72	0.25	0.23	0.34	51.72	1.5	1542.5	2.5	12.0	0.30	34.76
		EKO	2.43	0.62	0.25	0.31	50.85	2.9	1490.4	7.3	16.3	0.47	58.25
		EKO	2.72	0.67	0.61	0.33	51.28	3.3	1572.2	6.7	17.2	0.47	63.09
	UF	EKO	2.27	0.24	0.20	0.38	50.96	1.7	1529.6	3.1	11.7	0.29	32.44
		EKO	2.51	0.21	0.19	0.36	50.61	1.6	1391.3	2.5	10.6	0.25	29.58
		EKO	2.77	0.29	0.16	0.36	50.56	0.8	1288.1	2.7	10.3	0.26	29.38
		EKO	1.02	0.12	0.19	0.45	52.57	0.9	1483.8	1.4	7.6	0.20	20.19
		EKO	1.23	0.08	0.15	0.45	50.84	0.8	1205.1	1.3	7.0	0.16	17.08
		EKO	1.24	0.09	0.18	0.48	49.77	0.8	1219.4	1.5	6.7	0.15	17.25
		EKO	1.10	0.08	0.15	0.42	50.28	0.8	1162.2	1.4	6.5	0.17	17.00
		EKO	1.30	0.08	0.14	0.42	46.34	0.9	1101.0	1.2	7.1	0.20	17.76
		EKO	2.71	0.26	0.28	0.56	47.79	0.9	1065.6	4.0	10.3	0.29	36.22
		EKO	2.75	0.22	0.29	0.55	47.94	1.5	1177.2	3.3	9.2	0.25	31.12
Well 5	UF	**EKO**	**17.78**	**0.78**	**0.51**	**0.60**	**41.30**	**4.5**	**835.1**	**9.7**	**11.2**	**0.31**	**41.91**
		EKO	*9.48*	*0.35*	*0.56*	*0.66*	*47.45*	*2.0*	*1042.0*	*5.8*	*11.5*	*0.31*	*40.47*
		EKO	**15.51**	**0.63**	**0.48**	**0.59**	**43.45**	**3.3**	**789.9**	**7.8**	**11.6**	**0.31**	**40.74**
		EKO	**16.48**	**0.67**	**0.52**	**0.65**	**42.11**	**3.9**	**851.7**	**10.2**	**11.6**	**0.31**	**41.00**
		EKO	2.58	0.18	0.21	0.72	51.90	0.8	1298.3	3.3	11.7	0.32	41.27
		EKO	2.29	0.17	0.17	0.65	52.87	0.5	1300.8	2.7	11.7	0.32	41.54
		EKO	2.50	0.17	0.16	0.67	52.54	0.6	1310.9	3.0	11.8	0.32	41.80
		EKO	2.54	0.18	0.16	0.65	52.52	0.5	1321.6	2.7	11.8	0.32	42.07
		TOR	2.13	0.22	0.14	0.50	50.90	0.8	1083.3	3.7	11.9	0.32	42.33
		TOR	2.05	0.20	0.14	0.90	51.59	0.7	1019.5	3.3	11.9	0.32	42.60
		TOR	2.09	0.24	0.20	0.52	52.71	0.7	1149.0	3.0	11.9	0.32	42.87
		TOR	2.16	0.22	0.12	0.50	52.02	0.8	1148.5	4.2	12.0	0.33	43.13

Table 4: Major, minor and trace element concentrations in samples from wells 6 – 11; HC – hydrocarbon; NON-R – non-reservoir samples; RES – reservoir samples; dl - detection limit; bdl - below detection limit; italics – marly chalk; bold – marl

	HC content	Fm	SiO_2 %	Al_2O_3 %	Fe_2O_3 %	MgO %	CaO %	Rb PPM	Sr PPM	Zr PPM	Y PPM	Ho PPM	ΣREE PPM
		dl	**0.01**	**0.01**	**0.01**	**0.01**	**0.01**	**0.1**	**0.5**	**0.1**	**0.1**	**0.02**	
Well 6	NON-R	**EKO**	**11.25**	**0.36**	**0.27**	**0.42**	**47.64**	**1.5**	**1335.5**	**3.7**	**6.5**	**0.17**	**21.75**
		EKO	2.72	0.25	0.2	0.29	52.15	1.2	1449.9	2.9	10.9	0.23	41.73
	RES	EKO	4.14	0.21	0.02	0.40	51.27	1.3	1342.3	7.8	7.9	0.22	22.51
		TOR	1.07	0.10	0.23	0.28	53.98	0.4	1659.9	2.3	9.9	0.29	27.18
		TOR	1.40	0.20	0.09	0.34	54.09	1.1	1576.6	4.4	10.2	0.25	27.54
		TOR	1.60	0.21	0.02	0.33	53.94	0.9	1699.0	5.1	9.0	0.20	24.94
		TOR	1.33	0.30	0.14	0.33	53.96	1.2	2150.2	2.1	9.9	0.25	29.01
		TOR	1.40	0.29	0.02	0.31	54.28	1.4	1847.2	3.9	8.4	0.22	25.00
Well 7	NON-R	**EKO**	**21.49**	**3.59**	**1.45**	**0.72**	**38.41**	**23.5**	**1036.0**	**27.8**	**13.2**	**0.42**	**75.45**
		EKO	**14.35**	**1.74**	**0.75**	**0.39**	**44.41**	**11.4**	**1200.8**	**13.7**	**11.3**	**0.33**	**54.64**
		EKO	**25.13**	**2.48**	**0.99**	**0.48**	**37.97**	**12.8**	**1013.8**	**15.5**	**16.8**	**0.56**	**90.24**
		EKO	**10.92**	**0.53**	**0.26**	**0.17**	**47.35**	**3.2**	**1177.6**	**4.7**	**9.4**	**0.27**	**32.53**
		EKO	**19.45**	**1.69**	**0.62**	**0.37**	**43.48**	**7.5**	**1097.9**	**8.7**	**13.9**	**0.42**	**70.30**
		EKO	**10.32**	**0.29**	**0.27**	**0.21**	**48.48**	**1.8**	**1255.6**	**3.1**	**8.3**	**0.24**	**28.96**
		EKO	**16.96**	**1.22**	**0.51**	**0.30**	**44.73**	**6.4**	**1228.2**	**9.1**	**11.3**	**0.34**	**52.21**
		EKO	*8.88*	*0.94*	*0.33*	*0.20*	*47.83*	*4.8*	*1088.0*	*7.7*	*9.5*	*0.27*	*38.73*
		EKO	*5.23*	*0.59*	*0.25*	*0.16*	*50.47*	*2.7*	*1214.2*	*4.6*	*8.3*	*0.23*	*30.46*
		EKO	*5.95*	*0.54*	*0.23*	*0.17*	*50.01*	*2.6*	*1147.4*	*3.9*	*8.7*	*0.22*	*30.26*
		EKO	**11.90**	**1.16**	**0.38**	**0.26**	**46.78**	**6.2**	**1209.5**	**7.9**	**13.3**	**0.36**	**51.21**
		EKO	**11.40**	**1.45**	**0.44**	**0.30**	**47.97**	**8.0**	**1181.0**	**9.4**	**13.8**	**0.43**	**61.39**
		EKO	**22.21**	**3.09**	**1.01**	**0.71**	**39.02**	**14.0**	**1109.8**	**20.4**	**22.2**	**0.76**	**116.49**
		EKO	**15.74**	**0.72**	**0.47**	**0.27**	**45.12**	**2.7**	**1430.3**	**7.4**	**19.9**	**0.56**	**80.20**
		EKO	**34.95**	**1.94**	**0.74**	**0.46**	**33.13**	**8.5**	**1128.8**	**11.9**	**18.5**	**0.55**	**85.41**
		EKO	**37.23**	**3.70**	**1.41**	**0.77**	**29.22**	**19.2**	**928.1**	**24.5**	**11.0**	**0.41**	**74.68**
		EKO	**13.96**	**0.75**	**0.50**	**0.36**	**46.26**	**4.7**	**1501.1**	**6.8**	**13.8**	**0.45**	**56.99**
		EKO	**11.62**	**1.72**	**0.81**	**0.50**	**45.79**	**9.1**	**1572.9**	**10.3**	**15.0**	**0.43**	**69.61**
		EKO	**22.13**	**3.44**	**1.65**	**0.84**	**38.21**	**17.5**	**1349.5**	**21.8**	**18.6**	**0.62**	**101.89**
	RES	**EKO**	**34.83**	**1.64**	**0.47**	**0.35**	**33.70**	**3.8**	**1343.9**	**7.2**	**9.4**	**0.29**	**49.15**
		EKO	**39.92**	**6.34**	**1.00**	**1.08**	**25.47**	**45.1**	**1207.0**	**61.2**	**28.8**	**0.91**	**170.43**
		EKO	**13.60**	**1.72**	**1.22**	**0.68**	**46.23**	**6.7**	**1130.2**	**7.8**	**15.7**	**0.49**	**60.56**
		EKO	**10.34**	**1.00**	**0.22**	**0.42**	**48.30**	**3.1**	**1185.6**	**4.4**	**8.3**	**0.27**	**33.39**
		EKO	*9.71*	*0.56*	*0.15*	*0.24*	*48.72*	*2.8*	*1147.0*	*5.7*	*11.0*	*0.29*	*39.53*
		TOR	**10.08**	**0.97**	**0.27**	**0.28**	**48.59**	**5.8**	**1183.0**	**7.1**	**14.1**	**0.40**	**56.69**
		TOR	*6.31*	*0.54*	*0.17*	*0.23*	*50.89*	*2.4*	*1193.0*	*5.7*	*10.6*	*0.29*	*41.68*
		TOR	2.80	0.34	0.09	0.21	53.19	0.8	1517.3	1.8	10.3	0.26	31.55
		TOR	4.09	0.30	0.08	0.19	52.18	1.0	1325.6	2.0	10.2	0.26	32.24
		TOR	3.08	0.25	0.07	0.22	53.13	1.2	1523.7	2.5	9.7	0.24	28.22
		TOR	3.33	0.28	0.08	0.20	52.48	1.1	1525.9	2.0	11.6	0.28	32.59
		TOR	3.35	0.30	0.08	0.21	52.68	1.1	1463.0	9.6	11.3	0.30	31.64
		TOR	3.09	0.19	0.11	0.20	52.32	1.0	1377.8	6.0	12.7	0.31	34.48
		TOR	2.82	0.26	0.08	0.20	53.37	1.3	1400.3	2.7	13.1	0.35	38.50
		TOR	0.60	0.05	0.03	0.20	54.38	0.1	1732.6	0.7	8.4	0.21	18.60
		TOR	1.22	0.11	0.07	0.73	54.32	0.6	1407.6	1.4	9.3	0.23	23.61
		TOR	2.00	0.14	0.11	0.23	52.50	1.3	1309.2	2.8	8.1	0.17	30.12
		TOR	1.06	0.16	0.08	0.35	53.96	0.9	1436.4	1.6	8.9	0.19	24.13
		TOR	1.22	0.20	0.08	0.33	53.94	1.2	1401.4	2.5	9.3	0.23	27.32
		TOR	0.87	0.23	0.09	0.22	54.05	1.2	1329.4	2.2	9.5	0.26	28.60
		TOR	0.99	0.21	0.08	0.23	54.40	1.3	1348.2	1.5	8.5	0.21	23.74
		TOR	1.83	0.47	0.14	0.31	54.12	2.5	1283.1	5.5	11.8	0.33	37.00
		TOR	1.59	0.36	0.09	0.26	53.74	2.0	1290.6	2.3	10.0	0.26	30.68
		TOR	2.44	0.30	0.07	0.32	53.11	2.1	924.4	2.6	8.0	0.89	25.81
		TOR	2.43	0.26	0.10	0.39	53.98	2.0	838.4	3.6	6.8	0.16	22.19
		TOR	2.34	0.34	0.10	0.25	53.33	2.5	1116.5	2.3	8.0	0.20	24.93
		TOR	2.56	0.23	0.11	0.26	52.51	1.6	917.5	6.3	7.3	0.20	21.29
		TOR	2.88	0.56	0.14	0.33	53.18	3.6	1082.2	5.0	10.9	0.32	40.61
Well 8	NON-R	TOR	2.28	0.62	0.10	0.33	53.13	1.5	934.9	2.6	9.0	0.24	29.77
		TOR	0.93	0.17	0.06	0.32	54.61	0.8	939.0	13.4	6.6	0.17	19.45
		TOR	0.93	0.17	0.09	0.33	53.74	0.6	1072.4	2.2	6.4	0.20	20.81
		TOR	0.92	0.16	0.07	0.32	54.38	0.8	846.4	2.0	6.2	0.17	17.99
		HOD	*6.04*	*0.58*	*0.19*	*0.38*	*50.79*	*2.2*	*1261.4*	*3.8*	*12.9*	*0.39*	*54.56*
		HOD	4.76	0.43	0.21	0.34	51.46	2.8	1634.0	4.4	11.8	0.33	50.12
		HOD	3.98	0.61	0.23	0.36	51.62	4.2	1125.1	8.7	11.9	0.36	50.42
		HOD	3.54	0.43	0.18	0.38	51.74	2.4	1103.5	4.1	10.9	0.27	43.74
Well 9	NON-R	TOR	2.17	0.37	0.16	0.30	53.35	1.3	651.8	3.2	8.7	0.21	27.72
		TOR	**14.74**	**1.63**	**0.71**	**0.52**	**44.44**	**12.0**	**900.5**	**19.0**	**15.9**	**0.50**	**81.85**
		TOR	*5.49*	*0.67*	*0.25*	*0.27*	*50.48*	*3.2*	*846.5*	*7.2*	*15.3*	*0.48*	*65.87*
		TOR	4.97	0.93	0.36	0.32	51.18	4.5	1101.2	6.5	14.8	0.48	67.58
Well 10	RES	TOR	1.33	0.17	0.15	0.22	51.55	0.8	819.8	4.5	10.6	0.24	23.09
		TOR	2.22	0.44	0.17	0.25	50.65	2.4	742.6	2.6	9.2	0.19	21.90
	NON-R	TOR	1.09	0.20	0.10	0.29	53.97	1.0	893.9	8.1	5.1	0.12	15.65
		HOD	*6.22*	*0.80*	*0.27*	*0.41*	*50.55*	*4.1*	*950.4*	*5.0*	*13.4*	*0.46*	*63.90*
		HOD	2.24	0.33	0.14	0.28	53.16	1.9	870.6	6.8	9.1	0.27	33.92
Well 11	NON-R	TOR	1.55	0.20	0.11	0.33	52.85	1.0	770.7	5.0	6.9	0.16	19.52
		TOR	0.90	0.14	0.07	0.31	53.77	0.7	750.8	4.4	5.2	0.15	15.65
		TOR	0.99	0.14	0.13	0.32	53.18	0.8	865.8	1.5	5.2	0.18	16.94

Table 5: Major, minor and trace element concentrations in samples of insoluble residue from well 3; dl - detection limit; bdl - below detection limit; WF - waterflooded; UF - unflooded

	Flooding status	Fm		SiO2 %	Al2O3 %	Fe2O3 %	MgO %	CaO %	Rb PPM	Sr PPM	Zr PPM	Y PPM	Ho PPM	ΣREE PPM
			dl	**0.01**	**0.01**	**0.01**	**0.01**	**0.01**	**0.1**	**0.5**	**0.1**	**0.1**	**0.02**	
IR-Well 3	UF	EKO		74.96	8.73	1.58	1.16	1.18	39.00	96.6	37.80	24.30	0.80	139.82
		EKO		66.87	4.36	0.67	0.61	4.34	20.40	187.2	24.20	26.40	0.78	115.76
		EKO		66.78	5.91	1.02	0.82	3.53	25.20	166.2	32.90	30.50	0.91	145.58
	WF	EKO		72.04	4.88	0.70	0.65	1.43	24.10	119.4	31.20	29.50	0.94	135.37
		EKO		72.07	5.40	0.75	0.69	1.36	25.80	113.5	33.80	29.50	0.91	140.89

Wells 1, 2, 4 and 6 carry mainly clean chalk and only very few marls at the top of the sampled range. However, well 3 has consistently higher silica abundances between 5 and 10 %, representing between 67 -75 % of the non-carbonate phase (Table 5). Wells 2, and 5 contain a large amount of clastic material in the Ekofisk Formation but in the underlying Tor Formation clean chalk occurs. Well 7 shows this change at a deeper level, at the top of the Tor Formation.

MgO is slightly enriched with values above 0.4 % in only some chalk samples and in such cases this correlates with an enriched silica content pointing to clay minerals or other clastic phases. However, in wells 4 and 5 MgO is clearly more abundant in all lithotypes even in clean chalks, but does not correlate with silica.

No other major element shows any significant abundance in chalk samples. In marls and marly chalk (in bold, respectively italics in Table 3) Al_2O_3 and Fe_2O_{3t} are enriched together with silica pointing to feldspar and phyllosilicate abundance.

Clastic input can be monitored by certain trace elements, like rubidium (Rb) and zirconium (Zr), which occur solely in clastic material and are absent in carbonates. Their abundance together with Rare Earth Elements (REE), which are extremely depleted in all chemical sediments, would, when enriched, point to phyllosilicates or apatite, both enriched in the latter. Rb and Zr values in chalk samples are mostly below 2 % of the typical values

for the Post Archaean Australian Shale (PAAS; after Taylor and McLennan 1981) with threshold values of 4.2 ppm for Zr and 3.2 ppm for Rb (Frimmel, 2009). This applies to nearly all samples in the wells 1-7. Only in well 7 from the Ekofisk area some chalk samples are enriched in Zr, while this trend is very pronounced in all sampled wells 7 – 11 further North (Table 4).

The REE and yttrium (Y) concentrations normalized to the PAAS values reflect a general depletion of the REE by an average factor of 6 (Figures 5, 6). The enrichment in lanthanum (La), depletion of cerium (Ce) and a positive Y anomaly are a typical signature for influence of open marine seawater during precipitation of the carbonate (Bau and Dulski, 1996; Nozaki et al. 1997; Bau and Alexander, 2006). Shale-normalized REE plots of reservoir chalk samples (Figures 5; blue lines) and non-reservoir chalk samples (Figure 6; blue lines) have partly a typical pattern for seawater with a positive anomaly of La (calculated as 3xPr – 2xNd) and a pronounced positive Y anomaly.

At the same time, middle REE (Sm – Ho) should not be enriched in carbonates (Nozaki et al., 1997), and the only few chalk samples that show this feature also contain elevated Zr concentrations (6-7 ppm). Marly chalk samples (Figures 5, 6; yellow lines) generally

show a transition between typical REE pattern for chalk and a more enriched middle REE pattern for marls (Figures 5, 6; grey lines).

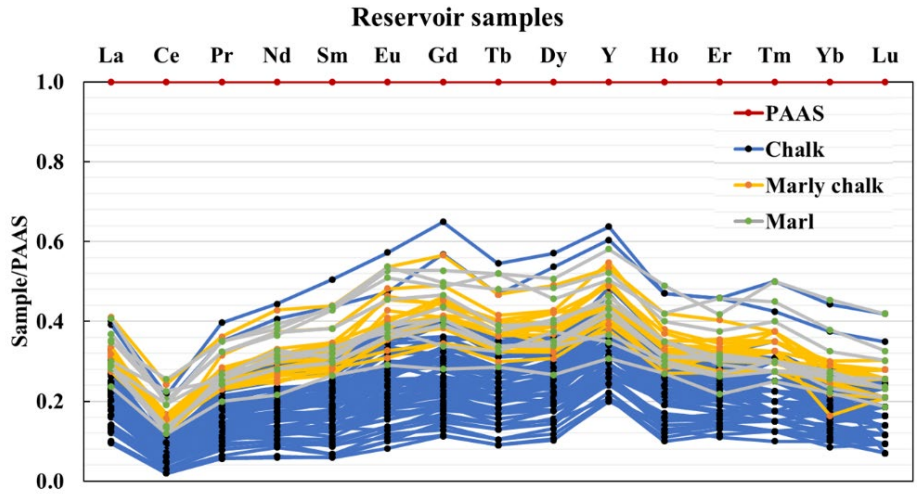

Figure 5: Shale normalized Yttrium and Rare Earth Element chemistry in selected reservoir chalk, whole rock samples categorized by amount of silica content: chalk (<5% silica, blue lines), marly chalk (5-10% silica, yellow lines) and marls (<10% silica grey lines)

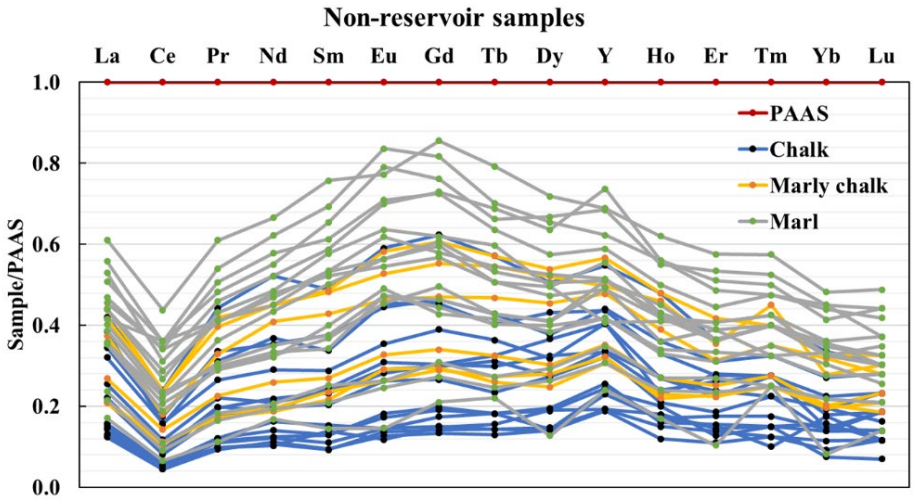

Figure 6: Shale normalized Yttrium and Rare Earth Element chemistry in selected non-reservoir chalk, whole rock samples categorized by amount of silica content: chalk (<5% silica, blue lines), marly chalk (5-10% silica, yellow lines) and marls (<10% silica grey lines)

Total REE (ΣREE) in chalk samples are mostly below 30 ppm and there are trends within the wells. Well 1 shows a variation between 10-33 ppm, so do samples from well 4 (17 – 36 ppm), while samples in wells 2, 6, 7 (18-30 ppm) and 5 (41 – 43 ppm) have a narrower range. Well 3 is affected by clastic material and among the marly chalks ΣREE varies immediately between 39 and 47 ppm. ΣREE from the northern wells 8, 9 and 10 are very variable (15-68 ppm) while samples from well 11 registered ΣREE well below 20 ppm. High Zr concentrations correlate partly with enriched ΣREE, but not in all samples.

Marly chalk and marl samples have mostly elevated ΣREE generally between 40 and 60 ppm, with one exception of a samples from well 7 which contains less than 30 ppm. Marls are significantly higher with values up to 200 ppm. The non-carbonate phase separates are comparable to shales with value close to, but often a slightly below a typical PAAS composition of 183 ppm (Taylor and McLennan, 1981).

Samples affected by clastic input are neglected when analyzing specific REE values for yttrium/holmium (Y/Ho) ratios. Y/Ho (Figure 7) average between 38 (Ekofisk Formation; blue markers) and 40 (Tor Formation; green markers) in the reservoir samples and appear slightly lower in the non-reservoir samples, averaging at 34 (Hod Formation, black markers) and 38 (Tor Formation, yellow markers). The same ratio calculated on the non-carbonate fraction composition (Table 5) has an average of 32, which is close to PAAS values. The reservoir chalk Y/Ho values are definitely below those from on-shore chalk at Stevns Klint (Denmark), but comparable to those from Liège quarry, Belgium (Andersen et al., 2018), Aalborg quarry (Denmark) and Mons basin (Belgium) (average 40, Minde et al., 2018). Several reservoir samples (Tor Formation) show higher values (over 50), which may point to either less clastic input or a less penetrative restricted fluid

flow that would have lowered the Y/Ho, or both. This will be studied in the nearest future intensively.

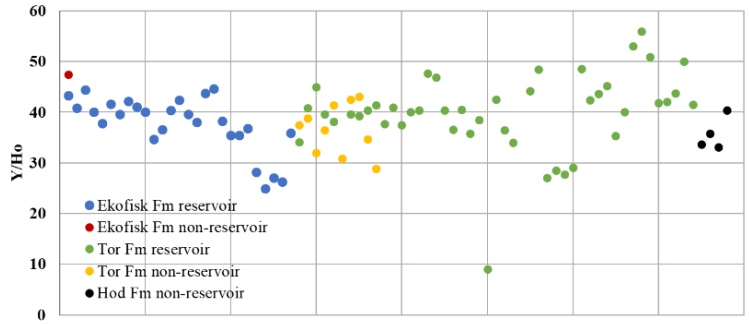

Figure 7: Y/Ho ratios in clean chalk (<5% silica content) whole-rock samples from all formations: the average for reservoir samples is 38 (Ekofisk Fm) and 40 (Tor Fm). Y/Ho ratios in non-reservoir samples are in average 38 (Tor Fm) and 34 (Hod Fm).

Abundances of sulfur (S) and barium (Ba) are interesting to notice, as well as strontium (Sr). The latter does not always correlate with increased CaO concentrations, which may point to a diagenetic overprint.

All other trace elements are depleted in the chalk samples, while several marly chalk samples show slight enrichments in Pb or Ni. Marls, like shales, or the insoluble residue samples from well 3, contain typical abundances of clastic sediments comparable to the typical Upper Continental crust (after McLennan et al., 2006).

4.6 Stable Isotope Geochemistry

Determined $\delta^{13}C$ values are comparable in all northern, non-reservoir samples, averaging at +1.7 ‰. Generally, the reservoir probes are slightly enriched in the heavy C isotope (i.e., higher $\delta^{13}C$), compared to the samples from the northern wells, averaging at +2.0 ‰, but remain within the expected range for unaltered Late Cretaceous chalk, between 1.0 and 2.5 $‰_{PDB}$ (Gradstein et al., 2012; Cramer et al., 2009).

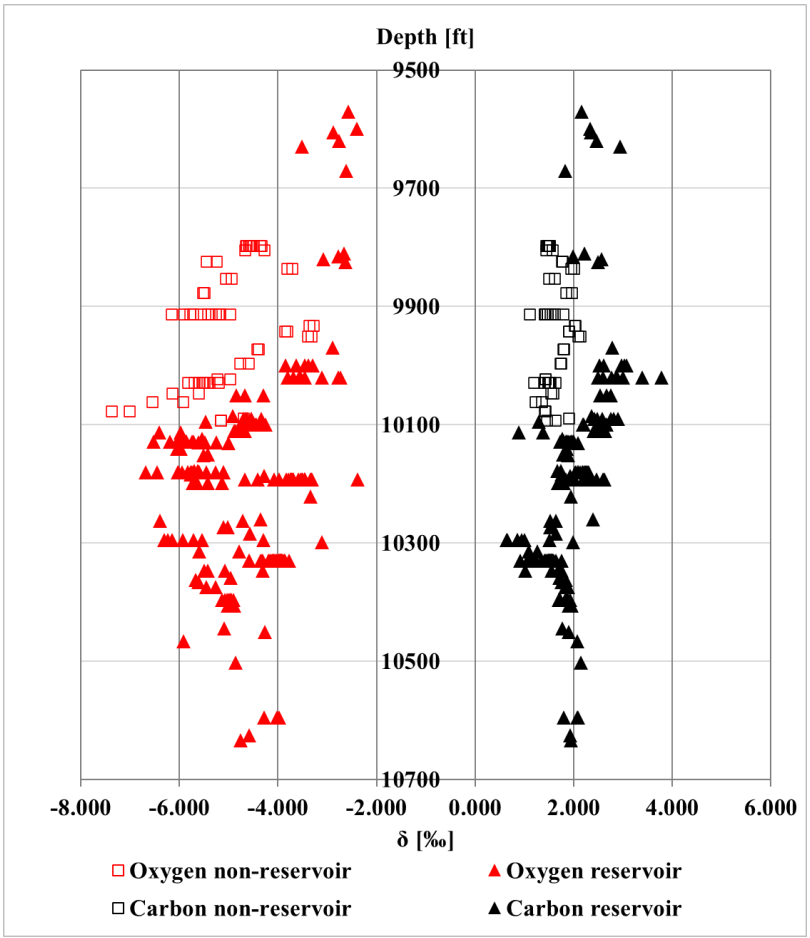

Figure 8: Oxygen (red markers) and carbon (black markers) stable isotope curves of reservoir (full triangles) and non-reservoir (empty squares) rock samples from shallower (top) to deeper layers (bottom)

Oxygen isotopic composition varies more than the carbon values in all wells, but it follows mainly a negative trend relative to burial depth (Figure 8, red markers). Reservoir samples register slightly higher $\delta^{18}O$ ratios than the northern well samples, -4.6 ‰ and -5.0 ‰ respectively, but are significantly lower than the estimated oxygen isotopic composition for Late Cretaceous chalk ranging between 0 and -1.5 ‰ (Scholle, 1977; Cramer et al., 2009).

Reservoir samples from the Ekofisk Formation (Figure 9; blue markers) stand out with higher oxygen isotope ratios (average of -4 ‰) compared to the rest of the samples (Figure 9). The $\delta^{13}C$ versus $\delta^{18}O$ cross plot shows sporadic positive covariations, typical for carbonate precipitation in marine/meteoric mixing zone (Allan and Matthews, 1982). Data points from Tor and Hod Formations, from both reservoir and non-reservoir wells scatter considerably and generally show stronger $\delta^{18}O$ disturbance than the Ekofisk reservoir samples.

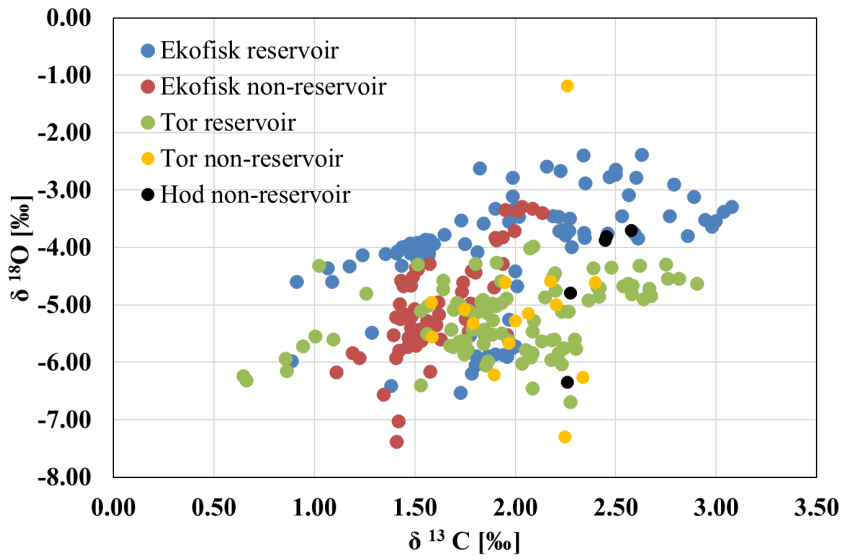

Figure 9: Cross-plot showing correlation between carbon and oxygen isotope ratios from reservoir and non-reservoir samples. Both reservoir (blue markers) and non-reservoir (red markers) from Ekofisk Formation show a brief positive linear correlation, while the rest of the data points scatter significantly.

5 Discussion

5.1 Petrology, mineralogy, and geochemistry

The optical petrography and SEM imaging revealed a sediment composition typical for Upper Cretaceous chalks, consisting of micritic carbonate matrix, microfossils and diverse but subordinated authigenic and detrital minerals. The deposition of coccolithosphores, the space between the whole and disintegrated calcite platelets, are the primary source of porosity that produces a good reservoir rock. The preserved calcite skeletons of foraminifers are efficient in enhancing the chalk porosity, as well as the void left after the dissolution of sponge spicules (Figures 2-4).

Another factor contributing to the high porosity and good permeability is the fracturing of the chalk as veins and interconnected crack networks. Further studies on the mechanical and chemical effects on porosity and permeability (e.g., grain coating, pressure conditions) can contribute to a more thorough description, but are not a part of this paper.

On the other hand, diagenetic processes reduce porosity, as often fractures, dissolved sponge spicules, and microfossils are entirely or partially filled by *in situ* precipitated calcite, or spar calcite cement. The stratigraphic lower reservoir chalk from Ekofisk Formation shows microfossils that are often deformed, or have collapsed walls, and filled with matrix material. This may be an effect of burial, or deformation related to tectonic activity, but based on the scarce geological information available, this cannot be evaluated. Nevertheless, compaction would normally reduce porosity in such a fragile rock. Hence, a process counteracting this geological process had to be present in early diagenetic phases (Scholle, 1977).

The geochemistry of the chalk samples (Tables 3, 4) showed, among the major elements, only minute enrichment in MgO in some samples and a typical limestone composition with low silica content. Quartz is the main non-carbonate phase with only few other silicates. Marly chalks and moreover marls are enriched in clastic material. However, no significant enrichments in any lithotype could be observed, which would point to a specific geological process, in terms of a changing depositional environment; the samples seem to be rather comparable. The existence of a higher clastic input may be related to tectonic movements and a short interruption of carbonate production. The latter can be caused by colder times and the former by exhumation of older clastic-dominated rock formations. However, no provenance studies have been made on the clastic material within chalk.

Nevertheless, chalks in the reservoir wells differ strongly in regards to the clastic contamination, with some wells only represented by marly chalks and marls within the Ekofisk Formation. The introduction of clastic material seems to start mostly at the bottom of the Ekofisk Formation and rarely already during deposition of the Tor Formation (Tables 3, 4). This variation is of utmost importance when modelling or estimating rock-fluid interactions in possible reservoirs.

Rare earth elements (REE) are sensitive monitors for a variation of geological aspects. The overall sum of REE for clean carbonates should be very low (close to the lower limit of detection) and higher values, like in this case, are an indication of terrestrial input and/or secondary fluid flow (Frimmel, 2009). Contamination with detrital materials, especially terrigenous clay minerals, can effectively alter REE signature patterns for marine deposits, increase the total REE (ΣREE) as well as the concentration of Zr, Th and Al (Frimmel, 2009).

Clastic input can undoubtedly be seen in the SEM, XRD and the whole-rock geochemistry. Besides kaolinite, the XRD, SEM-BSE-EDS

analyses showed a large variety of clay minerals and detrital grains. However, Al_2O_3 concentrations are low as such that future studies need to determine accurately the amount and type of clastic material in the different reservoirs or wells. Clays can possibly be introduced either by alteration of feldspar or as alteration product of volcanic glass, epiclastic material from explosive volcanism. As the main volcanic sources during the opening of the Atlantic Ocean were of mafic composition, subaerial explosive volcanism may have been rare to absent, and therefore the clays related to the alteration of glass are rather linked to sub-marine explosive processes and relicts of hyaloclastites.

Nevertheless, most of the chalk samples show typical geochemical patterns for limestones precipitates from seawater (Figures 5, 6). Y/Ho ratios, however, vary and mainly show a significant influence of non-seawater within the chalks (Bau, 1996). The origin of this fluid-flow and the timing of its circulation is unknown. The sparse appearance of secondary growth of minerals and low cementation points to an incomplete and only slight overprint.

The stable isotopic analyses of C and O show results typical for a marine depositional environment. Carbon isotope ratios align well with primary trends for Upper Cretaceous stages (Figure 10). Slightly lower values may be caused either by mixing of carbonate phases from different depositional environments, when the chalk is brecciated thus reworked, or by enrichment of organic carbon (i.e., higher ^{12}C) from meteoric origin, or they might reflect a colder environment, related to the water depth in which the carbonate precipitated. However, the narrow $\delta^{13}C$ variability compared to the $\delta^{18}O$ outrules strictly meteoric diagenesis and local positive C-O covariation suggests rather a marine-meteoric mixing zone (Allan and Matthews, 1982). The low Y/Ho ratios also point to the influence of meteoric/hydrothermal water and support this interpretation.

Oxygen isotopes on the other hand, are not primary, and considerable deviation from the Upper Cretaceous trends (i.e, 0 to -1.5 ‰) is seen in all samples. Previous studies showed that oxygen isotopes are subject to burial diagenesis, becoming increasingly negative with depth (Hudson, 1977; Scholle, 1977; Allan and Matthews, 1982), a trend seen here as well (Figure 8), although the alteration is not as severe, considering the burial depth.

Additionally, the marine-meteoric mixing zone, which may have influenced the carbon isotopes, and is also reflected in rather low Y/Ho ratios (Figure 7), can also explain the oxygen isotopes pattern, as strongly negative $\delta^{18}O$ values imply a different water input than of marine origin. Moreover, water temperature can influence oxygen isotopes, and warmer average temperatures can lower $\delta^{18}O$ values. Thus, paleotemperature fluctuations, or meteoric water input with different thermal gradient can plausibly explain the disturbed oxygen isotopes.

Analyses of the chemical composition of the ancient seawater show that the distribution of the REE does not suffer substantial changes compared to the present-day seawater pattern (Shields and Webb, 2004). Were there no other fluids besides the original seawater environment, the chalk should have retained the main characteristics of the original fluid environment. Although in this case the REE and Y pattern follows the typical open marine seawater signature, the overall depletion is less than what is expected for (pure) chalk deposits. The hydrothermal influence is clear in all wells, underlined by the presence of numerous minerals typically related to such an environment (pyrite, albite, sphalerite, etc.).

Further arguments supporting the presence of a secondary fluid are based on the Y and Ho concentrations, as they should have a positive linear correlation when chemical processes and not detrital ones dominate their abundance. The positive linear correlation between the abundance of the two elements in the geochemistry results indicates that the fractionation took place in a marine environment. However, the low

Y/Ho ratios (average 40, Figure 7) seen in the North Sea reservoir chalk are much below what is typical for seawater (Nozaki et al.,1997; Bau and Dulski, 1996; Bau and Dulski, 1999), and therefore reflect the presence of another fluid, assumingly fresh, meteoric/hydrothermal water, or intraformational water stored in rock successions. Such a fluid flow may have been triggered by the emergence of magma to produce the large volumes of extrusions during the Early Paleogene. This is, however, only speculation and needs to be substantiated with study of trapped seawater in lava vesicles of the Cenozoic extrusive rocks.

5.2 Diagenetic overprint

The occurrence of dolomite points to either a significant fluid flow to initiate dolomitization or to a slowly developing diagenesis. New dolomite crystals were detected in all thin sections from the Ekofisk area, mostly in pores and along fractures, but not in the northern, non-reservoir wells (Figure 4).

Clay minerals are most readily adjusted to the changes in the chemical conditions during burial. XRD analyses can identify such diagenetic changes, by considering the change in the mineral assemblage (e.g., from smectite to illite downwards). The presence of illite was observed in the XRD patterns (and confirmed with SEM analysis in Figure 3), but only in a few samples as a minor contributor to the non-carbonate mineral assemblage.

Areas in which pores are partly filled with secondary, re-worked material are observed (Figure 4), but this does not seem to be a significant, regional event rather active on a local area as geochemical data addressed.

Using stable isotope values as monitors for the influence of diagenetic processes when the ratios are not anymore primary has been

proposed in various contributions (compiled in Gomez Peral et al., 2007), most commonly corroborated with values from Mn, Fe, Mn/Sr ratio, 1000*Sr/Ca, Fe/Sr and Rb/Sr. According to this evaluation, none of the chalk samples in this study are pointing to any significant diagenetic overprint. Marly chalks and marls are affected by clastic input and the values of those samples cannot be considered. The only exception are Sr/Ca ratios which are definitely too high and can be affected by Sr-isotopes. The enrichment of Sr over Ca, which should rather have a character of positive correlation points to another Sr-bearing source, like baryte. This may be part of the rock either primary or introduced during migration of hydrocarbons and/or added during the drilling process. However, as all other indicators do not point to a strong diagenesis, we state that the change of the stable oxygen isotopes is not dominated by diagenetic processes. The amount of clastic detritus, not abundant enough to cause all the alterations seen in the geochemistry of the chalk, supports the assumption of another contaminant, most likely a secondary fluid, which also may comprise sufficient Mg to trigger dolomitization. Still, magmatic activity may have played a substantial role.

5.3 Influence of hydrocarbons and EOR fluids

It is unlikely that the presence of hydrocarbon fluids was the cause of the negative $\delta^{18}O$, as both the reservoir (Figure 10, green markers) and the non-reservoir successions (blue markers) show similar oxygen isotope pattern. By comparison, a number of Late Cretaceous samples of onshore chalk from Aalborg, Stevns Klint, Liège and Mons Basin (Andersen et

al., 2018) show isotopic values in concordance with the typical paleo-seawater isotopic composition (Figure 10; black diamonds).

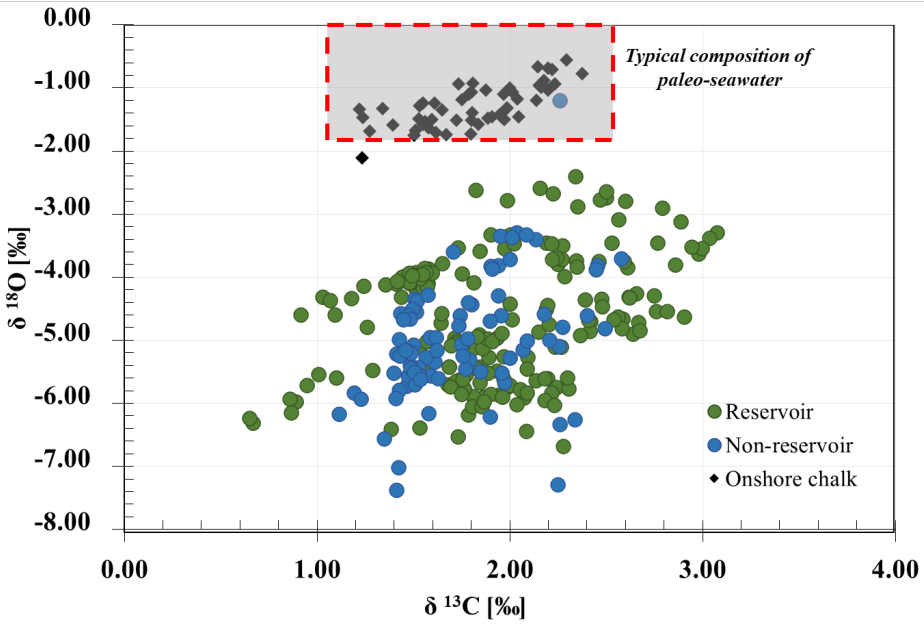

Figure 10: Cross plot of carbon and oxygen isotopic composition of offshore and onshore chalk from Danish outcrop locations (Andersen et al., 2018); the dashed red frame marks the expected plot area for undisturbed Cretaceous carbon and oxygen stable isotopes (after Gradstein et al., 2012).

A negative trend with depth is observed in both reservoir and non-reservoir samples (Figure 8) which may reflect burial lithification (Hudson, 1977). However, generally higher oxygen isotope ratios in reservoir compared to non-reservoir samples might be related to the presence of hydrocarbons. It may be that the processes that stabilized the chalk (early hydrocarbon entry, overpressuring, Nygaard et al., 1983; Brasher and Vagle, 1996) and were responsible for the early change of the REE concentrations, also retarded further change in the O isotope ratios during early, very low grade diagenesis.

The similarity between REE values of unflooded and flooded high porosity chalk (Table 3) excludes that artificial flooding events are

decisive for the observed negative oxygen ratio shift, which is therefore interpreted as natural, rather than anthropologic.

Field observations and laboratory studies confirm that NCS chalk is prone to mineralogical and textural changes when in contact with reactive EOR brines, and the effects of rock-fluid interactions are enhanced with higher injecting brine temperature (Austad et al., 2008; Madland et al. 2011; Megawati et al. 2015). The main mineralogical alterations are explained in terms of calcite dissolution and precipitation of new minerals such as magnesite, or anhydrite (Madland et al. 2011; Minde et al., 2018) and mineral alteration is most obvious close to the injection inlet (Minde et al., 2018; Kallesten et al., 2020). Production-related mineral alteration is possibly observed here as well. XRD analyses distinguished between flooded and unflooded samples in well 1, where the waterflooded cores had less calcite than the unflooded cores. Flooding temperature did not seem to make a difference, as both hot and cold waterflooded samples contained a similar amount of calcite.

However, samples from other wells that have been exposed to seawater injection do not show the same correlation. Most of the samples from well 2 as an example, although flooded, contained almost exclusively calcite. SEM analyses show that the mineral assemblage is similar in all reservoir wells and that the mineral and textural differences (e.g., presence of dolomite, pore morphology) are rather depositional, independent of flooding status (Figures 3, 4). Geochemistry results confirm this observation.

This does not necessarily rule out the effect of EOR fluids on chalk mineralogy, and the newly precipitated minerals might be more clearly seen closer to the brine injectors. However, this can only be resolved with a large sample set including well cores and drilled chalk less affected by artificial fluids.

The low diagenetic overprint, the presence of dolomite together with the often high amount of clastic material within the chalk is of

importance when testing onshore chalk as equivalent for the reservoir rocks in the context of smart water injection for EOR processes. Studies show that dolomite is less reactive to EOR fluids such as seawater than calcite (Shariatpanahi et al., 2016).

Further, pure chalk has a slower reaction rate to seawater than chalk with higher non-carbonate content, particularly clays (Madland et al., 2011). The introduction of clastic material into the Ekofisk Formation, often the host of hydrocarbon reservoirs, seems to be diachron and variable in its intensity. Wells 1 and 4 host chalk with silica content below 5 % and mainly between 1 and 3 %. In contrast well 3 contains only marly chalk and marls. Well 2 is characterized by an intercalation of clean chalk and marly chalk and finally wells 5 and 7 comprise a marly top versus a bottom enclosing clean chalk (Tables 3, 4). This variation is a very difficult issue when EOR techniques are applied and should be considered carefully.

6 Conclusions

Mineralogically, reservoir chalks from Ekofisk consist mainly of calcite; the silica is stored mostly in quartz and it represents a smaller, but significant proportion of the mineral composition of the chalk (1- 10 %). Corroborated results from XRD, SEM and geochemistry indicate the presence of other non-carbonate mineral phases like illite, smectite, kaolinite, which confirms a significant clastic input, a possible cause for the higher REE concentrations and lower Y/Ho ratios than expected in marine seawater precipitates, which may be triggered by the syn-depositional introduction of hydrothermal fluids or meteoric water.

Diagenesis that took place may have caused growth of dolomite and weak cementation, but the estimation of the diagenetic grade is yet not possible. Diagenetic dolomite exists together with sparse cementation, but an absence of significant chemical changes in elemental ratios (rather low Y/Ho ratios in relatively clean limestones) and elements used for monitoring diagenetic processes together with similar geochemical and isotope geochemical values for chalks from reservoir and non-reservoir areas, point to a circulation fluid which affected the rocks. This(these) fluid(s) may be of meteoric origin mixed with existing formation water. It is possible that the fluid was not very reactive with the larger minerals in the chalk but affected the grains on a very small scale, which is very difficult to monitor without using high-sensitive isotope data. The assumed fluid would have penetrated the formation rather early, and it may or may not have been related to hydrocarbon migration. This fluid may also have had sufficient Mg concentration to facilitate dolomite growth, and may as well have stabilized the rock, without weakening it and assisting in producing the reservoir at Ekofisk.

The chalk samples devoid of hydrocarbons show similar characteristics as the reservoir samples in terms of sediment composition, textures, and mineralogy. Both lithotypes, with and without

hydrocarbon accumulations, are clearly affected by a post-depositional process, which changed the oxygen isotope ratios to more negative values compared to many onshore chalk exposures, ruling out hydrocarbons as possible cause. Unlike the oxygen, the carbon isotopes seem to reflect Upper Cretaceous in all rocks.

There is no clear indication of chemical and mineral alteration due to EOR flooding of the reservoir chalk, possibly because the studied samples were far enough from the injectors where such effects would be more evident. Further studies on larger sample sets including flooded and unflooded fractured reservoir chalk can determine the spatial and temporal distribution of EOR fluid effects when the water chemistry, distance to the injectors, injection rate and time are known. Such data, together with knowledge of the North Sea reservoir chalk characteristics (typical Upper Cretaceous marine deposits, low diagenetic overprint, presence of dolomite and variable clastic input) offer a unique insight when considering potential EOR methods and can contribute to increased accuracy of chalk reservoir models.

Acknowledgements

The authors acknowledge the Research Council of Norway and the industry partners, ConocoPhillips Skandinavia AS, Aker BP ASA, Vår Energi AS, Equinor ASA, Neptune Energy Norge AS, Lundin Norway AS, Halliburton AS, Schlumberger Norge AS, and Wintershall DEA, of The National IOR Centre of Norway for support.

References

1. Allan, J. R., & Matthews, R. K. (1982). Isotope signatures associated with early meteoric diagenesis. *Sedimentology*, *29*(6), 797-817.
2. Andersen, P. Ø., Wang, W., Madland, M. V., Zimmermann, U., Korsnes, R. I., Bertolino, S. R. A., ... & Gilbricht, S. (2018).

Comparative study of five outcrop chalks flooded at reservoir conditions: chemo-mechanical behaviour and profiles of compositional alteration. *Transport in Porous Media*, *121*(1), 135-181.

3. Austad, T., Strand, S., Madland, M. V., Puntervold, T., and Korsnes, R. I. (2008) Seawater in Chalk: An EOR and Compaction Fluid. *SPE Reservoir Evaluation & Engineering: 11*(4), 648-654.
4. Bau, M. (1996). Controls on the fractionation of isovalent trace elements in magmatic and aqueous systems: evidence from Y/Ho, Zr/Hf, and lanthanide tetrad effect. *Contributions to Mineralogy and Petrology*, *123*(3), 323-333.
5. Bau, M., & Dulski, P. (1996). Distribution of yttrium and rare-earth elements in the Penge and Kuruman iron-formations, Transvaal Supergroup, South Africa. *Precambrian Research*, *79*(1-2), 37-55.
6. Bau, M., & Dulski, P. (1999). Comparing yttrium and rare earths in hydrothermal fluids from the Mid-Atlantic Ridge: implications for Y and REE behaviour during near-vent mixing and for the Y/Ho ratio of Proterozoic seawater. *Chemical Geology*, *155*(1-2), 77-90.
7. Bau, M., & Alexander, B. (2006). Preservation of primary REE patterns without Ce anomaly during dolomitization of Mid-Paleoproterozoic limestone and the potential re-establishment of marine anoxia immediately after the "Great Oxidation Event". *South African Journal of Geology*, *109*(1-2), 81-86.
8. Bjørlykke, K., & Høeg, K. (1997). Effects of burial diagenesis on stresses, compaction and fluid flow in sedimentary basins. *Marine and Petroleum Geology*, *14*(3), 267-276.
9. Brasher, J. E., & Vagle, K. R. (1996). Influence of lithofacies and diagenesis on Norwegian North Sea chalk reservoirs. *AAPG bulletin*, *80*(5), 746-768.
10. Cramer, B. S., Toggweiler, J. R., Wright, J. D., Katz, M. E., & Miller, K. G. (2009). Ocean overturning since the Late Cretaceous: Inferences from a new benthic foraminiferal isotope compilation. *Paleoceanography*, *24*(4).

11. D'Heur, M. (1991). West Ekofisk Field, Norway, Central Graben, North Sea (1). *AAPG Bulletin*, *75*(5), 946-968.
12. Dunham, R. J. (1962). Classification of carbonate rocks according to depositional textures. In: classification of Carbonate Rocks, *AAPG Mem.,* 108-121
13. Egeberg, P. K., & Saigal, G. C. (1991). North Sea chalk diagenesis: cementation of chalks and healing of fractures. *Chemical Geology*, *92*(4), 339-354.
14. Frimmel, H. E. (2009). Trace element distribution in Neoproterozoic carbonates as palaeoenvironmental indicator. *Chemical Geology*, *258*(3-4), 338-353.
15. Gennaro, M., Wonham, J. P., Sælen, G., Walgenwitz, F., Caline, B., & Faÿ-Gomord, O. (2013). Characterization of dense zones within the Danian chalks of the Ekofisk Field, Norwegian North Sea. *Petroleum Geoscience*, *19*(1), 39-64.
16. Gradstein, F. M., Ogg, J. G., Schmitz, M., & Ogg, G. (Eds.). (2012). *The geologic time scale 2012*. Elsevier.
17. Herrington, P. M., Pederstad, K., & Dickson, J. A. D. (1991). Sedimentology and Diagenesis of Resedimented and Rhythmically Bedded Chalks from the Eldfisk Field, North Sea Central Graben (1). *AAPG Bulletin*, *75*(11), 1661-1674.
18. Hjuler, M. L., & Fabricius, I. L. (2009). Engineering properties of chalk related to diagenetic variations of Upper Cretaceous onshore and offshore chalk in the North Sea area. *Journal of Petroleum Science and Engineering*, *68*(3-4), 151-170.
19. Howie, R. A., Zussman, J., & Deer, W. (1992). *An introduction to rock-forming minerals*. Longman.
20. Hudson, J. D. (1977). Stable isotopes and limestone lithification. *Journal of the Geological Society*, *133*(6), 637-660.
21. Jensen, T. B., Harpole, K. J., & Østhus, A. (2000, January). EOR screening for Ekofisk. In *SPE European Petroleum Conference*. Society of Petroleum Engineers.

22. Kallesten, E., Andersen, P. Ø., Berawala, D. S., Korsnes, R. I., Madland, M. V., Omdal, E., & Zimmermann, U. (2020). Modeling of Permeability and Strain Evolution in Chemical Creep Compaction Experiments with Fractured and Unfractured Chalk Cores Conducted at Reservoir Conditions. Society of Petroleum Engineers. *SPE Journal*. SPE-197371-PA.Madland, M. V., Hiorth, A., Omdal, E., Megawati, M., Hildebrand-Habel, T., Korsnes, R. I., ... & Cathles, L. M. (2011). Chemical alterations induced by rock–fluid interactions when injecting brines in high porosity chalks. *Transport in porous media*, *87*(3), 679-702.
23. Madland, M. V., Hiorth, A., Omdal, E., Megawati, M., Hildebrand-Habel, T., Korsnes, R. I., ... & Cathles, L. M. (2011). Chemical alterations induced by rock–fluid interactions when injecting brines in high porosity chalks. Transport in porous media, 87(3), 679-702.
24. McLennan, S. M., Taylor, S. R., and Henning, S. R. (2006). Composition, differentiation, and evolution of continental crust: constraints from sedimentary rocks and heat flow. *In Brown, M., and Rushmer T., eds. Evolution and differentiation of the continental crust. New York, Cambridge University Press,* p. 92–134.
25. Megawati, M., Madland, M. V., & Hiorth, A. (2015). Mechanical and physical behavior of high-porosity chalks exposed to chemical perturbation. *Journal of Petroleum Science and Engineering*, *133*, 313-327.
26. Minde, M. W., Zimmermann, U., Madland, M. V., Korsnes, R. I., Schulz, B., & Audinot, J. N. (2016, August). Fluid–flow during EOR experiments in chalk: insights using SEM–MLA, EMPA and Nanosims Applications. In *International Symposium of the Society of Core Analysts. Colorado, USA* (pp. 21-26).
27. Minde, M. W., Wang, W., Madland, M. V., Zimmermann, U., Korsnes, R. I., Bertolino, S. R., & Andersen, P. Ø. (2018). Temperature effects on rock engineering properties and rock-fluid chemistry in opal-CT-bearing chalk. *Journal of Petroleum Science and Engineering*, *169*, 454-470.

28. Nozaki, Y., Zhang, J., & Amakawa, H. (1997). The fractionation between Y and Ho in the marine environment. *Earth and Planetary Science Letters*, *148*(1-2), 329-340.
29. Nygaard, E., Lieberkind, K., & Frykman, P. (1983). Sedimentology and reservoir parameters of the Chalk Group in the Danish Central Graben. In *Petroleum Geology of the Southeastern North Sea and the Adjacent Onshore Areas* (pp. 177-190).
30. Peral, L. E. G., Poiré, D. G., Strauss, H., & Zimmermann, U. (2007). Chemostratigraphy and diagenetic constraints on Neoproterozoic carbonate successions from the Sierras Bayas Group, Tandilia System, Argentina. *Chemical Geology*, *237*(1-2), 109-128.
31. Scholle, P. A. (1977). Chalk diagenesis and its relation to petroleum exploration: oil from chalks, a modern miracle?. *AAPG Bulletin*, *61*(7), 982-1009.
32. Shariatpanahi, S. F., Hopkins, P., Aksulu, H., Strand, S., Puntervold, T., & Austad, T. (2016). Water based EOR by wettability alteration in dolomite. *Energy & Fuels*, *30*(1), 180-187.
33. Shields, G. A., & Webb, G. E. (2004). Has the REE composition of seawater changed over geological time?. *Chemical Geology*, *204*(1-2), 103-107.
34. Stoddart, D. P., Hall, P. B., Larter, S. R., Brasher, J., Li, M., & Bjorøy, M. (1995). The reservoir geochemistry of the Eldfisk field, Norwegian North Sea. *Geological Society, London, Special Publications*, *86*(1), 257-279.
35. Strand, S., Hjuler, M. L., Torsvik, R., Pedersen, J. I., Madland, M. V., & Austad, T. (2007). Wettability of chalk: impact of silica, clay content and mechanical properties. Petroleum Geoscience, 13(1), 69-80.
36. Sylte, J. E., Thomas, L. K., Rhett, D. W., Bruning, D. D., & Nagel, N. B. (1999, January). Water induced compaction in the Ekofisk field. In *SPE Annual Technical Conference and Exhibition*. Society of Petroleum Engineers.

37. Talukdar, M. S., & Torsaeter, O. (2002). Reconstruction of chalk pore networks from 2D backscatter electron micrographs using a simulated annealing technique. *Journal of petroleum science and engineering*, *33*(4), 265-282.
38. Taylor, S. R., & McLennan, S. M. (1981). The composition and evolution of the continental crust: rare earth element evidence from sedimentary rocks. *Philosophical Transactions of the Royal Society of London. Series A, Mathematical and Physical Sciences*, *301*(1461), 381-399.
39. Van Den Bark, E., & Thomas, O. D. (1981). Ekofisk: first of the giant oil fields in Western Europe. *AAPG Bulletin*, *65*(11), 2341-2363.
40. Wang, W., Madland, M. V., Zimmermann, U., Nermoen, A., Korsnes, R. I., Bertolino, S. R., & Hildebrand-Habel, T. (2018). Evaluation of porosity change during chemo-mechanical compaction in flooding experiments on Liège outcrop chalk. *Geological Society, London, Special Publications*, *435*(1), 217-234.

JPSE, https://doi.org/10.1016/j.petrol.2020.108164

Paper II: Validation study of water weakening research from outcrop chalks performed on Eldfisk reservoir cores

Kallesten, E., Cherif, Y., Madland, M.V., Korsnes, R.I., Omdal, E., Andersen, P.Ø., Zimmermann, U

Journal of Petroleum Science and Engineering (in press)

Paper II

JPSE, https://doi.org/10.1016/j.petrol.2020.108164

Validation study of water weakening research from outcrop chalks performed on Eldfisk reservoir cores

Emanuela I. Kallesten[1, 2], Yosra Cherif[1], Merete V. Madland[1, 2], Reidar I. Korsnes[1, 2], Edvard Omdal[3], Pål Østebø Andersen[1, 2], Udo Zimmermann[1,2]

1. University of Stavanger, Kristine Bonnevies vei 22, 4021 Stavanger, Norway
2. The National IOR Centre of Norway (same address as 1.)
3. ConocoPhillips, Ekofiskveien 35, 4056 Tananger, Norway

Keywords: reservoir chalk, waterflooding, enhanced oil recovery, creep compaction, testing at reservoir conditions

Abstract

Seawater injection for Enhanced Oil Recovery (EOR) purposes can increase the hydrocarbon recovery factor in carbonate reservoirs but are also responsible for weakening their mechanical strength. This study investigates the geomechanical behavior of oil-bearing reservoir chalk subject to reactive flow at reservoir conditions. The obtained results are compared with previous results from experiments on water-saturated outcrop chalks.

Two unwashed oil-bearing reservoir chalk cores from the Eldfisk Field in the North Sea are mechanically tested in a triaxial cell. The cores are saturated with NaCl brine prior to testing, in addition to residual oil. The cores' axial and radial deformations were monitored during hydrostatic stress loading and creep under constant 50 MPa stress, at 130° C. During the test, the cores were flooded with 0.657 M NaCl, 0.219 M $MgCl_2$, 0.219 M $MgCl_2$ + 0.130 M $CaCl_2$ and synthetic seawater (SSW). The average creep strain increased from 0.03 % to 0.04 % per day radially and from 0.03 % to 0.06 % axially after changing from the NaCl brine to

SSW brine. Flooding $MgCl_2$ brine after NaCl increased the average compaction rate from 0.05 % to 0.09 % per day radially and from 0.04 % to 0.07% per day axially. Adding $CaCl_2$ to the $MgCl_2$ brine reduced the average compaction rate from 0.05 % per day during $MgCl_2$ injection to 0.02 % per day both radially and axially, comparable to reports from outcrop chalk experiments. The brine composition-dependent creep compaction in the core flooding experiments was explained by dissolution of primary calcite, confirmed by Ion Chromatography, and precipitation of secondary Mg-bearing minerals, seen by Scanning Electron Microscopy (SEM) analytics.

Generally, the aforementioned results describing geomechanical behaviors of oil-bearing reservoir chalk cores under hydrostatic stress and thermochemical influence in this study are comparable to those from previous studies on outcrop chalk, thus supporting many years of laboratory research as applicable in the reservoir chalk context.

1 Introduction

Developing Improved Oil Recovery (IOR) techniques is central in the efforts for sustainability and resource optimization on the Norwegian Continental Shelf (NCS). The discovery of the Ekofisk Field in 1969, marked the beginning of remarkable advances in hydrocarbon production from chalk reservoirs in Norway. 50 years after its discovery, it is still one of the most prolific reservoirs on the NCS.

After the Ekofisk field had a peak in production rate from primary recovery by pore pressure depletion, the production rate decreased dramatically. The pore pressure depletion contributed to an increased effective stress (overburden minus pore pressure) in the reservoir. The resulting compaction facilitated hydrocarbon expulsion from the porous chalk, but also lead to seafloor subsidence (Teufel et al., 1991; Sulak and Danielsen, 1988; Hermansen et al., 1997; Hermansen et al., 2000).

Implementing the seawater injection at Ekofisk Field in 1987 contributed to reservoir re-pressurization and an increase in oil production rates. However, despite re-pressurization of the reservoir, high compaction rates continued in certain areas of the field (Schroeder et al., 1998; Hermansen et al., 2000), indicating that effective stress alone was not the only compaction driving mechanism. The interactions between chalk and the injected non-equilibrium seawater, referred to as water weakening is a likely contributor (Hermansen et al., 2000). Studies demonstrate a two-step water effect on chalk: an abrupt, instantaneous weakening occurring at the first water-chalk contact, followed by a creep-like deformation at a lower, stable rate (Schroeder et al., 1998; Korsnes et al., 2006). The initial, dramatic water weakening step explains much of the continued compaction of Ekofisk field, but the focus of this study is rather on the role of water chemistry in water weakening of chalk. Korsnes et al., 2006 demonstrated that while water weakening occurs regardless of the water composition, the magnitude of induced

weakening was more pronounced when injecting seawater than in case of distilled water.

Extensive laboratory studies on water-wet outcrop chalk showed that the chemical interplay between ions in the injected seawater and the rock itself, does indeed affect the geomechanical properties of chalk (Korsnes et al., 2006; Madland et al., 2011; Nermoen et al., 2015; Kallesten et al., 2020a). The processes identified as responsible for changing the geomechanical properties of chalk are chemical and mineralogical alterations that occur in the presence of surface active ions in the seawater, such as Ca^{2+}, Mg^{2+} and SO_4^{2-} through adsorption, calcite dissolution, substitution and new mineral precipitation. The rock, as a result, suffers morphological and textural changes that in the end are responsible for chalk weakening.

Korsnes et al., 2006 related water weakening during seawater flooding of chalk to the substitution of Ca^{2+} at the chalk surface with Mg^{2+} at elevated temperatures. It is suggested that due to the size difference between the two ions (Mg^{2+} is smaller than Ca^{2+}) this substitution is associated with causing structural changes at intergranular contacts which weaken the chalk. Madland et al. (2011) demonstrated that when flooding seawater the dissolution/substitution process not only leads to precipitation of new Mg-bearing minerals, but also anhydrite ($CaSO_4$) given the presence of sulfate molecules. Further, Madland et al. (2011) demonstrated that when injecting seawater or simplified seawater solutions such as $MgCl_2$ in chalk cores, it is likely that the fluid in the pores is undersaturated with respect to calcite and supersaturated with respect to other minerals, which leads to new mineral precipitation. However, the total produced calcium exceeds the limited number of surface sites, which indicates that the ion exchange or substitution does not occur indefinitely, and that dissolution remains the dominating mechanism. Based on this observation, Megawati et al. (2011) investigated the hypothesis that adding sufficiently high calcium concentration to the $MgCl_2$ brine will hinder the calcite dissolution and thus not weaken the chalk. The results confirmed this supposition and

they observed that by adding 0.130 mol/L $CaCl_2$ to the 0.219 mol/L $MgCl_2$ flooding brine, representing an increase of calcium concentration by a factor of 10 compared to the seawater composition, lead to a severe reduction in both excess calcium production and creep compaction rate of the chalk. Switching back to a non-equilibrium brine reactivated the calcite dissolution and accelerated the compaction.

Besides dissolution/precipitation processes leading to mineral replacement, the interactions between the pore fluid and the chalk surface may also include adsorption and desorption of surface-active ions (Ahsan and Fabricius, 2010; Megawati et al., 2013; Sachdeva et al., 2019a). Megawati et al., 2013 showed that adsorption of sulfate ions present in seawater on the chalk grains can lead to a negative surface charge that triggers the occurrence of repulsive forces at granular contacts, which consequently reduces the cohesion between grains, weakening the chalk. Nermoen et al., 2018 and Sachdeva et al., 2019a observed that Mg^{2+} can have a similar effect. Due to the non-equilibrium between $MgCl_2$ brine and calcite surface, magnesium ions adsorb on available chalk surface sites and as calcium ions desorb from the internal surface during flooding until equilibrium is reached. However, adsorption and desorption are considered as limited processes in this case, that occur only within the few first pore volumes of the injected reactive brine because of the finite number of available surface sites (Madland et al., 2011). Thereafter, the changes in magnesium and calcium concentrations in the effluents are dominated by the dissolution and precipitation processes. Both during the early and late time injection periods of $MgCl_2$ injection into outcrop it appears that very similar amounts of excess Ca is produced as Mg is retained (Madland et al 2011; Megawati et al 2015; Andersen et al 2018; Minde et al 2018). We hypothesize the same will take place with reservoir chalk samples.

In comparison to reactive brines, geochemical analysis from experiments with non-reactive flooding fluid (NaCl) at 130 °C concluded that in the absence of surface-active ions, chemical alterations such as adsorption, dissolution and precipitation of new minerals, are unlikely to

occur (Madland et al., 2011; Megawati et al., 2015; Minde et al., 2018; Wang et al., 2018). Nonetheless, NaCl flooding can dissolve calcite if flooded over a long time period, causing morphological changes such as grain rounding (Gautier et al., 2001). This was reported in outcrop chalk studies (Andersen et al., 2018) and according to Megawati et al., 2011 smoothened crystals corners and edges may lower the mechanical intergranular friction, and consequently enhance the creep development with time.

Another aspect in water weakening research is the presence of additional phases besides brine, as the wettability of chalk (whether the grain surfaces are more water-wet or oil-wet) plays an important role in flooding experiments on mechanical strength, geochemical and petrophysical changes and oil production (Strand et al., 2007; Hiorth et al., 2010; Sachdeva et al., 2019b). Sachdeva et al., 2019b found that water-wet chalk cores were weaker than mixed-wet (some grain surfaces are water-wet and others are oil-wet) when flooded with non-reactive brines (NaCl). However, injecting $MgCl_2$ and SSW lead to increasing creep rates in both water-wet and mixed-wet cores alike, indicating that the presence of oil in the pores does not avert the flooding brine from the intergranular contacts and therefore does not hinder the weakening effects of reactive flow on chalk as described above.

Not least, mineralogy plays an important role in rock-fluid interactions (Andersen et al., 2018; Fabricius and Borre, 2007; Hjuler and Fabricius, 2007; Hiorth et al., 2010; Madland et al., 2011; Minde et al., 2018; Strand et al., 2007; Kallesten et al., 2020b). Madland et al., 2011 pointed out that pure chalk (high calcite content) has a slower reaction rate than chalk with higher non-carbonate content (particularly silicates, clays). Therefore, despite the rather predictable mineralogy and petrology of chalk, important aspects such as the depositional environment, stress history, diagenesis, burial depth can strongly influence its engineering properties and a direct transfer of data from outcrop chalk to reservoir chalk is not always appropriate (Scholle, 1977; Brasher and Vagle, 1996; Hjuler & Fabricius, 2009; Minde et al., 2016).

As an example, North Sea offshore chalks are deeply buried, with depths often exceeding 3 km, whereas onshore chalks such as Danish chalks have relative shallow maximum palaeo-burial depths ranging between 500 – 750 m (Japsen, 1998; Japsen and Bidstrup, 1999; Japsen, 2000).

Most of the chalk research, however, is performed on outcrop chalk, due to the scarcity and high cost of reservoir test material. Yet, in an effort to identify the most suitable outcrop analogues to the North Sea reservoir chalk, studies of chalk from exposures with a comparable mineralogy, permeability, porosity environment and sedimentary age as reservoir chalk concluded that in spite of the mineralogical, diagenetic differences, laboratory tests on certain chalk outcrops can nontheless provide valuable information for further research (Collin et al., 2002; Hjuler and Fabricius, 2009; Jarvis, 2006). The studies recommend outcrop chalk such as the Belgian Liège chalk as a possible mechanical analogue to Ekofisk field and the Danish Aalborg chalk is considered comparable to Valhall reservoir chalk in terms of geo-mechanical properties. Still, the studies urge to careful consideration when selecting suitable outcrop chalk as reservoir chalk substitutes for mechanical testing.

Conducting laboratory tests on actual reservoir chalk cores is a unique opportunity to validate results and behavior seen in laboratory tests on outcrop chalk. For that purpose, this study investigates the behavior of reservoir chalk when tested with procedures giving significant responses in outcrop chalk. The core material is from Eldfisk Field, the second largest producing field in the Greater Ekofisk area, located in the Southern tip of the NCS. Mineralogically the Eldfisk chalk consists almost entirely of calcite (96 – 97 %), while the non-carbonate phase is mainly quartz, kaolinite and scarce dolomite, feldspar, pyrite, apatite and smectite-illite (Madsen, 2010).

The study will replicate the test conditions used previously on outcrop chalk (Madland et al., 2011; Megawati et al., 2011; Korsnes et al., 2013; Megawati et al., 2015; Zimmermann et al., 2015; Andersen et al., 2018; Minde et al., 2018; Nermoen et al., 2018; Wang et al., 2018;

Sachdeva et al., 2019b). Two reservoir chalk cores will be tested in triaxial cells under hydrostatic stress conditions, and flooded with NaCl, seawater, $MgCl_2$ and $MgCl_2$ with added $CaCl_2$ (to reduce calcite dissolution) at 130° C, over several weeks. The focus will be on axial and radial strain measurements in response to hydrostatic loading and creep and variation in flooding brine. Also, the effluent concentrations will be monitored throughout the test by collecting effluent probes regularly, in order to detect possible changes in ionic concentration compared with the concentrations of the injecting fluid. Finally, Scanning Electron Microscopy will investigate the mineralogy and texture of the flooded chalk. The results will allow a direct comparison between reservoir chalk from the North Sea and the outcrop chalk tests in terms of geomechanical behavior and geochemical effects of injecting brine chemistry. Specific research questions we seek to answer are:

- Will $MgCl_2$ brine and seawater, which are reactive to outcrop chalk, also be reactive to Eldfisk reservoir chalk in terms of mineralogical changes?
- Will switching from an inert brine (NaCl) to a reactive brine lead to enhanced compaction during creep?
- Will $MgCl_2$ brine injection, followed by injecting $MgCl_2$ brine with added high $CaCl_2$ concentration result in reduced compaction rate?
- Will Mg^{2+} loss and Ca^{2+} gain be identical when $MgCl_2$ is injected into reservoir chalk?

Knowledge of the reservoir chalk behavior in the same test conditions as the outcrop chalk will verify the relevance of outcrop chalk testing for the North Sea context, will refine the search of an outcrop analogue to reservoir chalk, but also enhance the accuracy of reservoir models relevant to the NCS, and eventually contribute to increase efficiency of the EOR techniques from existing and future chalk reservoirs.

2 Sample set, experimental procedures, and methods

2.1. *Sample set*

This study focuses on tests performed on two reservoir chalk cores (E2 and E3, Figure 1) from the Ekofisk Formation (Eldfisk field). Although ideally several cores should be tested, the two cores studied here are a rare opportunity considering the limited availability for laboratory testing and the cost of obtaining reservoir cores. The cores contained saturation of reservoir oil and they have not been exposed to EOR fluids. To maintain the cores as close to their original state as possible, the residual oil and salts were not removed prior to testing. Core E2 contained a visible fissure on the top facet, which did not seem to penetrate the entire core.

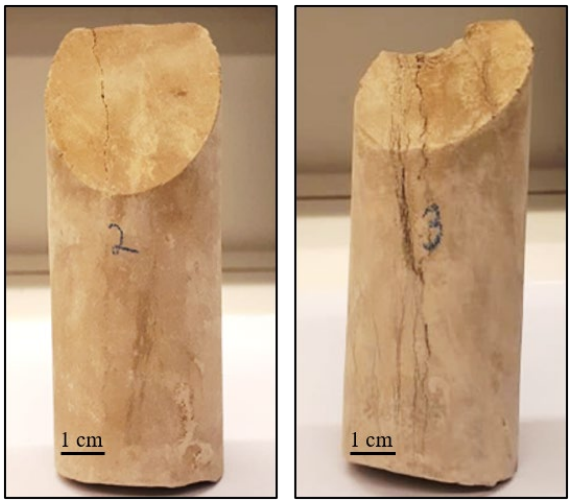

Figure 1: Chalk cores E2 (left) and E3 (right) before testing

To obtain a cylindrical shape with parallel end facets compatible with the testing equipment, the cores' irregular end facets were cut with a Struers Discotom-5 cutting machine and grinded with a Delta LF-350 machine. The excess end pieces were stored for a later study investigating possible mineralogical differences between untested and

tested chalk. The porosity of the obtained cylinders was measured by gas pycnometry. Because the cores were unwashed, the measured porosity represents effective values rather than true porosity. The dimensions and porosity of the cores are listed in Table 1.

Table 1: Dimensions and effective porosity of the tested cores

Core ID	*Length [mm]*	*Diameter [mm]*	*Effective porosity [%]*
E2	*53.00*	*37.93*	*18.00*
E3	*52.40*	*37.98*	*18.93*

2.2. *Injecting brines*

Four different brines were used for core flooding, henceforth generically identified by and referred to according to their composition: 0.657 M sodium chloride (NaCl), 0.219 M magnesium chloride ($MgCl_2$), 0.219 M magnesium chloride spiked with 0.130 M calcium chloride ($MgCl_2$+$CaCl_2$) and synthetic seawater (SSW). Apart from SSW, the rest of the brines were prepared with distilled water (DW) in equilibrium with calcite. 0.1 g/L calcite powder was added to DW and stirred at room temperature. The solution was then filtered through a 0.22 μm filtrate paper, to remove all undissolved calcite and used further for preparation of the sodium chloride and magnesium chloride brines. The ionic strength of the monosalt brines was set to match the ionic strength of seawater. A summary of the injecting brine compositions is shown in Table 2, discounting calcite equilibration of DW.

Calcite equilibration makes sodium chloride brine inert, thus avoiding textural alteration in contact with chalk. This would provide a contrast in comparison to the reactive brines (magnesium chloride and synthetic seawater) which contain surface-active ions such as Mg^{2+}, Ca^{2+} and SO_4^{2}, an indication of the effect of rock-fluid interactions when injecting reactive brines through chalk.

Table 2: Chemical composition of the flooding brines; here, ionic composition of sodium chloride and magnesium chloride without considering calcite equilibration

Injecting brine	NaCl	$MgCl_2$	$MgCl_2$ + $CaCl_2$	SSW
Ionic strength [-]	0.657	0.657	1,047	0.657
Cl^- [mole/L]	0.657	0.438	0,698	0.525
Na^+ [mole/L]	0.657			0.450
Mg^{2+} [mole/L]		0.219	0,219	0.045
SO_4^{2-} [mole/L]				0.024
Ca^{2+} [mole/L]			0,130	0.013
HCO_3^- mole/L]				0.002
K^+ [mole/L]				0.010

2.3. *Triaxial cell test setup and procedures*

Both cores were saturated with NaCl in vacuum conditions before cell mounting and were continuously flooded with the same brine during the first stages of the test (Table 3). The injecting rate was 0.023 ml/min, equivalent of approximately 3 pore volumes (PVs) per day. The effluent brine was collected throughout the test at regular intervals; the first 9 – 12 PVs (i.e., 3 – 4 days) after changing to a new brine were sampled 4 times per day, and thereafter once per day. Comparison of the effluent composition to the original injecting brine provides an insight in the rock-fluid interactions during the test.

The triaxial cell is equipped with an outer heating jacket and a regulating system (Omron E5CN) with precise Proportional Integral Derivative (PID) temperature control (±1.0 °C). The system includes two Quizix QX-2000HC pumps that control the axial and confining pressures independently, and a fluid injection pump (Gilson 307HPLC) as well as a backpressure regulator that controls the pore pressure. A schematic diagram representing the triaxial cell setup such as the one used in this study can be found in Nermoen et al., 2016.

During cell mounting, perforated drainage disks with the same diameter as the cores are placed at both brine-saturated core ends to

ensure an evenly distributed fluid flow across the core. Additionally, a steel spacer (19.3 mm length) was placed on top to compensate the limited core length. The cores are isolated from the oil bath in the confining chamber by a heat shrinkage sleeve (fluorinated ethylene propylene –FEP, 0.5 mm wall thickness). Throughout the test, any changes in core diameter (radial strain) were measured with an extensometer (GCTS DEF-5000), placed at mid length of the core. An external axial linear variable displacement transducer (LVDT, ±0.05 mm) positioned on top of the cell piston, which is carefully lowered to slight core contact, monitored changes in the cores' length (axial strain). The cell piston applies a 0.55 MPa pressure, to slightly overcome the piston friction, without causing any notable core deformation. NaCl brine flooding started shortly after the triaxial cell mounting was complete and the procedure continued once the differential pressure across the core (measured between the upstream pore line and the downstream) becomes stable. Both tests are performed at 130 °C, representative to the reservoir temperature of Eldfisk field (Cook and Brekke, 2004; Puntervold and Austad, 2008).

At the beginning of the hydrostatic loading, the confining pressure was 1.2 MPa, while the pore pressure was set to 0.7 MPa. For the rest of the test, the pore pressure was kept constant. Hydrostatic loading started with increasing the confining pressure from 1.2 MPa to 50 MPa at a constant 0.1 MPa/min rate. Since with increasing confining pressure the friction associated with the piston also rises, the piston pressure was adjusted accordingly, and finally set to 4.7 MPa.

Once the hydrostatic loading was complete, the pressures were kept constant for the rest of the test, allowing the cores to deform (creep) over several weeks while flooded with different brines. A summary of the stress and flooding sequence for the tests is shown in Table 3.

Table 3: Duration of each stress phase correlated to flooding sequences for cores E2 and E3

	E2		E3	
Injecting Brine	**Hydrostatic loading [days]**	**Creep at 50 MPa [days]**	**Hydrostatic loading [days]**	**Creep at 50 MPa [days]**
NaCl	*0.3*	*6.7*	*0.3*	*6.7*
SSW	-	*19*	-	-
$MgCl_2$	-	-	-	*28*
$MgCl_2$ + $CaCl_2$	-	-	-	*23*
DW	-	*3.0*	-	*3.0*

The core diameter over the length of the core is not constant after testing at hydrostatic stress conditions, and new core bulk volume expected to appear after hydrostatic testing was estimated from the sum of truncated circular cones with diameter D_i measured at height h_i along the core (5), assuming symmetric radial deformation at each h_i.

$$V_b = \sum_i \frac{\pi h_i}{12} \left(D_i^2 + {D_{i+1}}^2 + D_i D_{i+1}\right) \quad (5)$$

After testing, both cores were flooded with DW to avoid salt precipitation. Additionally, the cleaning process for core E3 included injection with methanol and toluene to eliminate any possible hydrocarbon residue and prepare for SEM analyses.

2.4. *Ion Chromatography*

The ionic concentrations of the injected and produced brines were measured with a Dionex Ion Chromatography System (ICS)-5000$^+$. Dionex IonPac AS20 and IonPac CS19 were used as anion and cation exchange columns, respectively. Prior to the analyses, the original brine and effluent samples were diluted 500 times with DW in a Gilson GX-271 dilution machine. The ionic concentrations of Na^+, Cl^-, Mg^{2+}, Ca^{2+} and SO_4^{2-} were measured against standard solutions with known concentrations.

2.5. *Electron Microscopy*

Fresh surfaces of the flooded material from core E3, were examined with Field Emission Gun-Scanning Electron Microscope (Zeiss Supra 35VP FEG-SEM) to obtain visual images of the grains and the rock structure on μm scale. The measurements were performed in high vacuum mode with an accelerating voltage of 15 kV, aperture size of 30 μm, and a working distance between 8 and 9 mm. The electron microscope is equipped with Energy-Dispersive X-Ray Spectroscope (EDS) with a spot size between 1 and 2 μm, which was applied to determine the mineralogical and elemental composition of the analyzed chalk surfaces. The EDS was calibrated after a dolomite standard from "Astimex Standards Limited" before the sample was analyzed.

The dry, tested core was cut in half longitudinally, then one of the halves was cut in four transverse slices, numbered from P1 to P4 from the core inlet to the outlet, respectively. The method focused on a fragment with a fresh surface from slice P1 (inlet), coated with palladium in an Emitech K550 sputtering device.

3. Results

3.1. *Mechanical testing*

Both cores were tested in the same triaxial cell, following the same stress sequence as described in section 2.4, at 130 °C.

Eldfisk reservoir core E2 was loaded hydrostatically up to 50 MPa while

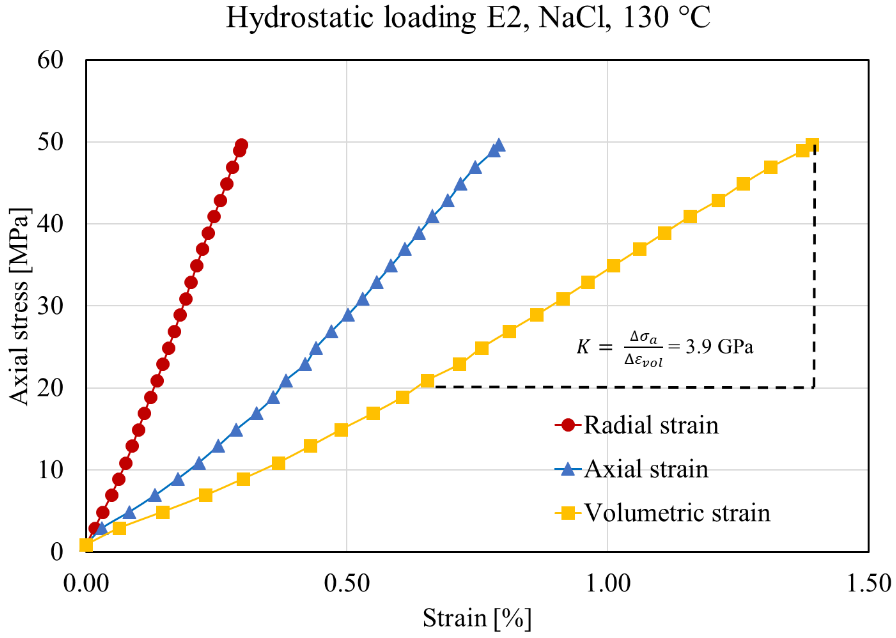

Figure 2: Stress-strain relationships during hydrostatic loading of core E2

flooding NaCl at an injection rate equal to 3 PVs/day. The axial stress versus axial, radial and volumetric strain are plotted in Figure 2. The core was compacted both axially (Figure 2, blue line) and radially (Figure 2, red line) but did not yield (stress-strain relationship remains linear). The recorded axial and radial strains at the end of this phase were approximately 0.8 % and 0.3 % respectively. The calculated bulk modulus (K) from the linear slope of axial stress against volumetric strain as shown in Figure 2 (yellow line), was 3.9 GPa.

NaCl injection continued during the first 6.7 days of the creep phase (Figure 3). The axial and radial strain rates (percent/day) stabilized at approximately 0.03 %/day. The injecting brine was then changed to synthetic seawater, SSW, for the rest of the creep phase.

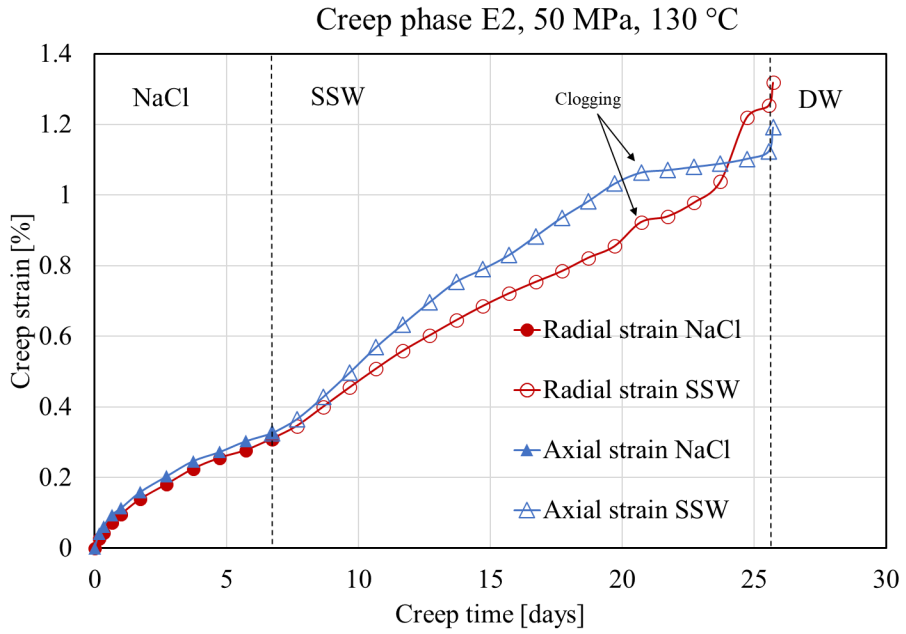

Figure 3: Axial strain (blue lines) and radial strain (red lines)) for core E2 during NaCl injection (filled markers) and SSW injection (empty markers) during creep at 50 MPa hydrostatic stress

As Figure 3 shows, the compaction accelerated shortly after initiating SSW injection (empty markers) compared to the compaction rate during NaCl injection (full markers). Thereafter, the core continued to deform at an almost constant rate until day 21 of creep. Changing the injection brine to SSW increased the average strain rates from 0.03 % to 0.04 % per day radially and from 0.03 % to 0.06 % per day axially, considering the average strain rate for 5 days prior to and after brine change. The flattening of radial and axial creep after day 21 was most likely caused by clogging of the outlet tube. This increased the pore pressure and thereby reduced the effective stress, and consequently the axial

deformation rate. This period is not included in the average strain rate evaluation. As soon as the cleaning procedure was initiated with distilled water injection (DW section, Figure 3), the axial strain rate increased sharply, supporting the assumption of outlet tube clogging due to salt precipitation during flooding. As the precipitates were removed, the pore pressure decreased, the effective stress increased, also inducing a sharp increase in axial strain.

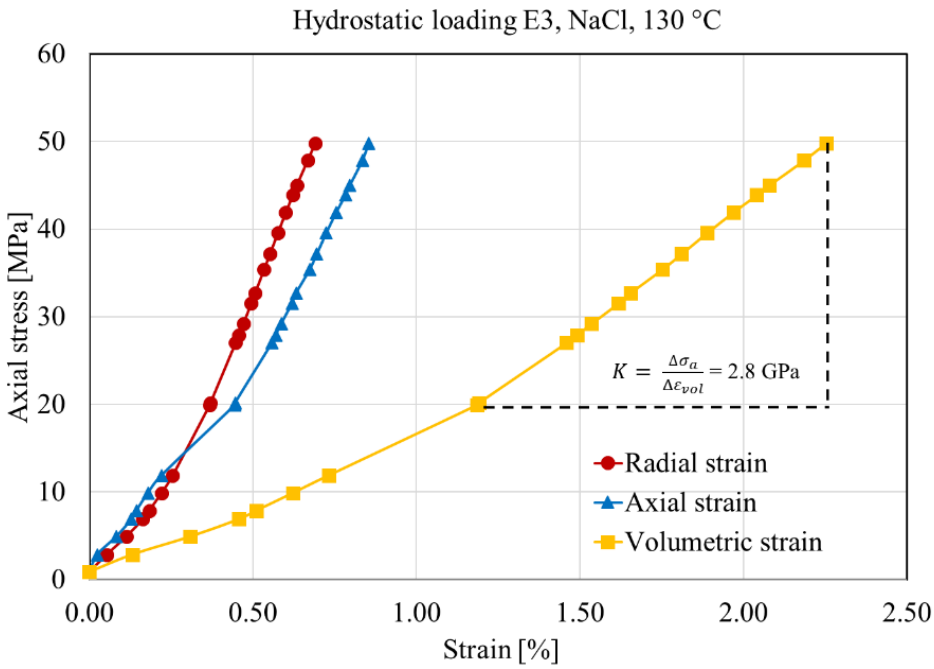

Figure 4: Stress-strain relationships during hydrostatic loading of core E3

During the first 24 days of creep, E2 deformed more in the axial direction (Figure 3, blue line) compared to radial (Figure 3, red line), and more clearly so during SSW injection. However, after 24 days, the radial creep strain accelerated, exceeding the axial strain for the remaining creep period. This unexpected behavior might have been caused by an instrumental error (loosening of the chain of extensometer) or by weakening of the central part of the core.

Mechanical testing of Eldfisk reservoir core E3 started with the same conditions as the previous test, with hydrostatic loading from a confining pressure of 1.2 MPa to 50 MPa, while injecting NaCl at a constant 3 PVs/day rate. The axial stress versus axial and radial strains are plotted in Figure 4. The axial strain (Figure 4, blue line) and radial strain (Figure 4, red line) reached 0.86 % and 0.69 % respectively at the end of the isotropic loading phase. The yield point was not observed for E3. The bulk modulus (K) could be calculated from the linear slope of axial stress versus volumetric strain within the elastic phase as shown in Figure 4, and it was equal to 2.8 GPa.

The deformation of E3 at constant stress and pore pressure conditions (creep) was studied for 58 days with continuous logging of the axial and radial strains. The creep compaction profile of E3 is shown in Figure 5. The core was initially flooded with 0.657 M NaCl for the first 6.7 days of creep before flow of 0.219 M $MgCl_2$ started. Axial creep strain (Figure 5, blue line) and radial creep strain (Figure 5, red line) at the end of NaCl flow (Figure 4, full markers) were approximately 0.5%, stabilizing at an average deformation rate of 0.04 % per day.

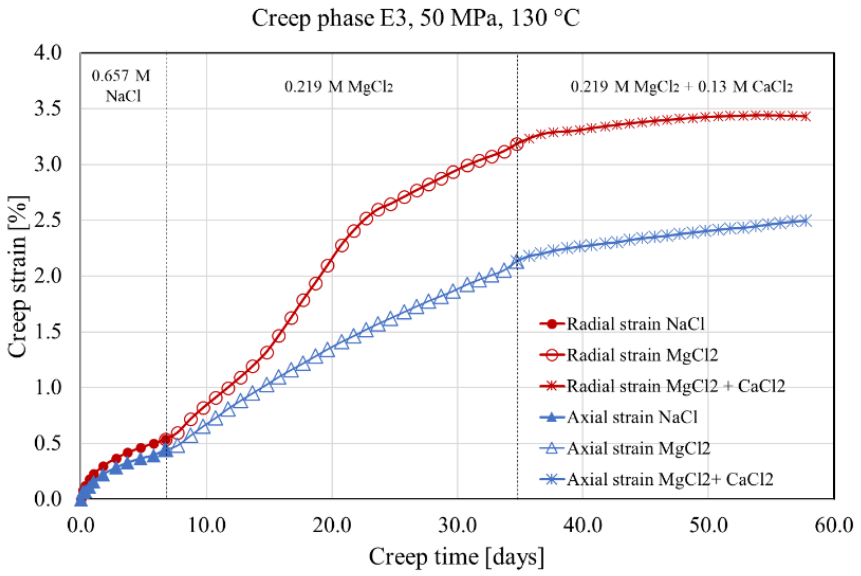

Figure 5: Axial strain (blue lines) and radial strain (red lines) for core E3 during NaCl injection (filled markers), $MgCl_2$ (empty markers) and $MgCl_2$ spiked with $CaCl_2$ (cross markers) during creep at 50 MPa hydrostatic stress

However, the switch to injection of $MgCl_2$ (Figure 5, empty markers) led to an abrupt increase in the deformation rates both axially and radially. Figure 5 shows how the radial strain (red line) increased significantly especially until day 22 of creep, then the core continued to deform, but with a lower rate until a strain of 3.2% was recorded. During the same period, the axial strain increased continuously up to 2.1% at 34.7 days. In average, the strain rate per day during the first 5 days of $MgCl_2$ flooding increased compared to the average strain rates during the last 5 days of NaCl injection, from 0.05 % to 0.09 % radially and from 0.04 % to 0.07 % axially.

The injection of 0.219 M $MgCl_2$ + 0.130 M $CaCl_2$, (Figure 5, day 35, cross markers) caused a reduction in the deformation rate compared to the deformation rate while flooding only 0.219 M $MgCl_2$. Comparing the average strain rates over the last $MgCl_2$ injection and the first 10 days

after adding $CaCl_2$ to the flooding medium, the compaction rate changed from approximately 0.05 % to 0.02 % per day both radially and axially.

3.2. *Effluent analyses*

The effluent profiles from test E2 focused on the concentrations of the following ions: magnesium, calcium, and sulphate. Figure 6 shows the ion chromatography analysis of E2, flooded with 0.657 M NaCl and SSW.

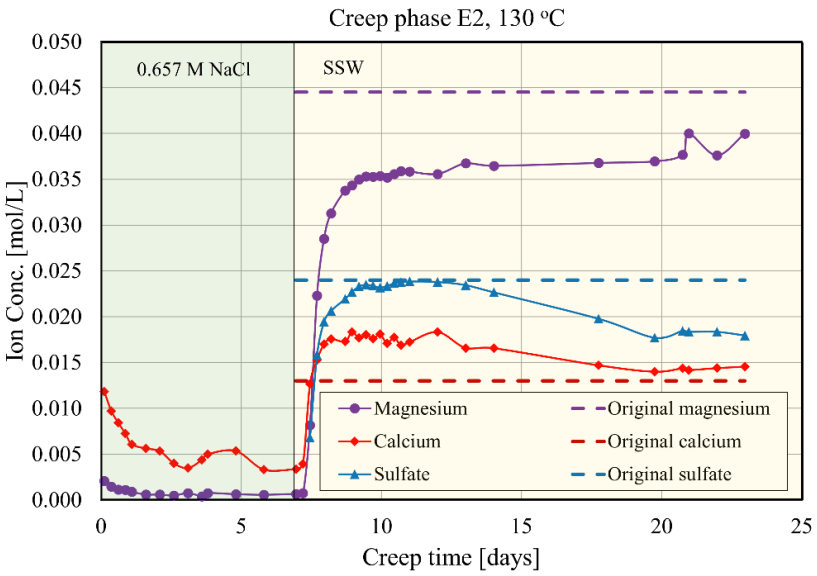

Figure 6: Magnesium (purple line), calcium (red line) and sulfate (blue line) concentrations of effluents [mol/L] during creep time [days] and flooding of inert (green shade) and reactive (yellow shade) brines of core E2. Dashed lines indicate original ion concentrations.

During NaCl flooding, the concentrations of sodium and chloride (neither shown) were generally stable throughout the whole experiment with values close to their injected concentration. From the profile of E2, a small magnesium peak of ~ 0.002 mol/L (Figure 6, purple line) appeared in the beginning of the creep phase, but it decreased relatively fast and the magnesium concentration in the effluent at this stage stabilized around zero. A larger calcium peak of ~ 0.01 mol/L (Figure 6, red line) was observed initially. The calcium concentration also generally

decreased, with a brief fluctuation (day 3) and it stabilized at ~ 0.003 mol/L.

Magnesium loss was detected throughout Synthetic Seawater (SSW) flooding, in comparison to the original brine concentration; the magnesium concentration in the effluent increased to 0.035 mol/L in the first 6 PVs transitioning from NaCl injection. For the rest of the creep phase, the concentration increased slowly, up to 0.04 mol/L, but remained clearly below the injected concentration, by approximately 11 %.

Excess calcium is produced during SSW injection, and the effluent calcium concentration showed an increasing trend up to 0.018 mol/L, from day 8 to day 10, exceeding the injected concentration of 0.013 mol/L, Thereafter, a decrease in the calcium concentration down to ~ 0.014 mol/L at day 20 was found, where it stabilized over the last three creep days, still 0.001 mol/L above the original concentration of 0.013 mol/L.

The sulphate concentration in the effluent (Figure 6, blue lines) reached the original SWW concentration after two days of SSW injection. Later during creep (from day 13) the sulfate concentration started a decreasing trend for the next 7 days, finally stabilizing around 25 % below the injected concentration.

For core E3, the effluent profiles were based on the concentrations of magnesium (Mg^{2+}) and calcium (Ca^{2+}). When flooding with NaCl, the effluent concentrations of Na^{+} and Cl^{-} were practically the same as the injected, i.e. 0.657 mol/L. A small calcium peak of 0.01 mol/Lwas found initially (Figure 7, red line), but it rapidly went down to negligible values.

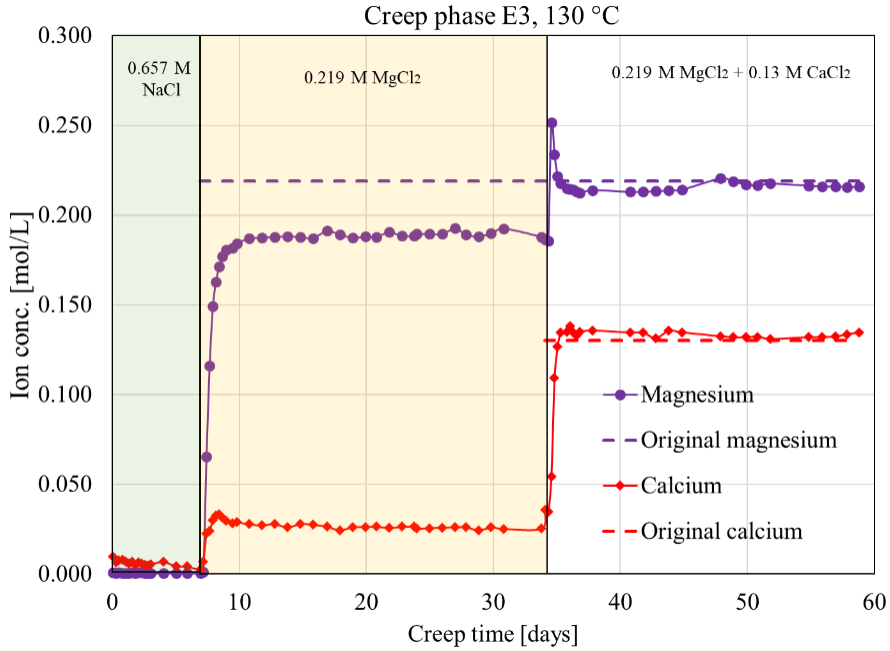

Figure 7: Magnesium (purple line), calcium (red line) and sulfate (blue line) concentrations of effluents [mol/L] during creep time [days] and flooding with inert bine (green shade) magnesium chloride (yellow shade) and calcite-enhanced magnesium chloride (unshaded) of core E3. Dashed lines indicate original ion concentrations.

When changing from NaCl to $MgCl_2$, a transient behavior in calcium production and magnesium retention can be observed in Figure 6 (red line, respectively purple line). A calcium peak starts, when introducing $MgCl_2$, from a concentration of ~ 0.003 mol/L before the production of calcium increases to a maximum value of 0.033 and stabilizes at 0.026 mol/L around day 10 of creep. This corresponded with loss of magnesium, as the concentration in the sampled effluent increased from

0 and stabilizes at ~ 0.190 mol/L, clearly below the injected concentration of 0.219 mol/L.

When 0.130 M $CaCl_2$ was added to the flooding brine in the period between 34 and 59 days of creep, an immediate response in the calcium production and magnesium retention occurred. As seen in Figure 6, the produced calcium concentration increased and slightly exceeded 0.130 mol/L (by ~0.01 mol/L), then it gradually decreased over the next 15 days and the difference between the effluent calcium concentration and that of the injected brine became negligible. Complementary to the calcium profile, a large peak in the magnesium effluent concentration with a maximum value of 0.252 mol/L can be observed. Thereafter, the magnesium concentration decreased quickly (~1-2 days), but only slightly below (~0.01 mol/L) the injected concentration, unlike during the previous brine injection. After ~15 d the effluent concentration was practically identical to that of the injected.

Generally, the evolution of magnesium and calcium concentrations are mirrored, retention of magnesium corresponding closely to excess production of calcium. This in in agreement with previous experimental studies (Madland et al. 2011; Megawati 2011, 2015; Andersen et al. 2012, 2018; Minde et al. 2018) which show that when injecting brines containing reactive Ca and Mg ions, the dissolution of calcite and precipitation of magnesite can occur in a substitution-like way, as the moles Ca production is the same as moles Mg retention, as described by the reaction:

$$CaCO_3(s) + Mg^{2+}(aq) \leftrightarrow MgCO_3(s) + Ca^{2+}(aq).$$

3.3. *Field Emission Gun-Scanning Electron Microscopy (FEG-SEM) – core E3*

Mineralogical and compositional analysis by Scanning Electron Microscopy (SEM) combined with Energy-dispersive X-ray spectroscopy (EDS) have been performed at the inlet of the Eldfisk core E3, which has been exposed to 81 PVs $MgCl_2$ and 75 PVs $MgCl_2$ +

$CaCl_2$. FEG-SEM images from the flooded core are shown in Figures 7 and 8. Chemical alteration is shown in Figure 8 by the occurrence of newly formed minerals in open pore spaces, mostly inside foraminifer shells.

The crystals appear as trigonal aggregates and the EDS spectrum indicates a high magnesium content (Figure 8, right). The sharp edges indicate in-situ, post-depositional precipitation. An unequivocal interpretation of the new mineral crystals is difficult because of their small sizes (~ 1µm), although it is likely to assume they are magnesite , as precipitation of magnesite has been confirmed in several studies on outcrop chalk flooded with $MgCl_2$ brine (Zimmermann et al., 2015; Andersen et al., 2018; Wang et al., 2018; Minde et al., 2020).

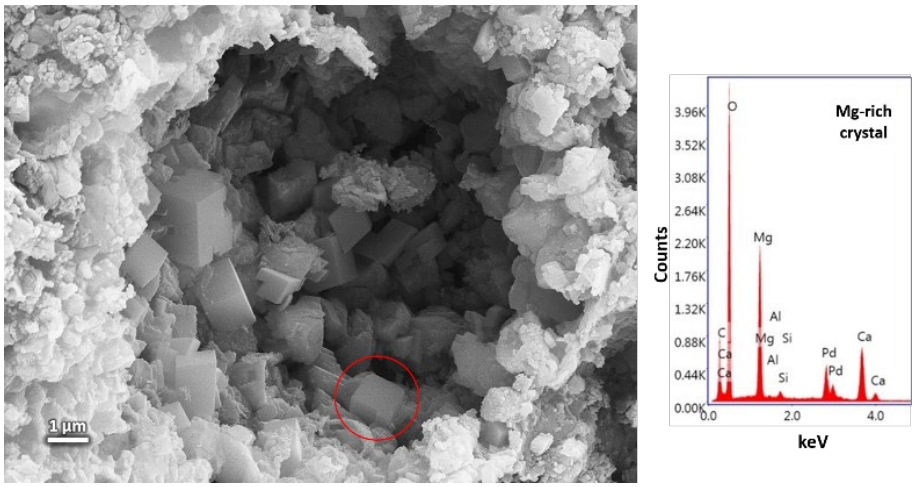

Figure 8: Left: SEM micrograph of flooded chalk fragment from the inlet of core E3; red circle shows Mg-rich crystal. Right: EDS spectrum of the encircled crystal, possibly magnesite.

In addition, the SEM image and the EDS analysis reveal the presence of flakey clay minerals containing both magnesium and silicon (Figure 9, red circle). These Si-Mg-rich minerals are also interpreted to be newly grown clay minerals as a result of injection of Mg-rich brines, a process observed in outcrop chalk studies as well (Madland et al., 2011; Minde et al., 2018; Minde et al., 2020). The SEM micrograph in Figure 9 also

shows unbroken microfossils are still present, along with occurrence of clay minerals and quartz. A part of these clay minerals is believed to be kaolinite originally present in the core before flooding. This is indicated by the EDS analysis in Figure 9 (right) which shows high aluminum and silicon weight percent around 23.4 and 24.3 % respectively, in addition to minor occurrence of magnesium, ~ 0.3 wt %, that probably remained from flooding with $MgCl_2$.

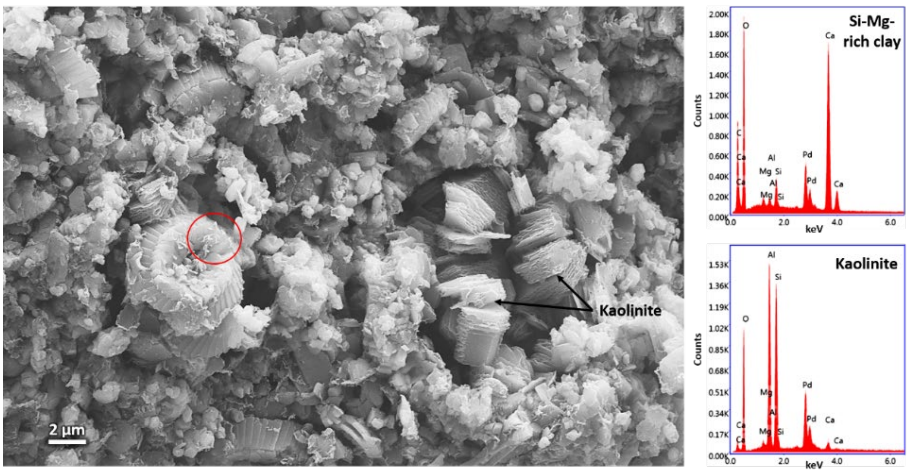

Figure 9: SEM micrograph of flooded E3 containing fibrous Si-Mg-rich minerals precipitated on cocolith surfaces (red circle) and most likely kaolinite growth inside foraminifer cavity; Right: EDS analysis of these two mineral phases

4. Discussion

The results from geomechanical testing of Eldfisk reservoir chalk cores in controlled laboratory conditions give a unique insight into the compaction behavior of reservoir chalk exposed to thermo-chemical influence, under hydrostatic stress conditions. A direct comparison between this study and the outcrop chalk experiments is difficult, given that the test parameters are not identical (i.e., different stress values, test time). However, under hydrostatic stress conditions, at 130° C and exposed to chemical perturbation, generally Eldfisk reservoir chalk showed similar behavior as outcrop chalk described in Madland et al.,

2011; Megawati et al., 2011; Korsnes et al., 2013; Megawati et al., 2015; Zimmermann et al., 2015; Andersen et al., 2018; Minde et al., 2018; Nermoen et al., 2018; Wang et al., 2018; Sachdeva et al., 2019a in terms of mechanical and chemical response. This not only validates such experiments on outcrop chalk as relevant for reservoir chalk, but it also confirms the observations made by Sachdeva et al., 2019b, that the initial wettability of the chalk cores was inconsequential regarding the effect of the imposed fluids on the mechanical behavior of chalk. The presence of hydrocarbons in the cores used in this study did not seem to hinder the water weakening effect, indicating that application of rock-fluid interactions observed in water-wet experiments can be valid also in a reservoir context.

4.1 *Mechanical behavior in hydrostatic loading phase*

Hydrostatic loading caused a linear stress-strain relationship in both tests, E2 and E3, and neither of the cores yielded, i.e., the deformation rate did not increase in respect to the hydrostatic loading rate. Madland et al., 2011 reported yield point at approximately 8 MPa for outcrop chalk from Liège under the same stress and thermochemical conditions (hydrostatic stress, NaCl at 130° C). The difference in yielding behavior may be related to chalk porosity (41 % in Madland et al., 2011 tests compared to 18-19 % in this study) as chalk's mechanical strength increases with decreasing porosity (Risnes and Flaageng, 1999). Also, the nature of the saturation fluid can influence the core stiffness (Sachdeva et al., 2019b), so that the presence of residual oil in may have stiffened the reservoir cores.

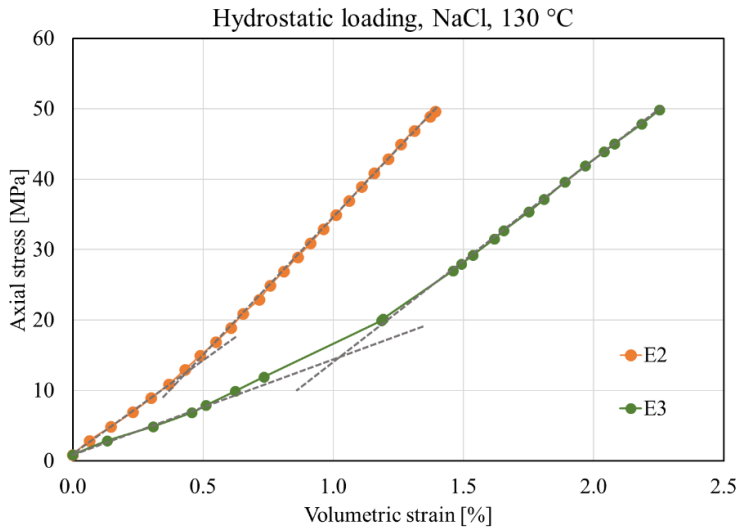

Figure 10: Change in axial stress [MPa] - volumetric strain [%] relationship during hydrostatic loading

However, a non-linear stress-strain behavior is observed in the beginning of the loading at approximately 15 MPa (Figure 10) where the strain rate decreases and the stress-strain linearity slope increases by 23 % for core E2 and 44 % for core E3. This could be related to the condition of the cores, as commonly noticed in rocks under large stresses (Fjær et al., 2008), especially in rocks that contain fine/small-scale cracks. As the confining pressure increases, the fine cracks are compressed, resulting in a relatively higher initial strain. As the crack aperture closes, the compression of the core becomes more difficult, thus, the rate of deformation becomes lower promoting a new elastic phase of linear stress-strain from which the bulk modulus is estimated.

Although the test conditions were the same for both cores (same hydrostatic loading rate, NaCl injection at 130 °C) the bulk modulus (K-modulus) differs between the two cores (3.9 GPa for E2 and 2.8 GPa for E3). The lower bulk modulus of E3 at the end of the loading phase also corresponds to a higher radial strain compared to E2, by a factor of 2.3, which contributed to a lower volumetric strain rate. This can be related

to a brief, abrupt piston pressure cycle during test setup, when the piston pressure jumped from 0.55 MPa to 4.8 MPa, as the piston touched the core. This could have caused an expansion of the core diameter and axial compaction. The difference in radial strain between the two cores may also be related to the closure of fissures during hydrostatic loading; given that the two cores had almost the same initial effective porosity, this may be an indication that core E3 contained larger or more vertical fissures than core E2. The observation that the discrepancy in radial strain was evident only during loading phase, with increasing confining pressure, also supports this suggestion; during the first approximately 7 days of creep, when the stress was kept constant and before changing the injecting brine, the radial strain was comparable between the two cores. However, since both cores generally show the similar response to stress and brine chemistry, suggests that for this type of test, where the focus is primarily on the qualitative assessment of the results, the initial physical condition of the cores was not of essence.

Although the cores did not yield, despite the high confining pressure (50 MPa), their deformation was not elastic, as the accumulated strain during testing was irreversible. The estimated volumetric strain after unloading was approximately 5 % for E2 and 8 % for E3.

4.2 *Effect of NaCl injection during creep*

During flooding of E2 and E3 with NaCl, ion chromatograph analysis detected dissolution of calcite in the beginning of the creep phase (Figures 11 and 12). Thereafter, the calcium concentration in the effluents decreased down to 0.003 mol/L in both tests before changing the injected brine, implying that NaCl is weakly reactive towards the chalk surface. However, the interaction between chalk and NaCl is negligible and comparable to observations from Nermoen et al, 2016 and Andersen et al., 2018 where the concentration of produced calcium when flooding NaCl through outcrop chalk cores at 130°C stabilized between 0.002 – 0.004 mol/L.

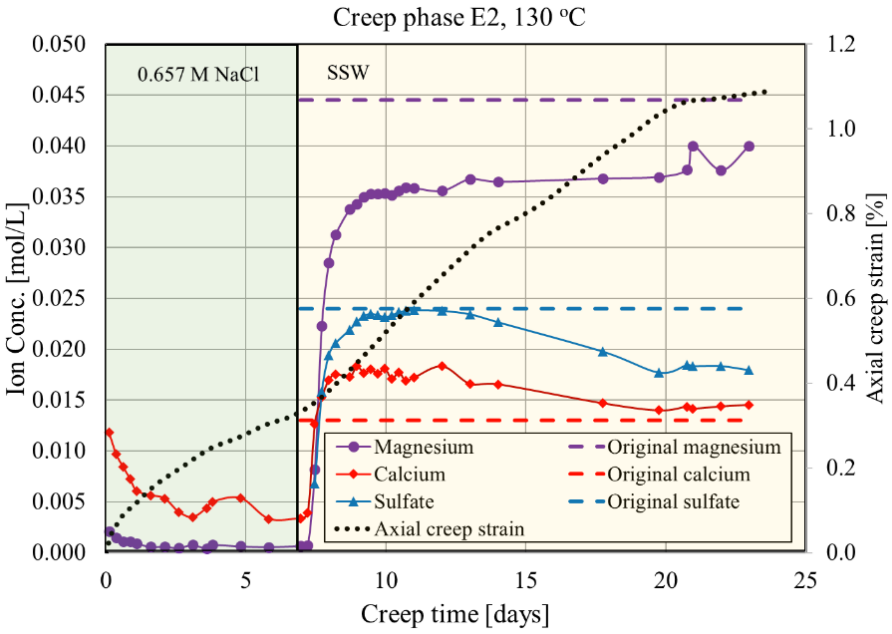

Figure 11: Axial deformation (dotted black line) and magnesium (purple line), calcium (red line) and sulfate (blue line) concentrations of effluents [mol/L] during creep time [days] and flooding inert (green shade) and reactive (yellow shade) brine of core E2. Dashed lines indicate original ion concentrations.

The deformation during the first approximately 7 days of hydrostatic creep follows a typical curve for porous rocks (Figure 11, 12, black dotted line). The transient (primary) creep, recognized by a diminishing deformation rate, is followed by steady state deformation (secondary creep), where the strain rate is constant. An acceleration of strain rate may occur over time, (tertiary creep), usually associated with high effective stresses, which leads rapidly to core failure (Hudson, 1993; Fjær et al., 2008). However, this is not the case here. The cores did not fail, indicating that the increasing deformation rate observed in both tests after changing injecting brines is not related to chalk poroelastic behavior. Since the test setup provides that other test parameters that could influence strain rate, such as stress, temperature, or brine injection rate (Nermoen et al., 2016; Sachdeva et al., 2019 b) remain the same

throughout the creep phase, the change in strain rate can only be the result of the change of injecting brine composition.

4.3 *Effect of SSW injection during creep*

The effect of the major divalent ions i.e. magnesium, calcium and sulphate, on the mechanical response of the Eldfisk core E2, have been emphasized during the continuous flow of seawater throughout the creep phase. In Figure 11, both the axial creep strain (dotted black line) and the concentrations of the surface active ions in seawater (Mg^{2+}, Ca^{2+}, and SO_4^{2-}) present in the effluents are plotted versus creep time for core E2.

The core's axial creep rate increases compared to when injected with NaCl, while at the same time magnesium ions are retained in the core and calcium ions are produced. The excess calcium and the loss of magnesium can be explained by dissolution of calcite and precipitation of magnesium-bearing minerals, seemingly the ongoing processes during seawater injection.

Additionally, the decrease in concentration of sulphate ions when flooding the core with seawater at 130°C, together with clogging in the outlet steel tubing after ~ 20 days of SSW injection, point toward the precipitation of new minerals such as anhydrite, $CaSO_4$ (Heggheim et al., 2005; Hiorth et al., 2008; Madland et al., 2008). Also, the sum of measured magnesium concentration and the additional amount of calcium ions in the effluent are lower than the magnesium concentration of the injected brine, i.e. 0.0445 mol/L, which can confirm the occurrence of anhydrite precipitation (Madland et al., 2011). Due to anhydrite formation, the fluid in the pores would be undersaturated with respect to calcium, which promotes calcite dissolution.

4.4 *Effect of $MgCl_2$ injection during creep*

$MgCl_2$ represents a simplified aqueous chemistry of seawater, and it is injected specially to investigate the effect of magnesium ions on the mechanical strength of chalk. When core E3 is injected with $MgCl_2$, after switching from NaCl, a clear physical response is observed. The

chemically induced creep deformation is reflected in the plot of axial strain along (dotted black line) with the effluent concentration profiles as a function of creep time in Figure 12.

A steady considerable amount of excess calcium (red line) was produced, approximately 0.026 mol/L, while a substantial amount of magnesium (purple line) was retained in the core (approximately 0.03 mol/L) as the $MgCl_2$ flooding commenced. This calcium production, indicative of calcite dissolution is significantly higher than that observed during NaCl injection and it is in the same range as the calcium production described in Andersen et al., 2018 from experiments on outcrop chalk from Liège, Mons (Belgium) and Stevns Klint (Denmark).

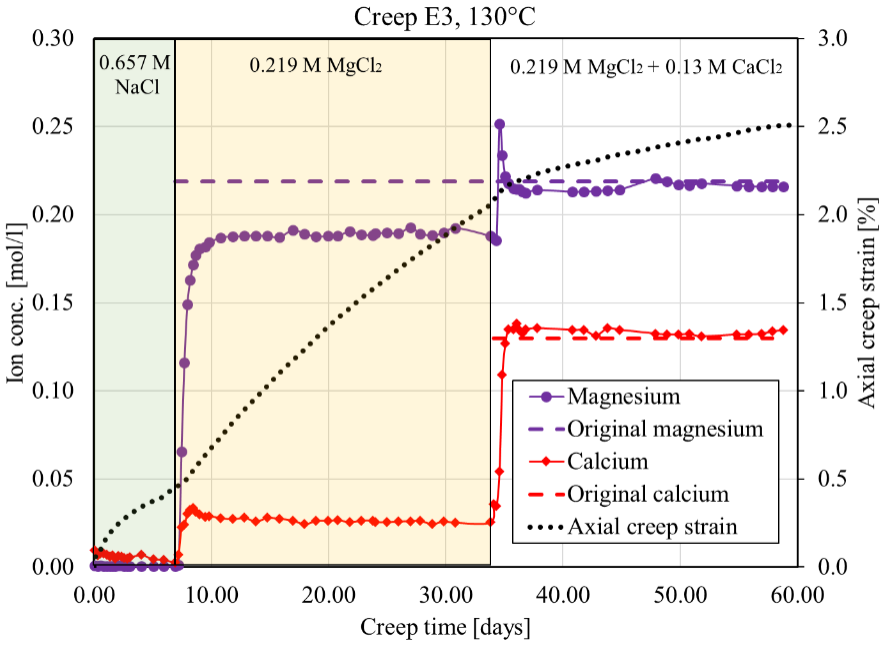

Figure 12: Axial deformation (dotted black line) and magnesium (purple line) and calcium (red line) concentrations of effluents [mol/L] during creep time [days] and flooding inert brine (green shade) magnesium chloride (yellow shade) and calcite-enhanced magnesium chloride (unshaded) of core E3. Dashed lines indicate original ion concentrations.

At the same time, the axial strain rate increased (Figure 12, dotted line) as a response to the non-equilibrium nature of the rock-fluid interface. Chemically induced deformation has been observed in multiple earlier

studies on outcrop chalk (Madland et al., 2008; Madland et al., 2011; Megawati et al., 2015; Andersen et al., 2018; Minde et al., 2018; Wang et al., 2018) which explain it as a result of calcite dissolution enhanced by precipitation of magnesium-bearing minerals.

This is seen here as well, newly precipitated magnesium-bearing minerals also having been detected in the inlet of E3 by SEM-EDS analysis (Figure 8). Although not clearly identified, due to their minute size, these newly precipitated crystals are most likely magnesite, agreeing to previous studies on outcrop chalk at similar conditions (Korsnes et al., 2013; Zimmermann et al., 2015, Minde et al., 2018). Magnesium-rich minerals have higher densities than calcite, thereby, less volume is occupied in the core as magnesite and other magnesium-bearing minerals precipitate at the expense of calcite. This is likely to contribute to the enhancement of creep strain. However, future studies comparing the mineral and geochemical composition of the cores before and after testing will allow a more comprehensive evaluation of the physical and compositional changes induced by the rock-fluid interactions.

4.5 *Effect of adding $CaCl_2$ to $MgCl_2$*

Adding $CaCl_2$ to $MgCl_2$ produced a similar effect as described in Megawati et al. (2011). Figure 12 shows that as soon as $CaCl_2$ is added to the $MgCl_2$ brine, the magnesium (purple line) and calcium concentrations (red line) lay steady around the original ion concentrations of the injected brine, together with a clear reduction in creep compaction rate (dotted black line). Andersen and Berawala (2019) explained this phenomenon by mathematical modeling where the creep compaction was driven both by a stress component and a dissolution rate component. Reducing or eliminating the dissolution rate would result in strongly reduced compaction rate, but not a full stop. Accordingly, the compaction reduction here was clear, but not as severe as seen in the study by Megawati et al. (2011) on outcrop chalk (Liège, Gulpen Fm) where the deformation nearly ceased. This may be due to textural differences between the two chalk cores or the different test parameters

(creep stress at 11.6 MPa in Megawati et al. 2011 compared to 50 MPa in this study, and over different periods of time).

5. Conclusions

Hydrostatic loading and creep compaction with continuous brine injection was performed on two Eldfisk reservoir chalk cores. The ion concentrations of the effluent water samples have been analyzed chemically, and a sample from the inlet of the core flooded with magnesium chloride brines has been analyzed by SEM-EDS. Thereafter, the geomechanical behavior of Eldfisk cores have been compared with previous results obtained from onshore outcrop chalks. The main conclusions can be summarized as follows:

- Production of excess calcium and retention of magnesium while flooding seawater-like brines are explained by of dissolution of primary calcite and precipitation of secondary Mg-bearing minerals. It is probable that the retention of sulphate ions in SSW enables anhydrite precipitation.
- Dissolution and precipitation processes seem to be key driving mechanisms for chemical creep compaction in the flooding experiments of reservoir core chalk.
- The creep deformation rate depended on the flooding brine: SSW and $MgCl_2$ injection caused excess production of calcium (calcite dissolution) which correlated with enhanced water weakening of Eldfisk cores compared to when flooding NaCl brine. Adding calcium to $MgCl_2$ stopped calcium production, which resulted in clear attenuation of the creep strain.
- The Eldfisk reservoir chalk cores behaved in a comparable manner to outcrop cores under similar test conditions (stress and thermochemical exposure) in terms of rock-fluid interactions (such as dissolution and precipitation processes as mentioned above) and geo-mechanical behavior (i.e., water weakening), despite the natural differences between the chalk types (depositional environments, stress history, diagenetic grade, mineralogy) and the wettability phase. This indicates that observations of the effect of water-

weakening mechanisms on outcrop chalk can also be valid for reservoir chalk.

Acknowledgement: The authors acknowledge the Research Council of Norway and the industry partners, ConocoPhillips Skandinavia AS, Aker BP ASA, Vår Energi AS, Equinor ASA, Neptune Energy Norge AS, Lundin Norway AS, Halliburton AS, Schlumberger Norge AS, and Wintershall DEA, of The National IOR Centre of Norway for support.

References

1. Ahsan, R., & Fabricius, I. L. (2010, June). Sorption of magnesium and sulfate ions on calcite. In *72nd EAGE Conference and Exhibition-Workshops and Fieldtrips* (pp. cp-161). European Association of Geoscientists & Engineers.
2. Andersen, P. Ø., Wang, W., Madland, M. V., Zimmermann, U., Korsnes, R. I., Bertolino, S. R. A., ... & Gilbricht, S. (2018). Comparative study of five outcrop chalks flooded at reservoir conditions: chemo-mechanical behaviour and profiles of compositional alteration. *Transport in Porous Media*, *121*(1), 135-181.
3. Andersen, P. Ø., & Berawala, D. S. (2019). Modeling of Creep-Compacting Outcrop Chalks Injected with Ca-Mg-Na-Cl Brines at Reservoir Conditions. *SPE Journal*.
4. Boyle, R. A defence of the doctrine touching the spring and weight of the air [1669]. *The Work of the Honourable Robert Boyle*, *1*.
5. Brasher, J. E., & Vagle, K. R. (1996). Influence of lithofacies and diagenesis on Norwegian North Sea chalk reservoirs. *AAPG bulletin*, *80*(5), 746-768.
6. Collin, F., Cui, Y. J., Schroeder, C., & Charlier, R. (2002). Mechanical behaviour of Lixhe chalk partly saturated by oil and water: experiment and modelling. *International journal for numerical and analytical methods in geomechanics*, *26*(9), 897-924.

7. Cook, C. C., & Brekke, K. (2004). Productivity preservation through hydraulic propped fractures in the Eldfisk North Sea chalk field. *SPE Reservoir Evaluation & Engineering*, *7*(02), 105-114.
8. Fabricius, I. L., & Borre, M. K. (2007). Stylolites, porosity, depositional texture, and silicates in chalk facies sediments. Ontong Java Plateau–Gorm and Tyra fields, North Sea. *Sedimentology*, *54*(1), 183-205.
9. Fjær, E., Holt, R. M., Horsrud, P., Raaen, A. M., and Risnes, R. (2008) Petroleum related rock mechanics *(2nd ed. ed. Vol. 53),* 50;257.
10. Gautier, J. M., Oelkers, E. H., & Schott, J. (2001). Are quartz dissolution rates proportional to BET surface areas?. *Geochimica et Cosmochimica Acta*, *65*(7), 1059-1070.
11. Heggheim, T., Madland, M. V., Risnes, R., & Austad, T. (2005). A chemical induced enhanced weakening of chalk by seawater. *Journal of Petroleum Science and Engineering*, *46*(3), 171-184.
12. Hermansen, H., Thomas, L. K., Sylte, J. E., & Aasboe, B. T. (1997, January). Twenty five years of Ekofisk reservoir management. In *SPE annual technical conference and exhibition*. Society of Petroleum Engineers.
13. Hermansen, H., Landa, G. H., Sylte, J. E., & Thomas, L. K. (2000). Experiences after 10 years of waterflooding the Ekofisk Field, Norway. *Journal of Petroleum Science and Engineering*, *26*(1-4), 11-18.
14. Hiorth, A., Cathles, L. M., Kolnes, J., Vikane, O., Lohne, A., & Madland, M. V. (2008, October). Chemical modelling of wettability change in carbonate rocks. In *10th Wettability Conference, Abu Dhabi, UAE* (pp. 1-9).
15. Hiorth, A., Cathles, L. M., & Madland, M. V. (2010). The impact of pore water chemistry on carbonate surface charge and oil wettability. *Transport in porous media*, *85*(1), 1-21.
16. Hjuler, M. L., & Fabricius, I. L. (2009). Engineering properties of chalk related to diagenetic variations of Upper Cretaceous onshore

and offshore chalk in the North Sea area. *Journal of Petroleum Science and Engineering*, *68*(3-4), 151-170.

17. Hudson, J. N. (1993). Comprehensive rock engineering, principals, practice and projects, volume 3, Rock testing and site characterization. Ed. Pergamon Press. Oxford, 119-121.
18. Japsen, P. (1998). Regional velocity-depth anomalies, North Sea Chalk: a record of overpressure and Neogene uplift and erosion. *AAPG bulletin*, *82*(11), 2031-2074.japsen
19. Japsen, P., & Bidstrup, T. (1999). Quantification of late Cenozoic erosion in Denmark based on sonic data and basin modelling. *Bulletin of the Geological Society of Denmark*, *46*, 79-99.
20. Japsen, P. (2000). Fra Kridthav til Vesterhav. Nordsøbassinets udvikling vurderet ud fra seismiske hastigheder. *Change*, *24*, 165-173.
21. Jarvis, I. (2006). The Santonian-Campanian phosphatic chalks of England and France. *Proceedings of the Geologists' Association*, *117*(2), 219-237.
22. Kallesten, E. I., Andersen, P. Ø., Madland, M. V., Korsnes, R. I., Omdal, E., & Zimmermann, U. (2020a). Permeability Evolution of Shear Failing Chalk Cores under Thermochemical Influence. *ACS omega*, *5(16)*, 9185-9195.
23. Kallesten, E., Andersen, P. Ø., Berawala, D. S., Korsnes, R. I., Madland, M. V., Omdal, E., & Zimmermann, U. (2020b). Modeling of Permeability and Strain Evolution in Chemical Creep Compaction Experiments with Fractured and Unfractured Chalk Cores Conducted at Reservoir Conditions. Society of Petroleum Engineers. *SPE Journal*. SPE-197371-PA.
24. Korsnes, R. I., Madland, M. V., & Austad, T. (2006, April). Impact of brine composition on the mechanical strength of chalk at high temperature. In *Eurock* (pp. 133-140).
25. Korsnes, R. I., Zimmermann, U., Madland, M. V., Bertolino, S. A. R., Hildebrand-Habel, T., & Hiorth, A. (2013, November). Tracing Fluid Flow in Flooded Chalk under Long Term Test Conditions.

In *First EAGE West Africa Workshop 2013-Subsurface Challenges in West Africa* (pp. cp-348). European Association of Geoscientists & Engineers.

26. Madland, M. V., Midtgarden, K., Manafov, R., Korsnes, R. I., Kristiansen, T., & Hiorth, A. (2008, October). The effect of temperature and brine composition on the mechanical strength of Kansas chalk. In *International Symposium SCA*.
27. Madland, M. V., Hiorth, A., Omdal, E., Megawati, M., Hildebrand-Habel, T., Korsnes, R. I., ... & Cathles, L. M. (2011). Chemical alterations induced by rock–fluid interactions when injecting brines in high porosity chalks. *Transport in porous media*, *87*(3), 679-702.
28. Madsen, H. B. (2010). Silica diagenesis and its effect on porosity of upper Maastrichtian chalk–an example from the Eldfisk Field, the North Sea. *Bulletin of the Geological Society of Denmark*, *20*, 47-50.
29. Megawati, M., Andersen, P. Ø., Korsnes, R. I., Evje, S., Hiorth, A., & Madland, M. V. (2011). The effect of aqueous chemistry ph on the time-dependent deformation behaviour of chalk experimental and modelling study. *Pore2Fluid IFP Energies nouvelles Paris, Nov*, 16-18.
30. Megawati, M., Hiorth, A., & Madland, M. V. (2013). The impact of surface charge on the mechanical behavior of high-porosity chalk. *Rock mechanics and rock engineering*, *46*(5), 1073-1090.
31. Megawati, M., Madland, M. V., & Hiorth, A. (2015). Mechanical and physical behavior of high-porosity chalks exposed to chemical perturbation. *Journal of Petroleum Science and Engineering*, *133*, 313-327.
32. Minde, M. W., Zimmermann, U., Madland, M. V., Korsnes, R. I., Schulz, B., & Audinot, J. N. (2016, August). Fluid–flow during EOR experiments in chalk: insights using SEM–MLA, EMPA and Nanosims Applications. In *International Symposium of the Society of Core Analysts. Colorado, USA* (pp. 21-26).
33. Minde, M. W., Wang, W., Madland, M. V., Zimmermann, U., Korsnes, R. I., Bertolino, S. R., & Andersen, P. Ø. (2018).

Temperature effects on rock engineering properties and rock-fluid chemistry in opal-CT-bearing chalk. *Journal of Petroleum Science and Engineering*, *169*, 454-470.

34. Minde, M. W., Zimmermann, U., Madland, M. V., Korsnes, R. I., Schulz, B., & Gilbricht, S. (2020). Mineral replacement in long-term flooded porous carbonate rocks. *Geochimica et Cosmochimica Acta*, *268*, 485-508.
35. Molenaar, N., & Zijlstra, J. J. P. (1997). Differential early diagenetic low-Mg calcite cementation and rhythmic hardground development in Campanian-Maastrichtian chalk. *Sedimentary Geology*, *109*(3-4), 261-281.
36. Nermoen, A., Korsnes, R. I., Hiorth, A., & Madland, M. V. (2015). Porosity and permeability development in compacting chalks during flooding of nonequilibrium brines: Insights from long-term experiment. *Journal of Geophysical Research: Solid Earth*, *120*(5), 2935-2960.
37. Nermoen, A., Korsnes, R. I., Aursjø, O., Madland, M. V., Kjørslevik, T. A., & Østensen, G. (2016). How stress and temperature conditions affect rock-fluid chemistry and mechanical deformation. *Frontiers in Physics*, *4*, 2.
38. Nermoen, A., Korsnes, R. I., Storm, E. V., Stødle, T., Madland, M. V., & Fabricius, I. L. (2018). Incorporating electrostatic effects into the effective stress relation—Insights from chalk experiments. *Geophysics*, *83*(3), MR123-MR135.
39. Puntervold, T., & Austad, T. (2008). Injection of seawater and mixtures with produced water into North Sea chalk formation: Impact of fluid–rock interactions on wettability and scale formation. *Journal of Petroleum Science and Engineering*, *63*(1-4), 23-33.
40. Risnes, R., & Flaageng, O. (1999). Mechanical properties of chalk with emphasis on chalk-fluid interactions and micromechanical aspects. *Oil & Gas Science and Technology*, *54*(6), 751-758.

41. Sachdeva, J. S., Muriel, H., Nermoen, A., Korsnes, R. I., & Madland, M. V. (2019 a). Chalk Surface Area Evolution during Flow of Reactive Brines: Does Oil Play a Role?. *Energy & Fuels*, *33*(6), 4890-4908.
42. Sachdeva, J. S., Nermoen, A., Korsnes, R. I., & Madland, M. V. (2019 b). Impact of Initial Wettability and Injection Brine Chemistry on Mechanical Behaviour of Kansas Chalk. *Transport in Porous Media*, *128*(2), 755-795.
43. Scholle, P. A. (1977). Chalk diagenesis and its relation to petroleum exploration: oil from chalks, a modern miracle?. *AAPG Bulletin*, *61*(7), 982-1009.
44. Schroeder, C., Bois, A. P., Maury, V., & Halle, G. (1998, January). Water/chalk (or collapsible soil) interaction: Part II. Results of tests performed in laboratory on Lixhe chalk to calibrate water/chalk models. In SPE/ISRM Rock Mechanics in Petroleum Engineering. Society of Petroleum Engineers.
45. Strand, S., Hjuler, M. L., Torsvik, R., Pedersen, J. I., Madland, M. V., & Austad, T. (2007). Wettability of chalk: impact of silica, clay content and mechanical properties. *Petroleum Geoscience*, *13*(1), 69-80.
46. Sulak, A. M., & Danielsen, J. (1988, January). Reservoir aspects of Ekofisk subsidence. In *Offshore Technology Conference*. Offshore Technology Conference.
47. Teufel, L. W., Rhett, D. W., & Farrell, H. E. (1991, January). Effect of reservoir depletion and pore pressure drawdown on in situ stress and deformation in the Ekofisk field, North Sea. In *The 32nd US Symposium on Rock Mechanics (USRMS)*. American Rock Mechanics Association.
48. Wang, W., Madland, M. V., Zimmermann, U., Nermoen, A., Korsnes, R. I., Bertolino, S. R., & Hildebrand-Habel, T. (2018). Evaluation of porosity change during chemo-mechanical compaction in flooding experiments on Liege outcrop chalk. *Geological Society, London, Special Publications*, *435*(1), 217-234.

49. Zimmermann, U., Madland, M. V., Nermoen, A., Hildebrand-Habel, T., Bertolino, S. A., Hiorth, A., ... & Grysan, P. (2015). Evaluation of the compositional changes during flooding of reactive fluids using scanning electron microscopy, nano-secondary ion mass spectrometry, x-ray diffraction, and whole-rock geochemistryCompositional Changes during Flooding. *AAPG Bulletin*, *99*(5), 791-805.

ACS Omega 2020, 5, 9185 – 9195

Paper III: Permeability evolution of shear failing chalk cores under thermochemical influence

Kallesten, E., Andersen, P.Ø., U., Madland, M.V., Korsnes, R.I., Omdal, E., Zimmermann, U.

ACS Omega 2020, 5, 9185 – 9195

Paper III

ACS OMEGA

http://pubs.acs.org/journal/acsodf

Article

Permeability Evolution of Shear Failing Chalk Cores under Thermochemical Influence

Emanuela I. Kallesten,* Pål Østebø Andersen, Merete V. Madland, Reidar I. Korsnes, Edvard Omdal, and Udo Zimmermann

Cite This: *ACS Omega* 2020, 5, 9185−9195

Read Online

ACCESS | Metrics & More | Article Recommendations

ABSTRACT: Development of petroleum reservoirs, including primary depletion of the pore pressure and repressurization during water injection naturally, leads to changes in effective stresses of the formations. These changes impose mechanical deformation of the rock mass with subsequent altering of its petrophysical properties. Besides mechanical compaction, chalk reservoirs on the Norwegian Continental Shelf also seem susceptible to mineralogical and textural changes as an effect of the injecting fluid's chemical composition and temperature. Understanding such chemical and thermal effects and how they interplay with the mechanical response to changes in effective stresses could contribute to improved prediction of permeability development during field life. This article presents results from mechanical testing of chalk cores of medium-porosity (32%) outcrop chalk (Niobrara Formation, Kansas) in triaxial cells. The experimental setup allows systematic combinations of fluctuating deviatoric stress, temperature (50 and 130 °C), and injecting fluid (calcite-equilibrated sodium chloride, calcite-equilibrated sodium sulfate, and reactive synthetic seawater) intended to replicate in situ processes, relevant to the North Sea chalk reservoirs. Deviatoric loading above yield resulted in a shear failure with a steeply dipping fracture of the core and a simultaneous increase in permeability. This occurred regardless of the brine composition. The second and third deviatoric loadings above yield did not have the same strong effect on permeability. During creep and unloading, the permeability changes were minor such that the end permeability remained higher than the initial values. However, sodium sulfate-injected cores retained most of the permeability gain after shear fracturing compared to sodium chloride and synthetic seawater series at both temperatures. Synthetic seawater-injected cores registered the most permeability loss compared to the other brines at 130 °C. The results indicate that repulsive forces generated by sulfate adsorption contribute to maintain the fracture permeability.

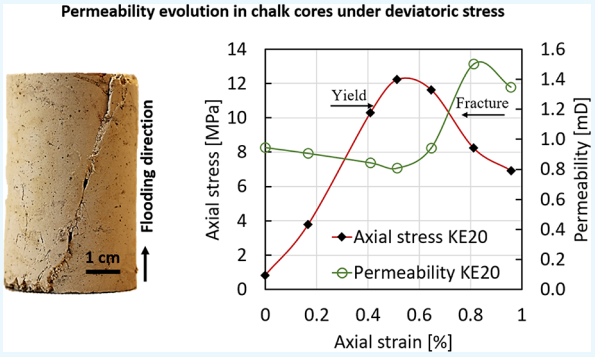

1. INTRODUCTION

Water-related improved oil recovery (IOR) techniques have a documented effect on hydrocarbon production in naturally fractured chalk reservoirs, and the success story of seawater injection at the Ekofisk field (North Sea, Norway) is closely linked to fracture permeability. With the matrix permeability evaluated in the range of 1−5 mD, the Ekofisk field chalk accommodates a natural fracture system that enhances the total reservoir permeability by a factor of 50.[1]

After several years of primary oil recovery by pore pressure depletion, the effective stress (overburden minus pore pressure) increased, causing the compaction mechanisms of the reservoir chalk to resume. This did not only lead to severe seafloor subsidence and challenges for the production facilities but also lead to significant changes in the physical and mechanical properties of the rock. Yet, despite years of compaction, loss of permeability was not detected.[2,3] Sulak[2] stated that, even though matrix permeability declined with matrix compaction, the effect was of no apparent consequence to the effective permeability. This seeming paradox indicated that fracture permeability, in another order of magnitude compared to the matrix permeability, dominates the effective permeability evolution. Additionally, Teufel[3] pointed out that the deviatoric nature of the reservoir stress state seems to govern the permeability of fractures such that steeply dipping fractures aligned with the maximum horizontal stress, as seen at Ekofisk, will suffer the least permeability loss. The study also underlined the different permeability behaviors under hydrostatic conditions, where permeability declines steadily with increasing hydrostatic stress.

Received: December 28, 2019
Accepted: April 1, 2020
Published: April 13, 2020

This behavior is clearly demonstrated[4−7] and does not capture permeability changes under deviatoric stresses, typical for reservoirs.

Stress anisotropy was also one of the reasons why field-wide implementation of seawater injection at the Ekofisk field in 1987 was remarkably successful. Teufel and Rhett[8] showed that decreasing effective mean stress by water injection while maintaining a large shear stress leads to increasing fracture density and fracture surface area and to significantly increased reservoir permeability.

Maintaining high fracture permeability, on the other hand, is not without challenges as production-related changes such as primary depletion of the pore pressure and repressurization during water injection continuously alter the effective stresses of the successions.[9,10] Such stress history affects the physical properties of porous rocks and their mechanical strength,[11,12] generating a complex porosity−permeability behavior in porous rocks. Studies of fracture permeability response to fluctuating effective stress[13−15] in porous rocks show less permeability changes with each stress cycle, and in any case, the loss of permeability seems irreversible. However, these studies only focus on stress-related permeability and do not incorporate other permeability-altering parameters, specific to carbonates. Ekofisk field observations of continued high compaction rates in certain areas even after repressurization and at constant pressure indicated the activity of other compaction mechanisms than only increasing effective stress and identified the chalk contact with nonequilibrium cold seawater as a likely cause.[16]

Field observations and laboratory studies remark that the temperature of the injecting fluid also contributes to continuous changes in the reservoir stress state; cold injecting fluid cools down the rock, causing it to contract and leading to a decrease in effective stress and increased permeability.[8,17] In a study of mechanical behavior of chalk cores exposed to temperature cycling, Voake et al.[18] observed more irreversible strain in chalk cores that experienced temperature fluctuations compared to cores tested at constant temperature.

Additionally, the fluid temperature plays an important role in how the fluid interacts with the reservoir rock. Chalk reservoirs found on the Norwegian Continental Shelf seem susceptible to mineralogical and textural changes, and their mechanical stability is dependent on the injected fluid's chemical composition and temperature.[7,19−26] Studies show that high temperature enhances the rock−fluid interactions and their effects are more obvious than at lower temperature. Particularly, ions such as Mg^{2+} and SO_4^{2-}, which are present in seawater, are responsible for the main chemical and mineralogical alterations in chalk (adsorption, calcite dissolution, and precipitation of new minerals). While seawater-like brines injected at increasing temperatures have a positive effect on the IOR potential,[27] they also reduce the mechanical strength of chalk, affect its elastic properties,[28] and lead to precipitation of permeability-inhibiting minerals such as anhydrite and gypsum.[23]

In the above review, most of the research has been conducted on whole cores to study the effect of systematically changing effective stress, temperature, and brine composition and see the resulting impact in terms of rock−fluid interactions, compaction, porosity, and permeability. Kallesten et al.[29] modeled chemical creep compaction in a fractured core subject to hydrostatic stresses but concluded that more experimental data were needed to characterize the fracture. A limited number of studies have considered fractured cores, deviatoric stress, or doing repeated stress cycles. Unique to the present study is that we generate fractured cores under deviatoric stress conditions and conduct repeated stress cycles while flooding inert or reactive brines at different temperatures, relevant to the chalk fields on the Norwegian Continental Shelf. The main aim is to see how different experimental conditions under stress cycles are able to affect the permeability of the system by investigating the interplay between varying parameters (stress state, temperature, and brine chemistry) and their combined effect on permeability evolution in chalk at such conditions. The test setup is designed to replicate the production-related dynamics of a chalk reservoir by considering shear-fractured outcrop chalk cores exposed to cyclic deviatoric stress states while systematically changing either the test temperature or the injected brine. In this way, different combinations of the experimental setup highlight the individual contribution of temperature, brine chemistry, and cyclic deviatoric stress on permeability evolution. The results will help answer the following:

- How do deviatoric stress cycles affect permeability?
- Is there any difference in permeability evolution when superimposing temperature or chemistry changes to the deviatoric stress cycles?
- Are these individual effects concurring or competing?

A better understanding of coexisting factors that affect reservoir permeability could bridge the gap toward an improved prediction of permeability development during field life.

2. EXPERIMENTAL PROCEDURES AND METHODS

This article presents results from mechanical testing of 12 chalk cores in triaxial cells. Such tests allow systematic changes of stress, temperature, and injecting fluid, intended to replicate in situ processes at reservoir conditions.

2.1. Sample Set. The sample set consists of 12 outcrop chalk cores (Niobrara Formation, Kansas/Utah) of medium porosity for a chalk (32%, ±1%). Experimental and theoretical studies demonstrate that mechanical strength of chalk is orientation-dependent and that chalk deformation behavior differs when main stress is applied parallel or perpendicular to bedding.[30,31] To ensure comparability between the tests, all cores are drilled from the same block collection and in the same direction. Further, the cores are cut to an average length of 75 mm and lathed to a diameter of 38.1 mm. The length−diameter ratio of approximately 2 should accommodate the steeply dipping shear fracture plane typical for deviatoric loading.[32]

2.2. Injecting Brines. The injecting brines define three test series: calcite-equilibrated sodium chloride (CE-NaCl), calcite-equilibrated sodium sulfate (CE-Na_2SO_4), and reactive synthetic seawater (SSW). By equilibrating the two former brines with calcite, no mineralogical interactions are expected, although surface reactions would be more likely. CE-NaCl is inert in all practical aspects and serves as a standard in comparison to CE-Na_2SO_4 and SSW brines. The concentrations of NaCl and Na_2SO_4 are designed to match the ionic strength of SSW (Table 1). The injection rate is 2 pore volumes (PVs)/day. After testing, the cores are flooded with 4 PVs distilled water (DW) to avoid salt precipitation.

2.3. Porosity and Permeability Calculation. For porosity calculation, the dry shaped cores were saturated with distilled water under vacuum conditions. The initial porosity (φ) is given by the ratio between pore volume (the difference in initial saturated and dry masses (M_{sat} and M_{dry}, respectively) divided by the density of distilled water (ρ_{dw})) and initial bulk volume ($V_{bulk,\ i}$)

https://dx.doi.org/10.1021/acsomega.9b04470
ACS Omega 2020, 5, 9185−9195

Table 1. Chemical Composition of Flooding Brines; Sodium Chloride (NaCl) and Sodium Sulfate (Na_2SO_4) Ionic Composition Here before Calcite Equilibration

flooding brine	NaCl	Na_2SO_4	SSW
ionic strength	0.657	0.657	0.657
Cl^- (mole L^{-1})	0.657	0.585	0.525
Na^+ (mole L^{-1})	0.657	0.633	0.450
SO_4^{2-} (mole L^{-1})		0.024	0.024
Ca^{2+} (mole L^{-1})			0.013
HCO_3^- (mole L^{-1})			0.002
Mg^{2+} (mole L^{-1})			0.045
K^+ (mole L^{-1})			0.010

$$\varphi = \frac{M_{\mathrm{sat},i} - M_{\mathrm{dry},i}}{\rho_{\mathrm{dw}} \times V_{\mathrm{bulk},i}} \quad (1)$$

The effective permeability (k) calculation is based on Darcy's law,[33] assuming a steady laminar fluid flow and symmetric axial and radial deformations

$$k = \frac{4\mu(L_i + \Delta L)Q}{\pi(D_i + \Delta D)^2 \Delta P} \quad (2)$$

where μ is the fluid viscosity as a function of salinity and temperature (cP; after El-Dessouky and Ettouny[34]), L_i is the initial length of the core (cm), ΔL is the change in core length (cm), Q is the flow rate (cm^3/s), D_i is the initial diameter of the core (cm), ΔD is the mean change in core diameter (cm), and ΔP is the pressure drop over the core during flooding (atm).

Uncertainties involved in the permeability calculation include fluid viscosity $\mu \pm 2\%$, change in core length $\Delta L \pm 0.7\%$, change in diameter $\Delta D \pm 1\%$, flooding rate $Q \pm 2\%$, and differential pressure $\Delta P \pm 0.075\%$. Permeability uncertainty Δk was estimated at $\pm 3\%$ by applying error estimation method shown in eq 3

$$\frac{\Delta k}{k} = \sqrt{\left[\frac{\Delta x}{x}\right]^2 + \left[\frac{\Delta y}{y}\right]^2 + \Delta\left[\frac{\Delta z}{z}\right]^2} \quad (3)$$

where x, ..., z are the measured values of the parameters with their respective Δx, ..., Δz uncertainty.[6]

A summary of the core properties before the mechanical testing (length, diameter, dry mass, saturated mass, porosity, permeability, and specific surface area) is listed in Table 2 and marked with index i (initial).

2.4. Triaxial Cell Tests. The triaxial cell is equipped with an outer heating jacket and a regulating system (Omron E5CN) with precise proportional integral derivative (PID) temperature control (±1.0 °C). The system includes two Quizix QX-2000HC pumps that control the axial and confining pressures independently and a fluid injection pump (Gilson 307HPLC) as well as a backpressure regulator that controls the pore pressure.

The cores are saturated with distilled water prior to cell mounting; they are isolated from the oil bath in the confining chamber by a heat shrinkage sleeve (fluorinated ethylene propylene, FEP; 0.5 mm in wall thickness). An extensometer surrounds the core at mid-length and measures the changes in diameter throughout the test (radial strain). Changes in the cores' length (axial strain) are monitored by an external axial linear variable displacement transducer (LVDT) placed on top of the cell piston.

Each series is performed at 50 °C, below the threshold for sulfate effects on chalk[35] and at 130 °C (reservoir temperature at Ekofisk) to trace the thermochemical effects on shear failing chalk cores injected with various brines. The low temperature tests require an initial heating to 130 °C to make sure that the shrinking sleeve is tight and uniform around the core, comparable to the tests at high temperature. During this stage, the injecting fluid is distilled water and brine injection only starting after the system had cooled down to 50 °C to avoid rock−brine interactions at high temperature.

Throughout the test, the confining pressure and pore pressure are constant at 1.2 and 0.7 MPa, respectively. In this way, the changes in effective stresses are a function of the increasing or decreasing axial stress. The cell piston is lowered carefully, and after core contact, it applies a pressure (0.5 MPa) that slightly overcomes the piston friction but causes negligible core deformation. The deviatoric tests start only when the triaxial cell has reached the right test temperature, the cores are brine-flooded with at least 2 PVs, the differential pressure is stable, and the system is in equilibrium (axial, radial strain rates close to 0).

2.5. Stress Cycles. The cores undergo the same stress sequence three times. The first step is axial loading at a constant injection rate (0.01 mL/min) above yield (defined by initiation of nonlinear stress−strain relationship) until shear failure (fracture formation) at which the value of axial stress drops. Immediately after, the axial pump is set to apply a constant

Table 2. List of Measurement Conditions and Core Properties before Testing[a]

flooding brine	T (°C)	core	L_i (mm)	D_i (mm)	$M_{\mathrm{dry},i}$ (g)	$M_{\mathrm{sat},i}$ (g)	φ_i (%)	k_i (mD)
CE-NaCl	50	KE4	70.3	38.12	134.6	162.7	32.6	1.24
	50	KE20	70.9	38.11	147.8	174.1	32.6	0.94
	130	KE44	76.5	38.10	159.9	188.0	32.2	0.64
	130	KE45	74.5	38.10	157.0	183.9	31.7	0.59
CE-Na_2SO_4	50	KE48	78.9	38.09	163.3	192.9	32.9	0.70
	50	KE75	75.9	38.14	158.3	186.4	32.4	0.62
	130	KE22	72.8	38.09	151.8	178.7	32.4	0.66
	130	KE55	75.9	38.10	157.3	185.5	32.6	0.61
SSW	50	KE47	75.4	38.10	155.9	184.1	32.9	0.81
	50	KE77	75.5	38.12	156.0	184.5	33.0	0.68
	130	KE51	77.1	38.10	161.7	189.9	32.1	0.58
	130	KE73	76.4	38.12	159.3	187.6	32.4	0.66

[a] T, temperature; L_i, initial length; D_i, initial diameter; $M_{\mathrm{dry},i}$, dry mass before testing; $M_{\mathrm{sat},i}$, saturated mass before testing; φ_i, initial porosity; k_i, initial permeability.

https://dx.doi.org/10.1021/acsomega.9b04470
ACS Omega 2020, 5, 9185−9195

pressure, slightly below the failure point, allowing the core to deform (creep) over 3 days. The axial pressure then returns to the starting point (0.5 MPa) at the same rate as loading. The second and third stress cycles, following the same procedure as the first, start after the system had reached equilibrium. In the second and third cycles, the creep phases are shorter (1 day).

3. RESULTS

Deviatoric loading above yield resulted without exception in a steeply dipping shear fracture along the core (Figure 1, left).

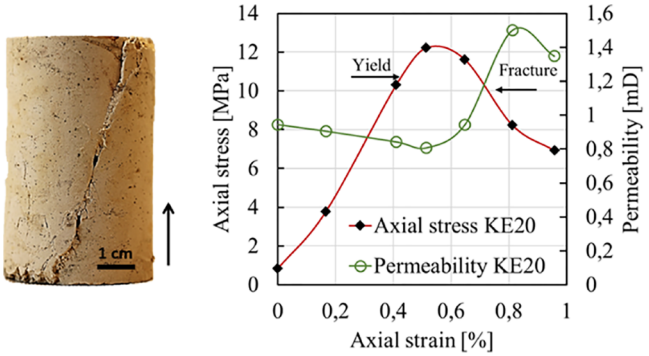

Figure 1. Right: High-angle shear fracture, typical for deviatoric loading at low confining pressure. The arrow indicates the flooding direction. Left: Typical example of axial stress−strain relationship (red curve) and permeability evolution (green curve) during first deviatoric loading above yield, here, data from the KE20 experiment (CE-NaCl series, 50 °C). Permeability generally decreases within the yield curve; the shear fracture event causes a concomitant drop in axial stress and an increase in permeability.

This is typical for compressive triaxial tests at low confining pressure, which allows the core to expand radially and facilitates well-organized shear failure between grains.[36] Figure 1 shows experiment KE20 (CE-NaCl series, 50 °C) to exemplify the typical permeability response (green curve) to first deviatoric loading above yield (red curve). Deviatoric loading within the yield curve (where the stress−strain relationship is linear) generally caused permeability decreases in all cores, in average, of 10% in the first cycle and 5% during second and third cycles compared to permeability values at the beginning of the respective cycles.

The shear fracture event, recognized by a drop in axial stress, initiated an abrupt increase in permeability, and generally, this occurred during the first loading. However, although all cores experienced the same deformation during the first loading, the mechanical strength of the cores and the degree of permeability rise differed. These differences should indicate the roles of injecting brine composition or temperature, the only two differing parameters in the test setup.

3.1. CE-NaCl Injection. Figure 2 shows permeability versus axial stress during deviatoric loading (left column) and permeability evolution in time during creep (right column) for the CE-NaCl test series. A clear distinction is seen between low temperature (blue curves) and high temperature (red curves) tests. As seen in Figure 2a, both cores tested at 50 °C (KE20 and KE4, blue lines) fractured at lower axial stress (11−12 MPa) than those tested at 130 °C (red lines, KE44 and KE45, 15−17 MPa). The shear fracture caused a drop in axial stress together with a clear rise in permeability (45% in average) and occurred mainly in the first loading. Test KE4 (50 °C), however, experienced a brief, unexpected pressure fluctuation in the beginning of the first loading at 5 MPa (Figure 2a), which might be related to an instrument error. This may have temporarily stabilized the core so that, at the end of the first deviatoric loading, the drop in axial stress from 11 to 9 MPa was an effect of microcracking, a precursor to fracturing.[37] A more pronounced shear fracture developed during the second loading cycle, leading to 1.75% axial deformation and 0.63% radial expansion, together with permeability rise by 36% (Figure 3b, blue triangles).

The mechanical strength decreased in all tests in the second loading (Figure 2b,c). The maximum axial stress was 3−4 MPa less compared to the first loading at 130 °C, while at 50 °C, the difference is approximately 5 MPa. Permeability increased in all tests after second loading but, unlike the first loading, by only less than 10% (excluding KE4).

Further, after the third loading, permeability decreased by 10% at 50 °C. Figure 2c (blue lines) shows that, after an initial decline during loading, the measured permeability remained constant. At 130 °C, on the other hand, it remained almost unchanged throughout the loading (Figure 2c, red lines).

The axial strain was the highest when the fracture occurred and it varied between 0.75 and 1.75% (Table 3), after which the cores experienced an average of 0.40% axial deformation at both temperatures. Radial strain does not correlate with the change in permeability so that more radial expansion does not necessarily lead to higher permeability.

Permeability seems unaffected by the degree of creep. Axial deformation during creep is a function of the applied axial stress, a value that was subjectively chosen for each core at each creep phase (Table 4). For example, in the KE44 test, the axial stress was 30% higher than KE45 at the same temperature, and it deformed three times more axially and six times more radially than KE45 during the first creep phase. Yet, permeability in both these tests is almost unchanged throughout the entire creep time (Figure 2d, red lines). The same trend is observed also in the creep phases 2 and 3, where the permeability does not register any significant changes. The two low temperature tests (KE4 and KE20), however, seem to decrease slightly during the first creep (Figure 2b, blue lines), but a direct comparison between the two tests is difficult because of the permeability fluctuations in KE4, which had not yet fractured properly at this point. During the second and third creep, on the other hand, the permeability only decreased somewhat in KE4 following the delayed clear shear fracture, but KE20 permeability stayed constant, similar to the high temperature tests (Figure 2e,f).

3.2. CE-Na_2SO_4 Fluid Injection. The results from the CE-Na_2SO_4 tests (Figure 3) show a similar permeability pattern as the CE-NaCl series. Permeability declined during the axial loading and increased with fracture formation in the first cycle (Figure 3a). Unlike the CE-NaCl tests, there is no clear maximum axial stress correlation between the high and low test temperatures. During the first loading cycle, the maximum axial stress was similar in three of the four tests, between 10 and 12 MPa, while KE22 withheld a maximum axial stress of 14 MPa. However, the high temperature tests registered the highest permeability increase when the shear fracture occurred, approximately double compared to the intact core permeability. At lower temperature, permeability increased with 50−80%. When comparing the first loading of the duplicate tests at each temperature, the magnitude of permeability rise correlates with the axial and radial strain: the higher the strain, the higher the permeability rise (Table 5).

https://dx.doi.org/10.1021/acsomega.9b04470
ACS Omega 2020, 5, 9185−9195

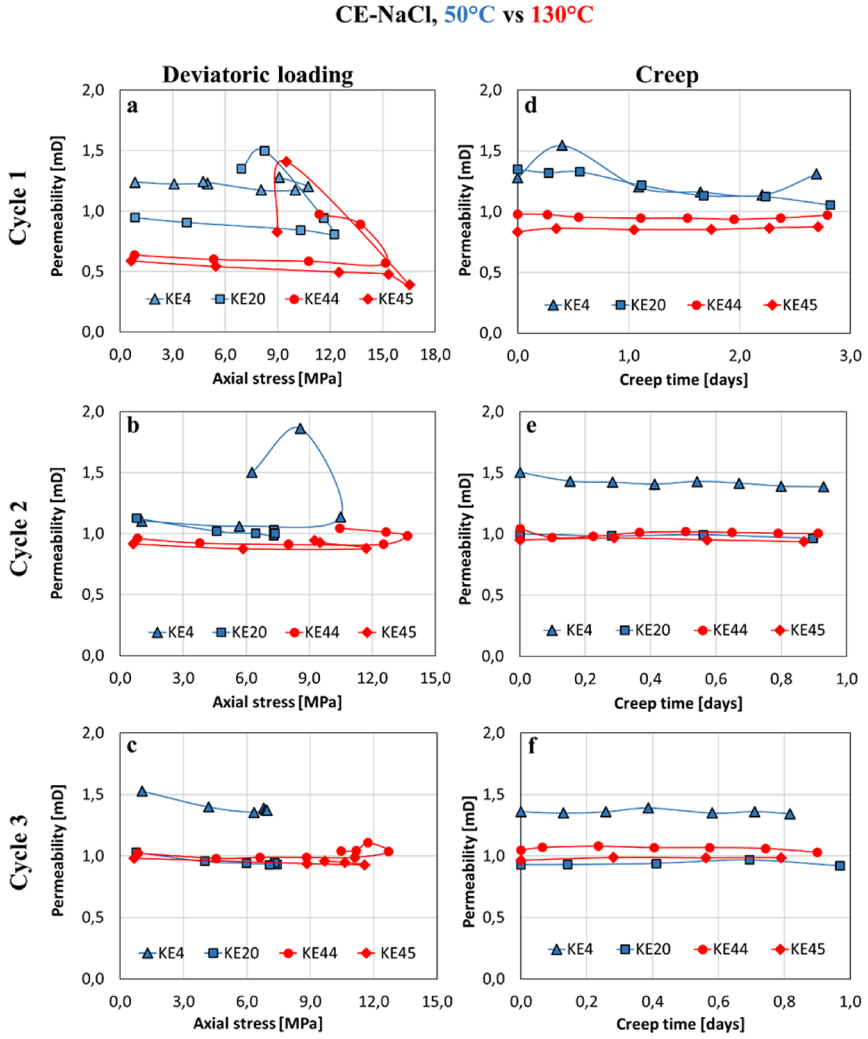

Figure 2. Permeability response to (a−c) axial stress and (d−f) creep in CE-NaCl experiments at 50 °C (blue lines) and 130 °C (red lines); the highest permeability increase is associated with core fracturing (a, and for KE4, b) after which no notable permeability change was observed. Creep under deviatoric conditions had a minimal effect on permeability evolution. The test temperature affected the mechanical strength during loading but did not play a decisive role in permeability during creep.

The mechanical strength decreased in all tests from the first cycle to the second and third cycles, regardless of test temperature (Figure 3b,c). Permeability increased in all experiments after the second loading cycle, this time by a factor of 2−4 more in the low temperature tests compared to the high temperature. This also corresponds to higher axial strain (0.62−0.98%) and radial strain (−0.2% in average) at low temperature compared to high temperature tests, which deformed in an average of 0.25% axially and below −0.1% radially at the same stage (Table 5).

The stress conditions in all three creep phases were similar (Table 6), and the cores sustained approximately 7 MPa constant axial stress and registered minor radial strain in all tests (between −0.02 and −0.06%). The axial strain varied somewhat with the temperature in the first creep phase so that, at low temperature, the axial strain was approximately double compared to the axial strain at 130 °C, but this had no clear effect on permeability.

The permeability generally declined after the first creep, mostly during the first creep day, after which it stabilized until the end of the creep phase (Figure 3d). Creep phases 2 and 3 (Figure 3e,f) induced minimal changes in permeability so that most of the permeability gain during the first loading cycle was retained throughout the test.

3.3. Synthetic Seawater Injection. The SSW-injected cores show similar permeability behavior as the CE-NaCl and CE-Na_2SO_4 series. As in the CE-Na_2SO_4 series, temperature did not play a distinguishing role in the maximum axial stress during the first loading cycle. Three of the tests fractured after a peak of approximately 12 MPa (Figure 4a), although performed at a different temperature. Core KE73 (130 °C, red diamonds) fractured after a maximum axial stress of 14 MPa. Although, generally, permeability increased after the first loading in all tests, there is no clear pattern in the rise magnitude (Table 7).

The strain−permeability correlation is seen here as well, where tests that showed higher permeability increase also experienced higher radial strain (Table 7). Core KE51 stands out with the highest permeability rise after the first loading (126%).

SSW flooding weakened the chalk cores similarly at both temperatures, showing an approximately 3−5 MPa decline in maximum axial stresses between the first loading and the subsequent loading phases. As in the CE-NaCl and CE-Na_2SO_4

https://dx.doi.org/10.1021/acsomega.9b04470
ACS Omega 2020, 5, 9185−9195

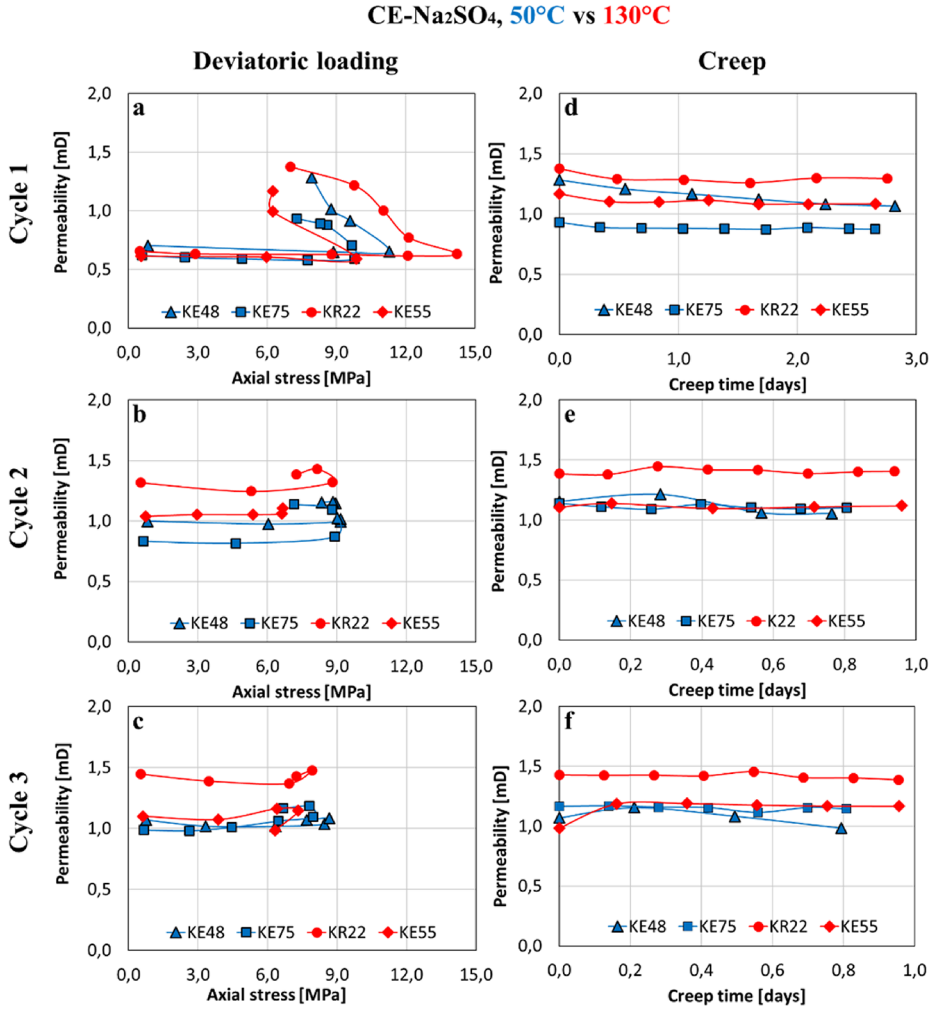

Figure 3. Permeability evolution in chalk cores flooded with CE-Na_2SO_4 brine at 50 °C (blue lines) and 130 °C (red lines) as a response to (a–c) deviatoric loading and (d–f) creep. Permeability rose clearly in the first loading cycle (a). After that, the permeability only registers minor changes regardless of temperature (b, c). Permeability remains almost unchanged during creep at both temperatures.

Table 3. Axial and Radial Strain (%) after Each Deviatoric Loading (CE-NaCl Series) and Permeability Change (%) Associated with Deviatoric Fracturing

			load 1			load 2		load 3	
flooding brine	T (°C)	core ID	axial strain (%)	radial strain (%)	permeability change (%)	axial strain (%)	radial strain (%)	axial strain (%)	radial strain (%)
CE-NaCl	50	KE4	0.88	−0.04	3	1.75	−0.63	0.48	−0.13
	50	KE20	0.96	−0.22	43	0.45	−0.67	0.28	−0.05
	130	KE44	0.75	−0.16	53	0.35	−0.09	0.38	−0.10
	130	KE45	1.04	−0.19	40	0.38	−0.08	0.44	−0.10

Table 4. Axial Stress (MPa) during Creep and Strain (%) after Each Creep Phase (CE-NaCl Series)

			creep 1			creep 2			creep 3		
flooding brine	T (°C)	core ID	axial stress (MPa)	axial strain (%)	radial strain (%)	axial stress (MPa)	axial strain (%)	radial strain (%)	axial stress (MPa)	axial strain (%)	radial strain (%)
CE-NaCl	50	KE4	6.9	0.14	−0.09	5.5	0.06	−0.01	5.5	0.03	0
	50	KE20	6.9	0.74	−0.68	6.8	0.21	−0.67	5.9	0.19	−0.05
	130	KE44	11.4	0.55	−0.2	10.4	0.14	−0.05	10.4	0.15	−0.05
	130	KE45	8.9	0.16	−0.03	9.2	0.07	−0.02	9.7	0.15	−0.05

series, permeability did not change significantly during deviatoric loadings 2 and 3.

Creep permeability trends were nearly parallel in all SSW experiments (Figure 4d–f), generally decreasing. End permeability was lowest in core KE51 (130 °C, Figure 4f, red bullets), which, throughout the test, lost more than half of the permeability gain after fracturing in loading 1. Core KE47 (50 °C) deformed at a high rate in all three creep cycles (Table 8),

https://dx.doi.org/10.1021/acsomega.9b04470
ACS Omega 2020, 5, 9185−9195

Table 5. Axial and Radial Strain (%) after Each Deviatoric Loading and Permeability Change (%) Associated with Shear Fracture during the First Loading

			load 1			load 2		load 3	
flooding brine	T (°C)	core	axial strain (%)	radial strain (%)	permeability change (%)	axial strain (%)	radial strain (%)	axial strain (%)	radial strain (%)
CE-Na_2SO_4	50	KE48	1.30	−0.25	+83	0.98	−0.23	0.40	−0.06
	50	KE75	1.02	−0.05	+50	0.62	−0.15	0.43	−0.12
	130	KE22	1.15	−0.39	+110	0.29	−0.07	0.28	−0.06
	130	KE55	0.97	−0.14	+90	0.22	−0.02	0.28	−0.05

Table 6. Axial Stress (MPa) during Creep and Strain (%) after Each Creep Phase (CE-Na_2SO_4 Series)

			creep 1			creep 2			creep 3		
flooding brine	T (°C)	core ID	axial stress (MPa)	axial strain (%)	radial strain (%)	axial stress (MPa)	axial strain (%)	radial strain (%)	axial stress (MPa)	axial strain (%)	radial strain (%)
CE-NA_2SO_4	50	KE48	7.7	0.33	−0.05	7.7	0.18	−0.03	7.7	0.15	−0.03
	50	KE75	7.2	0.59	−0.05	7.2	0.3	−0.06	6.7	0.15	−0.02
	130	KE22	7	0.16	−0.04	7.2	0.12	−0.04	7.2	0.12	−0.04
	130	KE55	6.2	0.27	−0.06	6.6	0.16	−0.04	6	0.19	−0.05

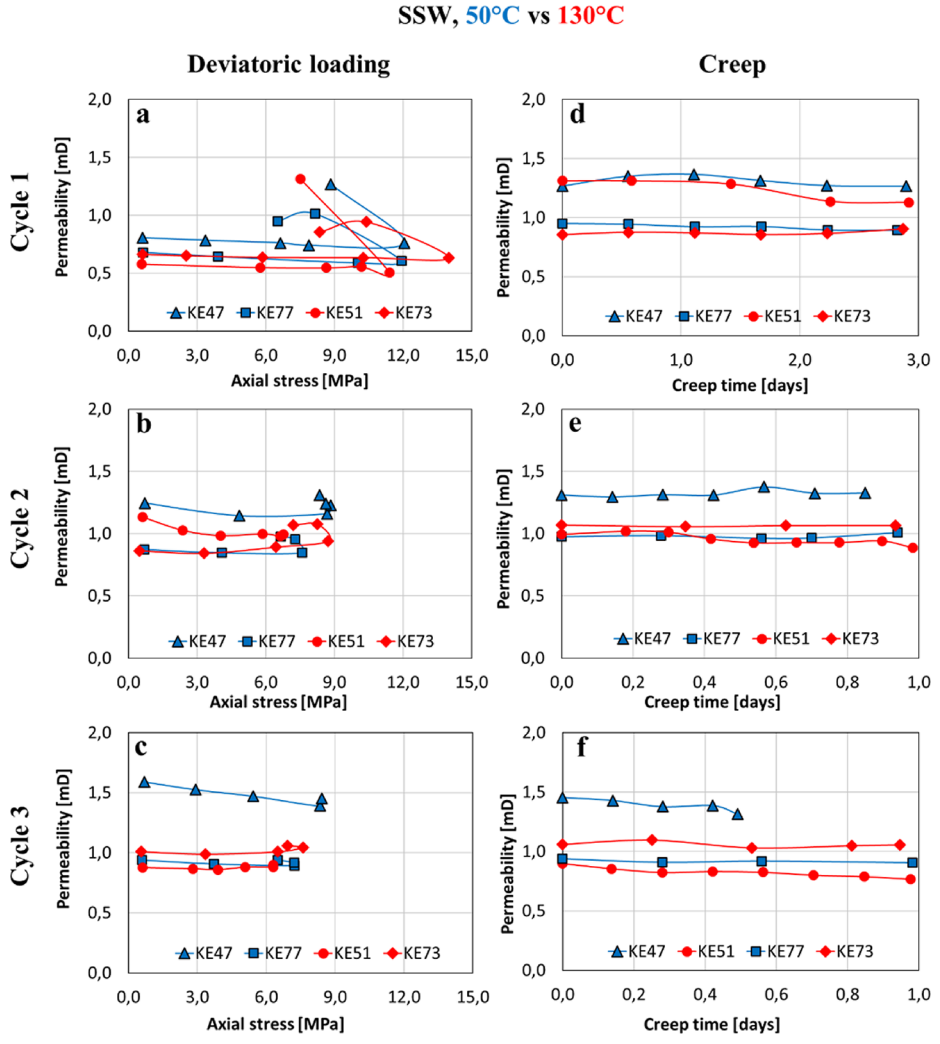

Figure 4. Permeability evolution in chalk cores flooded with SSW brine at 50 °C (blue lines) and 130 °C (red lines) as a response to (a−c) deviatoric loading and (d−f) creep. Permeability rose clearly in the first loading cycle as a result of shear fracturing (a). After that, the permeability registers minor changes regardless of temperature (b, c). Permeability remains almost unchanged during creep at both temperatures. Permeability of KE47 (blue triangles) declined more than all other tests in cycle 3 (c, f) as the core started to collapse.

https://dx.doi.org/10.1021/acsomega.9b04470
ACS Omega 2020, 5, 9185−9195

Table 7. Axial and Radial Strain (%) after Each Deviatoric Loading (SSW Series)

			load 1			load 2		load 3	
flooding brine	T (°C)	core ID	axial strain (%)	radial strain (%)	permeability change (%)	axial strain (%)	radial strain (%)	axial strain (%)	radial strain (%)
SSW	50	KE47	1.21	−0.16	+57	1.17	−0.31	0.41	−0.07
	50	KE77	0.77	−0.08	+40	0.39	−0.07	0.32	−0.05
	130	KE51	1.20	−0.24	+126	0.34	−0.06	0.20	−0.01
	130	KE73	0.67	−0.16	+29	0.49	−0.35	0.36	−0.11

Table 8. Axial Stress (MPa) during Creep and Strain (%) after Each Creep Phase (SSW Series)

			creep 1			creep 2			creep 3		
flooding brine	T (°C)	core ID	axial stress (MPa)	axial strain (%)	radial strain (%)	axial stress (MPa)	axial strain (%)	radial strain (%)	axial stress (MPa)	axial strain (%)	radial strain (%)
SSW	50	KE47	8.3	0.82	−0.23	8.2	1.16	−0.31	8.1		
	50	KE77	6.5	0.08	−0.01	6.6	0.08	−0.02	6.5	0.05	−0.01
	130	KE51	6.7	1.18	−0.36	6.8	0.31	−0.09	6.3	0.08	−0.02
	130	KE73	8.3	0.25	−0.07	7.2	0.11	−0.04	6.9	0.11	−0.04

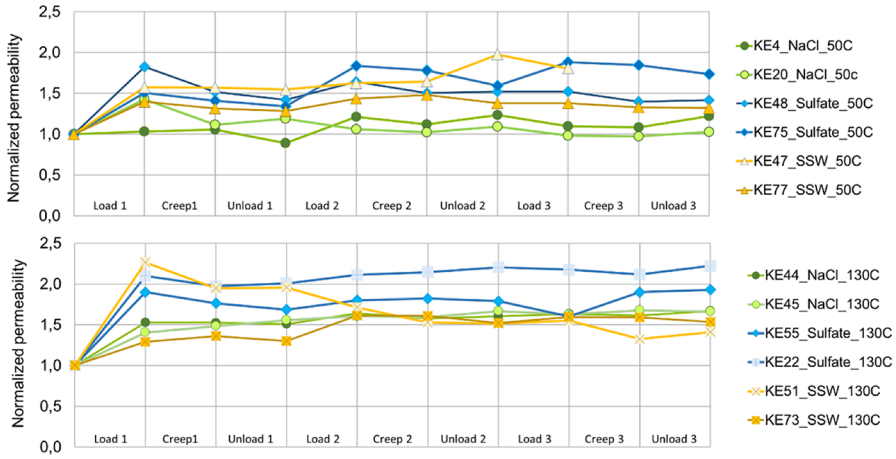

Figure 5. Overview of permeability evolution in all tested cores at 50 °C (top chart) and 130 °C (bottom chart). Permeability is normalized to the initial core permeability at the start of the first load; each line segment indicates the change in permeability during fluctuating stress states.

and the test was ultimately interrupted as the core collapsed. Yet, despite the accelerating creep conditions, the permeability decline rate is comparable to the other tests in this series.

4. DISCUSSION

The main drive in permeability change is the shear fracturing. Occurring mainly in the first deviatoric loading, the fracture serves as a "highway" for brine flow that induces a simultaneous permeability rise. The fracture dip angle is high and close to parallel to fluid flow due to the low confining pressure. The magnitude of permeability increase at this stage generally determines the cores' end permeability.

Figure 5 graphically displays the cumulative permeability evolution in all experiments, taking into account the unloading sequence as well. The first data point is the beginning of the first deviatoric cycle, and each line segment represents the permeability behavior during consecutive stress states. At both temperatures, end permeability of CE-Na_2SO_4-flooded cores is the highest. Megawati et al.[35] suggests that sodium sulfate brine injection at 130 °C does not cause new mineral precipitation such as anhydrite, but sulfate adsorption on chalk grains will change the chalk's surface charge and cause a disjoining force close to granular contacts. The disjoining force following sulfate adsorption may in fact explain why all CE-Na_2SO_4-flooded cores registered the highest permeability increase (Figure 5, blue lines).

On the other hand, SSW-flooded cores (yellow lines) gained least permeability at 130 °C, approximately half compared to CE-Na_2SO_4 series at the same temperature. That is most likely because SSW poses a different and more complex thermochemical scenario. According to previously mentioned studies,[23,30] SSW injection at 130 °C leads to both sulfate adsorption and mineralogical changes. Ca^{2+} substitution with Mg^{2+} and anhydrite ($CaSO_4$) precipitation contribute further to chalk weakening and alter fracture permeability. Particularly, anhydrite precipitation is a common permeability inhibitor, and Figure 5 shows that end permeability of both SSW-injected cores at 130 °C (yellow lines) lies below the other two series (CE-Na_2SO_4, blue lines, and CE-NaCl, green lines).

Another notable aspect from Figure 5 is that the degree of permeability rise related to fracturing (load 1) correlates with test temperature: overall, permeability increased 70%, in average, at the beginning of the tests at high temperature and only 40% average at low temperature. There was also higher variation in permeability rise among high temperature tests, compared to low temperature tests, where four out of six tests had an almost identical permeability increase. Additionally, end

https://dx.doi.org/10.1021/acsomega.9b04470
ACS Omega 2020, 5, 9185−9195

permeability at 130 °C increased, in average, by a factor of 1.7, while at 50 °C, the average increasing factor was 1.3.

Both stress and thermochemical test conditions impact the cores' mechanical strength to different degrees, generally decreasing throughout the test. Repetitive deviatoric loadings following the fracture formation do not seem to affect permeability as much as the shear fracturing event. This is in agreement with other studies[13,14] that, although performed under different thermochemical conditions than the present study, report that a second deviatoric stress cycle had a less effect on permeability evolution compared to the first cycle. The cycles naturally weaken the cores, with each loading−unloading adding more fatigue and deformation to the rock and altering its elastic properties.[11] The effect of temperature and injecting brine on the cores' mechanical strength is shown in Table 9.

Table 9. Maximum Axial Stress (MPa) during Deviatoric Loading under Different Thermochemical Conditions

			load 1	load 2	load 3
T (°C)	flooding brine	core ID	max. axial stress (MPa)	max. axial stress (MPa)	max. axial stress (MPa)
50 °C	CE-NaCl	KE4	11	10	7.0
	CE-NaCl	KE20	12	7.5	7.5
	CE-NA_2SO_4	KE48	12	9.1	8.6
	CE-NA_2SO_4	KE75	10	9.3	7.9
	SSW	KE47	13	8.9	8.4
	SSW	KE77	12	7.5	7.3
130 °C	CE-NaCl	KE44	15	14	13
	CE-NaCl	KE45	17	12	12
	CE-NA_2SO_4	KE22	14	8.8	8.6
	CE-NA_2SO_4	KE55	10	7.0	7.4
	SSW	KE51	11	6.6	6.7
	SSW	KE73	14	8.8	7.6

The CE-Na_2SO_4-injected cores at 50 °C registered the least mechanical strength decline (2−3 MPa) compared to the SSW (5 MPa) and CE-NaCl (4 MPa) series. At 130 °C, however, the CE-NaCl-injected cores retain most of their initial strength, while CE-Na_2SO_4 and, particularly, SSW series become weaker. This observation is in agreement with the previous studies[23,30] on SSW influence on the mechanical stability of chalk. Additionally, higher temperature intensifies the rock interactions with the injection brine.[7,19,23,24,30,35]

Creep conditions did not seem to override the permeability gain during fracturing. This is in agreement with other studies[3,6] that observed a low permeability decline in deviatoric conditions.

Table 10 summarizes the key changes recorded during each experiment. The net axial and radial strains are calculated as the percentage axial compaction and radial expansion, respectively, at the end of the test relative to the initial length and diameter respectively shown in Table 2.

In CE-NaCl and CE-Na_2SO_4 test series, the low temperature tests suffered more axial compaction than the high temperature tests. This correlates well with the end permeability: permeability increased only slightly in CE-NaCl-flooded cores at 50 °C (0 and 21%) but more clearly at higher temperature (66%). A similar pattern appears in CE-Na_2SO_4 tests. Low temperature cores experienced more compaction (2.5 and 2.8%) and less permeability increase (41 and 73%) than the cores flooded with CE-Na_2SO_4 at 130 °C (1.6% axial strain and a permeability increase by 95 and 122%). This indicates that, when flooding equilibrium brines that do not alter chalk mineralogy, brine temperature can play a significant role in mechanical compaction (strain), a key permeability-controlling factor.

This correlation is not clear in SSW series. Experiment KE47 failed before all stress sequences were complete so that the high compaction (4.3%) and high end permeability (+80%) are irrelevant in this argument. At 130 °C, KE51 deforms more axially (2.9%) than the second test at the same temperature (KE73, 1.3%) and end permeability is consequently lower with higher compaction, as in the previous two series.

There is little variation in net radial strain among the tests (between −0.2 and −0.8%, excluding KE47), indicating that flooding brine and temperature do not decisively affect fracture aperture, and any radial strain is rather stress-induced. Ultimately, there is no immediate correlation between the net radial strain and end permeability.

5. CONCLUSIONS

This study focuses on permeability evolution in fractured chalk cores exposed to cyclic deviatoric stress and thermochemical influence relevant to reservoir conditions. The test setup included three series, each with specific injecting brine: two calcite-equilibrated brines (CE-NaCl and Na_2SO_4) and one

Table 10. Summary of the Cores' Measured Axial and Radial Strain (%) and Permeability Changes

flooding brine	T (°C)	core ID	net axial strain (%)	net radial strain (%)	k_i (mD)	k_{end} (mD)	net permeability change (%)
CE-NaCl	50	KE4	3.0	−0.8	1.24	1.51	+22
	50	KE20	2.3	−0.7	0.94	0.97	+2.8
	130	KE44	1.7	−0.6	0.64	1.06	+67
	130	KE45	1.7	−0.5	0.59	0.98	+66
CE-Na_2SO_4	50	KE48	2.8	−0.6	0.70	1.00	+41
	50	KE75	2.5	−0.4	0.62	1.07	+73
	130	KE22	1.6	−0.6	0.66	1.46	+122
	130	KE55	1.6	−0.3	0.61	1.19	+95
SSW	50	KE47	4.3[a]	−1.0[a]	0.81	1.45[a]	+80[a]
	50	KE77	1.2	−0.2	0.68	0.90	+32
	130	KE51	2.9	−0.7	0.58	0.82	+41
	130	KE73	1.3	−0.5	0.66	1.02	+54

[a]Calculated values at the end of the third deviatoric loading prior to core collapse.

https://dx.doi.org/10.1021/acsomega.9b04470
ACS Omega 2020, 5, 9185−9195

nonequilibrium brine (SSW). Each test series was performed at 50 and 130 °C. Such flooding experiments highlight the interplay between the parameters. The results showed that stress-induced fracturing is the main permeability drive as permeability changed decisively only as a response to fracturing of the core. The deviatoric stress state together with low confining pressure induced shear fracturing at a steep angle (over 70°), close to the flooding direction. Subsequent deviatoric loadings had a little effect on permeability in all tests, regardless of injecting brine and test temperature. During creep, permeability generally declined slightly or remained unchanged. Our results indicate that, once chalk has fractured, the effective permeability is insensitive to compaction cycles and reactive flow, both at high and low temperatures.

The CE-Na_2SO_4 test series stand out with the highest final permeability at both temperatures. This is likely a result of sulfate adsorption on the chalk grain surface creating enough disjoining force at granular contact to preserve permeability. Additionally, calcite equilibration of the brine prevented calcium displacement and, consequently, anhydrite precipitation.

If flooding CE-Na_2SO_4 through fractured chalk seems to sustain the permeability gain related to shear fracturing, then flooding reactive brine such as SSW at a high temperature has a competing effect on permeability evolution. SSW test series registered most permeability loss at 130 °C, most likely due to chemical alteration, possibly precipitation of anhydrite.

However, all cores had a positive net permeability change. Despite fracturing and exposure to different stress states, temperatures, and brine conditions, core permeability at the end of the test seems to remain within the same order of magnitude as the original value, ranging between the initial value and double of the initial value. This indicates strong insensitivity to changes in reservoir conditions.

The results are repeatable, confirming permeability behavior for this experiment setup. Future studies should investigate the effects of longer-term stress cycles or several stress cycles at actual reservoir stress conditions on permeability evolution in fractured chalk cores. Additional analyses such as scanning electron microscopy can then verify the chemical alteration caused by reactive fluid flow in chalk, as suggested by Minde et al.,[38] and determine mineral alteration along the fracture or in the matrix. Although challenging to obtain, similar flooding experiments on actual reservoir chalk from the North Sea would provide important data for validating outcrop chalk test results and refining permeability models for the North Sea reservoir chalk. Especially, the importance of the adsorption mechanism to maintain fracture permeability in the field should be investigated further.

AUTHOR INFORMATION

Corresponding Author

Emanuela I. Kallesten − *University of Stavanger, 4021 Stavanger, Norway; The National IOR Centre of Norway, 4021 Stavanger, Norway;* orcid.org/0000-0002-3534-4386; Email: emanuela.i.kallesten@uis.no

Authors

Pål Østebø Andersen − *University of Stavanger, 4021 Stavanger, Norway; The National IOR Centre of Norway, 4021 Stavanger, Norway;* orcid.org/0000-0002-8552-094X

Merete V. Madland − *University of Stavanger, 4021 Stavanger, Norway; The National IOR Centre of Norway, 4021 Stavanger, Norway*

Reidar I. Korsnes − *University of Stavanger, 4021 Stavanger, Norway; The National IOR Centre of Norway, 4021 Stavanger, Norway*

Edvard Omdal − *ConocoPhillips, 4056 Tananger, Norway*

Udo Zimmermann − *University of Stavanger, 4021 Stavanger, Norway; The National IOR Centre of Norway, 4021 Stavanger, Norway*

Complete contact information is available at: https://pubs.acs.org/10.1021/acsomega.9b04470

Notes

The authors declare no competing financial interest.

ACKNOWLEDGMENTS

The authors acknowledge the Research Council of Norway and the industry partners, ConocoPhillips Skandinavia AS, Aker BP ASA, Vår Energi AS, Equinor ASA, Neptune Energy Norge AS, Lundin Norway AS, Halliburton AS, Schlumberger Norge AS, and Wintershall DEA, of The National IOR Centre of Norway for the support.

REFERENCES

(1) Sulak, R. M.; Danielsen, J. Reservoir Aspects of Ekofisk Subsidence. *J. Pet. Technol.* **1989**, *41*, 709−716.

(2) Sulak, R. M. Ekofisk field: the first 20 years. *J. Pet. Technol.* **1991**, *43*, 1−265.

(3) Teufel, L. W. Permeability of naturally fractured reservoirs. In *AAPG 1991 annual convention with DPA/EMD divisions and SEPM, an associated society;* AAPG: 1991, *75* (3), 680.

(4) Suri, P.; Azeemuddin, M.; Zaman, M.; Kukreti, A. R.; Roegiers, J. C. Stress-dependent permeability measurement using the oscillating pulse technique. *J. Pet. Sci. Eng.* **1997**, *17*, 247−264.

(5) Yale, D. P.; Crawford, B. Plasticity and permeability in carbonates: dependence on stress path and porosity. In *SPE/ISRM Rock Mechanics in Petroleum Engineering.* Society of Petroleum Engineers, 1998.

(6) Korsnes, R. I.; Risnes, R.; Faldaas, I.; Norland, T. End effects on stress dependent permeability measurements. *Tectonophysics* **2006**, *426*, 239−251.

(7) Minde, M. W.; Wang, W.; Madland, M. V.; Zimmermann, U.; Korsnes, R. I.; Bertolino, S. R. A.; Andersen, P. Ø. Temperature effects on rock engineering properties and rock-fluid chemistry in opal-CT-bearing chalk. *J. Pet. Sci. Eng.* **2018**, *169*, 454−470.

(8) Teufel, L. W.; Rhett, D. W. Failure of Chalk During Waterflooding of the Ekofisk Field. In *SPE Annual Technical Conference and Exhibition.* Society of Petroleum Engineers, 1992.

(9) Smart, B. G. D.; Somerville, J. M.; Edlman, K.; Jones, C. Stress sensitivity of fractured reservoirs. *J. Pet. Sci. Eng.* **2001**, *29*, 29−37.

(10) Moosavi, S. A.; Goshtasbi, K.; Kazemzadeh, E.; Bakhtiari, H. A.; Esfahani, M. R.; Vali, J. Relationship between porosity and permeability with stress using pore volume compressibility characteristic of reservoir rocks. *Arabian J. Geosci.* **2014**, *7*, 231−239.

(11) Ray, S. K.; Sarkar, M.; Singh, T. N. Effect of cyclic loading and strain rate on the mechanical behaviour of sandstone. *Int. J. Rock Mech. Min. Sci.* **1999**, *36*, 543−549.

(12) Bernabé, Y.; Mok, U.; Evans, B. Permeability-porosity relationships in rocks subjected to various evolution processes. *Pure Appl. Geophys.* **2003**, *160*, 937−960.

(13) Milsch, H.; Hofmann, H.; Blöcher, G. An experimental and numerical evaluation of continuous fracture permeability measurements during effective pressure cycles. *Int. J. Rock Mech. Min. Sci.* **2016**, *100*, 109−115.

(14) Kluge, C.; Blöcher, G.; Milsch, H.; Hofmann, H.; Nicolas, A.; Li, Z.; Fortin, J. Sustainability of fractured rock permeability under varying pressure. In *Poromechanics VI*; American Society of Civil Engineers: 2017, 1192−1199.

https://dx.doi.org/10.1021/acsomega.9b04470
ACS Omega 2020, 5, 9185−9195

(15) Hu, C.; Agostini, F.; Skoczylas, F.; Egermann, P. Effects of gas pressure on failure and deviatoric stress on permeability of reservoir rocks: initial studies on a Vosges sandstone. *Eur. J. Environ. Civ. Eng.* **2018**, *22*, 1004−1022.
(16) Hermansen, H.; Landa, G. H.; Sylte, J. E.; Thomas, L. K. Experiences after 10 years of waterflooding the Ekofisk Field, Norway. *J. Pet. Sci. Eng.* **2000**, *26*, 11−18.
(17) Uribe-Patiño, J. A.; Alzate-Espinosa, G. A.; Arbeláez-Londoño, A. Geomechanical aspects of reservoir thermal alteration: A literature review. *J. Pet. Sci. Eng.* **2017**, *152*, 250−266.
(18) Voake, T.; Nermoen, A.; Korsnes, R. I.; Fabricius, I. L. Temperature cycling and its effect on mechanical behaviours of high-porosity chalks. *J. Rock Mech. Geotech. Eng.* **2019**, *11*, 749−759.
(19) Austad, T.; Strand, S.; Høgnesen, E. J.; Zhang, P. Seawater as IOR fluid in fractured chalk. In *SPE international symposium on oilfield chemistry;* Society of Petroleum Engineers: 2005.
(20) Heggheim, T.; Madland, M. V.; Risnes, R.; Austad, T. A chemical induced enhanced weakening of chalk by seawater. *J. Pet. Sci. Eng.* **2005**, *46*, 171−184.
(21) Austad, T.; Strand, S.; Madland, M. V.; Puntervold, T.; Korsnes, R. I. Seawater in Chalk: An EOR and Compaction Fluid. In *International Petroleum Technology*; International Petroleum Technology Conference: 2008, *11* (04), 648−654, DOI: 10.2118/118431-PA.
(22) Korsnes, R. I.; Wersland, E.; Austad, T.; Madland, M. V. Anisotropy in chalk studied by rock mechanics. *J. Pet. Sci. Eng.* **2008**, *62*, 28−35.
(23) Madland, M. V.; Hiorth, A.; Omdal, E.; Megawati, M.; Hildebrand-Habel, T.; Korsnes, R. I.; Evje, S.; Cathles, L. M. Chemical Alterations Induced by Rock−Fluid Interactions When Injecting Brines in High Porosity Chalks. *Transp. Porous Media* **2011**, *87*, 679−702.
(24) Megawati, M.; Madland, M. V.; Hiorth, A. Mechanical and physical behavior of high-porosity chalks exposed to chemical perturbation. *J. Pet. Sci. Eng.* **2015**, *133*, 313−327.
(25) Bergsaker, A. S.; Røyne, A.; Ougier-Simonin, A.; Aubry, J.; Renard, F. The effect of fluid composition, salinity, and acidity on subcritical crack growth in calcite crystals. *J. Geophys. Res.: Solid Earth* **2016**, *121*, 1631−1651.
(26) Polat, C.; Parlaktuna, M. A study on the effect of the chemical composition of brine to improve oil recovery from carbonates. *Energy Sources, Part A* **2017**, *39*, 2151−2156.
(27) Zhang, P.; Tweheyo, M. T.; Austad, T. Wettability alteration and improved oil recovery by spontaneous imbibition of seawater into chalk: Impact of the potential determining ions Ca^{2+}, Mg^{2+}, and SO_4^{2-}. *Colloids Surf., A* **2007**, *301*, 199−208.
(28) Nermoen, A.; Korsnes, R. I.; Storm, E. V.; Stødle, T.; Madland, M. V.; Fabricius, I. L. Incorporating electrostatic effects into the effective stress relation—Insights from chalk experiments. *Geophysics* **2018**, *83*, MR123−MR135.
(29) Kallesten, E.; Østebø Andersen, P. Ø.; Berawala, D. S.; Korsnes, R. I.; Vadla Madland, M.; Omdal, E.; Zimmermann, U. Modelling of Permeability and Strain Evolution in Chemical Creep Compaction Experiments with Fractured and Unfractured Chalk Cores Conducted at Reservoir Conditions. *SPE J.* **2020** SPE-197371-PA (in press; available online April 2020) DOI: 10.2118/197371-PA.
(30) Korsnes, R. I.; Madland, M. V.; Austad, T.; Haver, S.; Røsland, G. The effects of temperature on the water weakening of chalk by seawater. *J. Pet. Sci. Eng.* **2008**, *60*, 183−193.
(31) Daigle, H.; Rasromani, E.; Gray, K. E. Near-wellbore permeability alteration in depleted, anisotropic reservoirs. *J. Pet. Sci. Eng.* **2017**, *157*, 302−311.
(32) Fjær, E.; Holt, R. M.; Horsrud, P.; Raaen, A. M.; Risnes, R. *Mechanical properties and stress data from laboratory analysis. In Petroleum Related Rock Mechanics*, 2nd Ed., Vol. *53*; Elsevier: 2008; pp 251−287.
(33) Darcy, H. P. G. *Les Fontaines publiques de la ville de Dijon. Exposition et application des principes à suivre et des formules à employer dans les questions de distribution d'eau, etc.*; V. Dalamont: 1856.
(34) El-Dessouky, H. T.; Ettouney, H. M. Thermodynamic Properties. In *Fundamentals of salt water desalination*, 1st ed.; Elsevier, 2002; pp 525−564.
(35) Megawati, M.; Hiorth, A.; Madland, M. V. The impact of surface charge on the mechanical behavior of high-porosity chalk. *Rock Mech. Rock Eng.* **2013**, *46*, 1073−1090.
(36) Risnes, R. Deformation and yield in high porosity outcrop chalk. *Phys. Chem. Earth A: Solid Earth Geod.* **2001**, *26*, 53−57.
(37) Dautriat, J.; Gland, N.; Dimanov, A.; Raphanel, J. Hydromechanical behavior of heterogeneous carbonate rock under proportional triaxial loadings. *J. Geophys. Res.: Solid Earth* **2011**, *116*, B01205.
(38) Minde, M. W.; Zimmermann, U.; Madland, M. V.; Korsnes, R. I.; Schulz, B.; Audinot, J. N. Fluid−flow during EOR experiments in chalk: insights using SEM−MLA, EMPA and Nanosims Applications. In *International Symposium of the Society of Core Analysts*; The Society of Core Analysts: 2016, 21−26.

https://dx.doi.org/10.1021/acsomega.9b04470
ACS Omega 2020, 5, 9185−9195

SPE Journal, https://doi.org/10.2118/197371-PA

Paper IV: Modelling of Permeability and Strain Evolution in Chemical Creep Compaction Experiments with Fractured and Unfractured Chalk Cores Conducted at Reservoir Conditions

Kallesten, E., Andersen, P.Ø., U., Berawala, D.S., Korsnes, R.I., Madland, M.V., Omdal, E., Zimmermann, U.

SPE Journal, in press

This paper is not in Brage for copyright reasons.

Paper IV